Feasibility of Beneficial Hurricane Modification by Carbon Black Seeding

By

William M. Gray

Department of Atmospheric Science
Colorado State University
Fort Collins, Colorado

NOAA N 22-65-75 (G)

Colorado State University

Department of Atmospheric Science

Paper No. 196

FEASIBILITY OF BENEFICIAL HURRICANE MODIFICATION BY CARBON DUST SEEDING

by

William M. Gray

Department of Atmospheric Science
Colorado State University
Fort Collins, Colorado

April 1973

ABSTRACT

The recent numerical models of hurricanes such as those of
Rosenthal (1970b, 1971a, 1971b) and Ooyama (1969), plus other model
and storm dynamic considerations indicate that the hurricane's inner
core circulation would weaken if the frictionally induced boundary layer
inflow into the storm center could be lessened by inducing some of it
to rise at a more distant radius.

It is hypothesized that a significant portion of the outlying boundary
layer inflow into the hurricane can be artificially induced to rise in
cumulus at a radius greater than the radius of the eye-wall cloud. This
can conceivably be accomplished by the interruption of solar radiation
by carbon black dust particles (radius ~ 0.1 micron) dispersed in the
boundary layer just beyond the hurricane's cirrus shield. Through the
use of 10-20 C-5A aircraft an artificially induced boundary layer heat-
ing of about $1^{\circ}C/hr.$ for 10 hours can be accomplished over an area of
40-80,000 km^2 at 10% areal coverage of carbon dust particles. This
not only produces extra thermal instability but also increases evapora-
tion rates from additional mixing downward of drier air from aloft.
The energy for this extra evaporation comes largely from the ocean
and not the air. The effects of this artificial solar heating at outer
radii should continue as the low level inflow progresses under the
cirrus shield.

The solar energy absorption amounts to about $\sim 2 \times 10^{10}$ cal/lb per
10 hours or about 4×10^{11} cal/dollar per 10 hours (Frank, 1973). This
is a tremendously powerful heat source, especially if it stimulates
an additional evaporation energy gain. Information gained from indi-
vidual cloud models such as that of López (1972), show that this low
level energy source can significantly enhance convective activity at
outer radii.

The Rosenthal (op. cit.) symmetric hurricane model indicates that
this extra heat source is enough to cause substantial reduction of the
maximum sustained surface winds ($\sim 30\%$) and kinetic energy ($\sim 60\%$)
in the hurricane's inner core in 18-24 hours while maintaining or
slightly increasing the outer vortex circulation and beneficial rainfall.
It is shown that if the assumptions of this model of modification are
correct, storm damage reduction to cost of modification ratios of up to
50-100 to 1 are possible. Adverse influences of pollution are shown
to be negligible. This modification hypothesis should be given careful
consideration.

TABLE OF CONTENTS

1. HURRICANE DESTRUCTION

Damage from hurricanes in the United States averages about $500 million per year (Howard, Matheson, and North, 1972). The global damage from all tropical storms is many times higher. Individual hurricanes such as Betsy (1965) and Camille (1969) can produce destruction equivalent to 3 times (or $1.5 billion) the U. S. annual storm damage. Most of this U. S. destruction comes from only one or two storms per year. In Asia, storms often bring much more destruction because of their higher frequency and the greater coastal population densities.

Man should attempt to reduce this heavy storm destruction while not significantly reducing the beneficial rains from these storms. This might be accomplished by significantly reducing the wind in the storm's inner core areas while maintaining the strength of the outer circulation which determines the large-scale water vapor convergence and the net rainfall production. In general, the precipitation from the outer regions of the hurricane is considered to be beneficial (Giddings, 1966; Sugg, 1968; Cry, 1967).

Hurricane Damage Related to Wind Speed. Hurricane property damage comes from three sources:

(1) coastal flooding damage due to wind-developed high water or storm surge;

(2) direct wind force damage;

(3) inland flooding from heavy precipitation

1

Coastal flooding is usually the largest source of damage, but this varies with individual storms. Saffir (1972) recently pointed out that in many cases wind force damage and/or inland flooding may produce as much or more destruction than the storm surge. The greatest hurricane damage usually occurs within a 150-200 km wide swath centered on the region of maximum winds to the right of the direction of movement of the storm's center. U. S. coastal hurricanes have their radius of maximum winds typically 40-50 km from the storm center. Destruction to the left side of the direction of storm motion is usually much less (Dunn and Miller, 1960).

The recent study of hurricane damage from all three damage sources by Howard, Matheson, and North(op. cit.) has indicated that U.S. hurricane destruction goes up dramatically with wind speed. They give a statistical relationship which shows cyclone destruction related to the storm's maximum sustained surface velocity raised to a power of 4. 3 (see Fig. 1-1).[1] If this is an accurate representation of storm damage, then a 20 to 25 percent reduction in maximum surface winds on the right side of the storm would reduce storm damage by as much as 50%, a most desirable modification goal.

----

[1] Although another research team (Jelesnianski and Taylor, 1972) studying only storm surge damage implies a more linear relationship between storm surge height and maximum wind speed, it is felt that the total hurricane destruction from all sources of wind and flooding damage is more related to the surface wind speed raised to a power considerably larger than one.

Flooding Damage. The massive study of rainfall associated with hurricanes by Schoner and Molansky (1956) and the data of Goodyear (1968) has documented the strong concentration of hurricane rainfall along the storm's central path. This is due to the very large amount of precipitation coming from eye-wall convection. Very heavy rainfall amounts (> 10-15 cm/24hrs) are typically concentrated in narrow strips of but 100-150 km straddling the storm's path as seen in Fig. 1-2. Heavy local flooding often occurs along the path of the storm center. The beneficial nature of the hurricane rainfall becomes questionable when flooding damage is large. If storm rainfall could be more evenly distributed and not concentrated in the storm center, flooding damage would be greatly reduced and the storm's rainfall would become more beneficial.

Storm Surge and Wind Damage. The storm wind and the surge heights go together. Although variations in the coastal shelf can greatly alter the height and character of the storm surge, high water levels would not be possible without a concentrated storm inner-core wind circulation. Fig. 1-3 shows the association of wind speed and storm ocean surge height information for Hurricane Debbie of 1969 as determined by Jelesinanski and Taylor (1972). Note the high correlation of storm surge height with wind speed and the strong concentration of the wind and water heights over a narrow width. This is thought to be typical of most hurricanes. The information of Graham and Hudson (1960) on surface winds near the center of hurricanes and the flight information
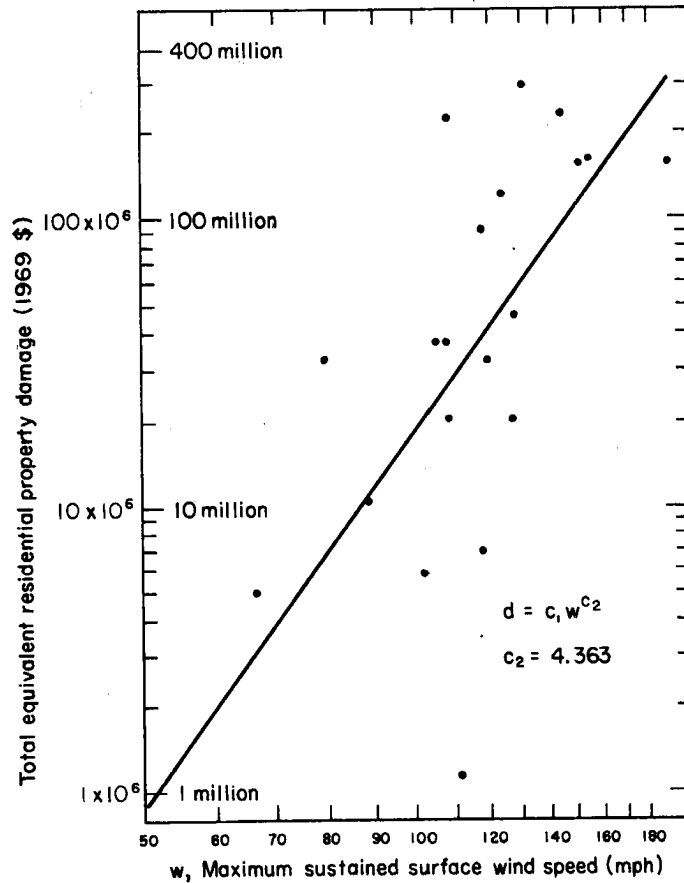
Fig. 1-1. Hurricane damage in the U. S. as related to storm's maximum sustained surface winds, as recently determined by Howard, Matheson, and North, 1972. Note how rapidly the damage increases with wind speed.
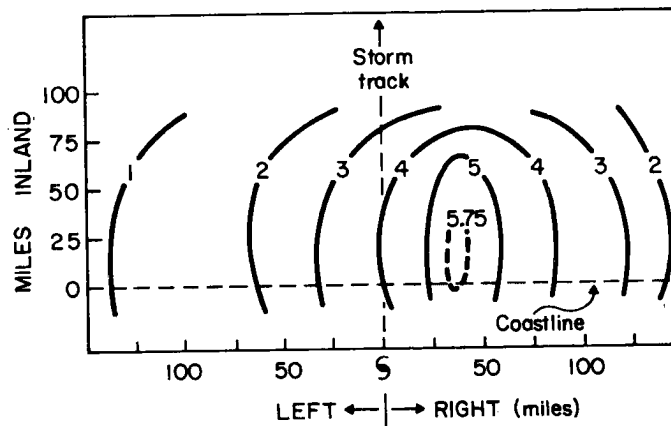

Fig. 1-2. Typical average 48-hour hurricane rainfall (in.) relative to the storm center and the coastline as determined by Goodyear (1968). Note concentration of rainfall near the hurricane center.
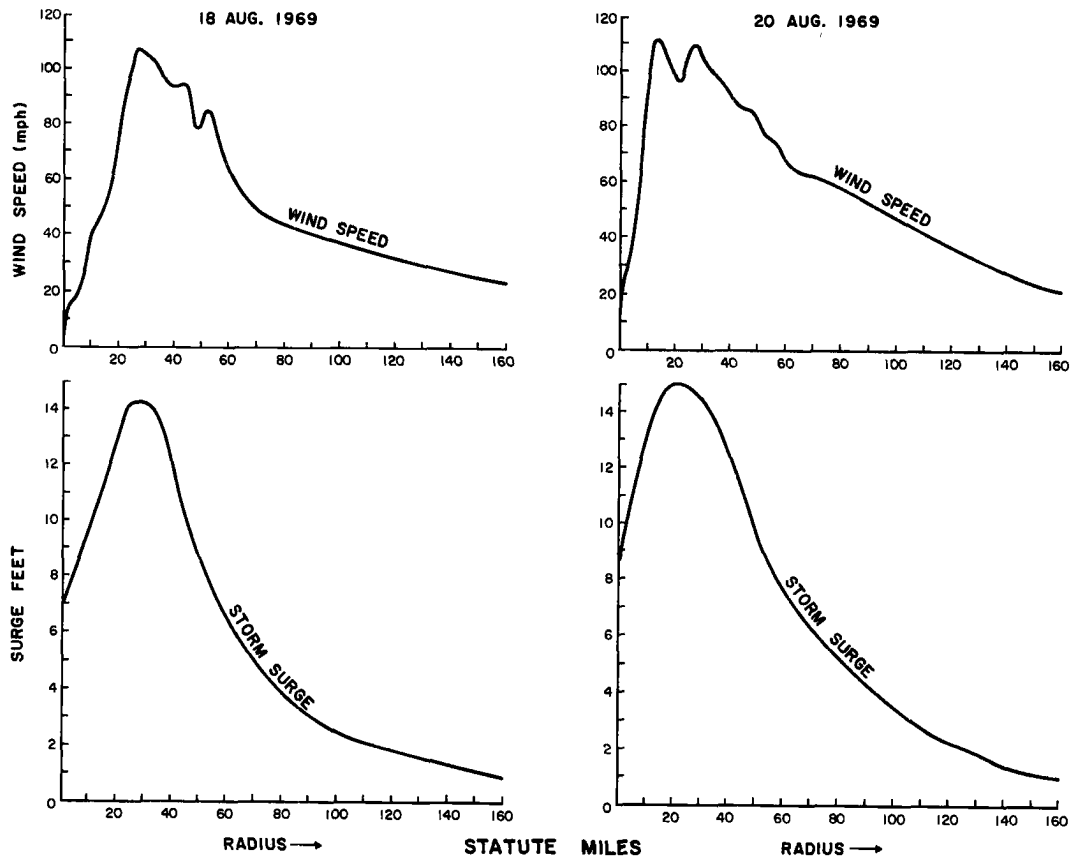
HURRICANE DEBBIE

Fig. 1-3. Relationship of wind speed and storm ocean surge height as determined by Jelesinanski and Taylor for Hurricane Debbie (1969). Note the strong correlation of the storm surge height with the wind speed and the concentration of the wind and surge height over a narrow inner radius width.

of Shea (1972) also verify the very concentrated nature of the winds in these storms.

Conclusion. Hurricane property damage increases exponentially with maximum sustained surface wind velocities. One source shows it increasing with the 4.3 power of the maximum sustained surface velocity. Hurricane induced wind damage, storm surge and precipitation destruction are concentrated in a narrow region 50-150 km wide

on the right side of the storm center. Destruction from these three influences would be greatly reduced if the hurricane's inner core of maximum winds could be reduced and the radial profile of wind velocity made more uniform.

2. HURRICANE STRUCTURE

The structure of hurricanes and their dynamics as determined by observational studies [Hughes (1952), Riehl (1954), Riehl and Malkus (1961), Miller (1964), Izawa (1964), Yanai (1961, 1968), Yanai and Nitta (1967), Sheets (1968), Bell and Tsui (1972), Hawkins and Rubsam (1968), Shea (1972)] and by model studies [Malkus and Riehl (1960), Riehl (1963), Ooyama (1969), Rosenthal (1970b, 1971a, 1971b), Anthes et al. (1971c), Gray (1967)] specify a low level (sfc to 850 mb) frictionally driven mass convergence toward the storm center which is related to the storm's overall surrounding cyclonic circulation. The hurricane could not exist without this low level frictionally forced convergence. This inflow is only partly related to the storm's central core of maximum wind velocity, however. The inner core wind intensity is also related to the radius to which this frictionally driven inflow penetrates to the storm center.

Fig. 2-1 is a typical surface pressure map surrounding a hurricane in the trade winds. It is surrounded by anticyclones to the north and sometimes also to the east and west. The arrows on this figure show the typical angle the surface wind makes with the low level pressure pattern. Over the tropical oceans the surface wind crosses the isobars to lower pressure at an angle of about 10 degrees (Gray, 1972a). Note how far the cyclonic circulation extends out from the storm center -- often to radii up to 12-15 degrees of latitude. This produces a low level frictional inflow from large distances. Much of this outer inflow occurs
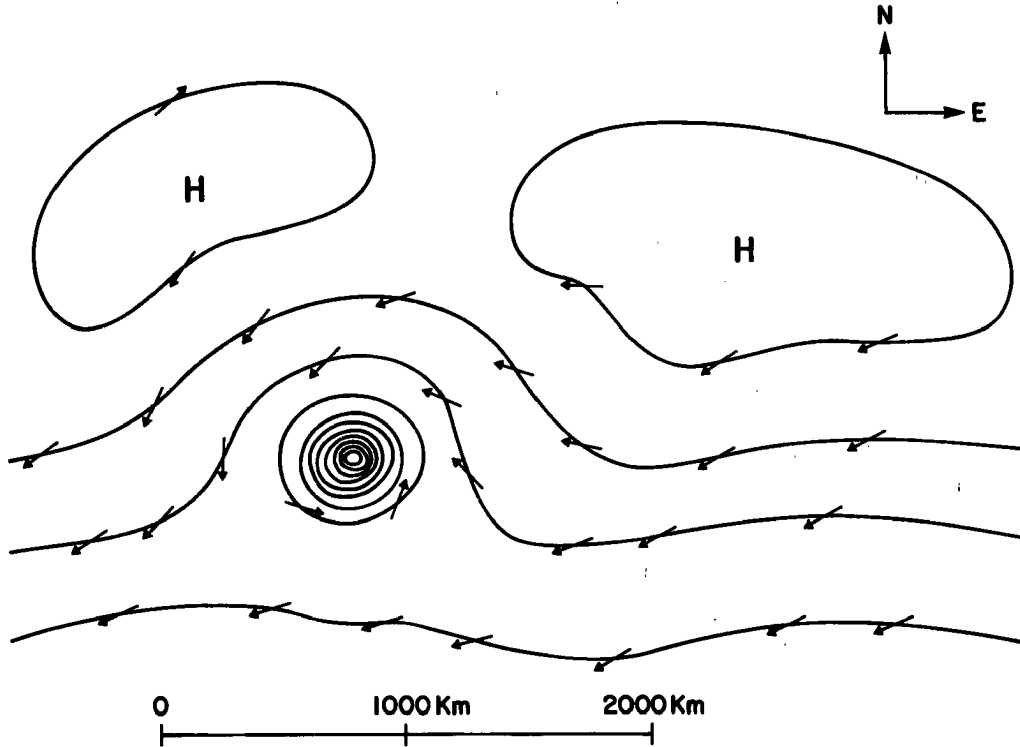
7

Fig. 2-1. Typical surface pressure (solid lines) and surface winds
(arrows) surrounding a hurricane-typhoon in the trade winds.
Note how far out from the storm center the cyclonic winds
and the surface inflow extend.

in clear conditions. Hurricane cloudiness typically extends out from

the storm center to 3-4° radius. Fig. 2-2 shows NOAA satellite pic-

tures of typical hurricane and typhoon cloud clusters. Note the large

clear (or moat) area surrounding the hurricane cloud cluster regions.

The hurricane's wind intensity is partially related to the width of its

cloud cluster areas as discussed by Fritz, Hubert, and Timchalk

(1966) – see Fig. 2-3. Weaker storms typically have a smaller inner

area of cloudiness. The most intense storms have cloud diameters of

up to 8-9° latitude. These relationships are invalid for some storms,

however. Fig. 2-4 (from LaSeur and Hawkins, 1963) shows a radial
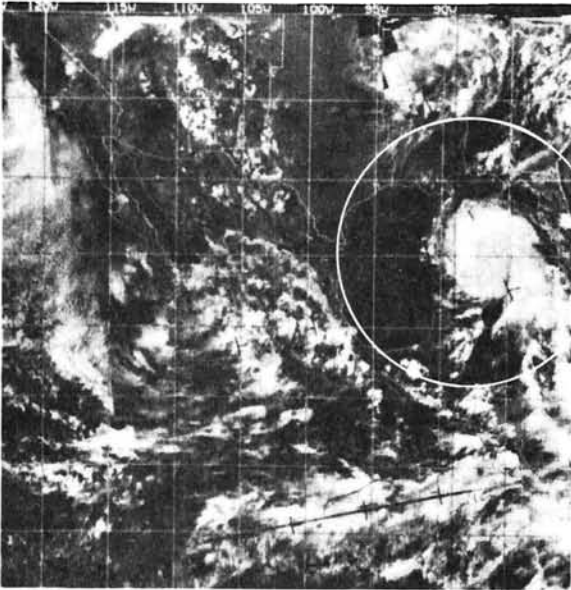
Hurricane Camille (25°N,87°W)
16 Aug 1969
Central Pressure ~905mb
Maximum Winds ~140kts
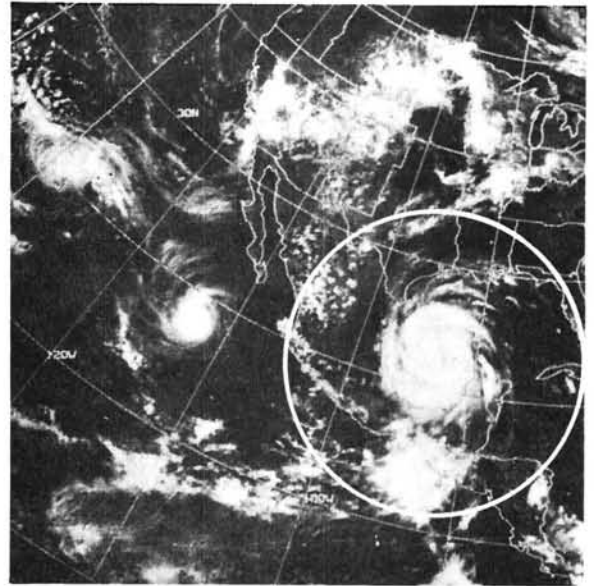
Hurricane Beulah (23°N, 95°W)
18 Sept. 1967
Central Pressure~950mb
Maximum Winds~100kts
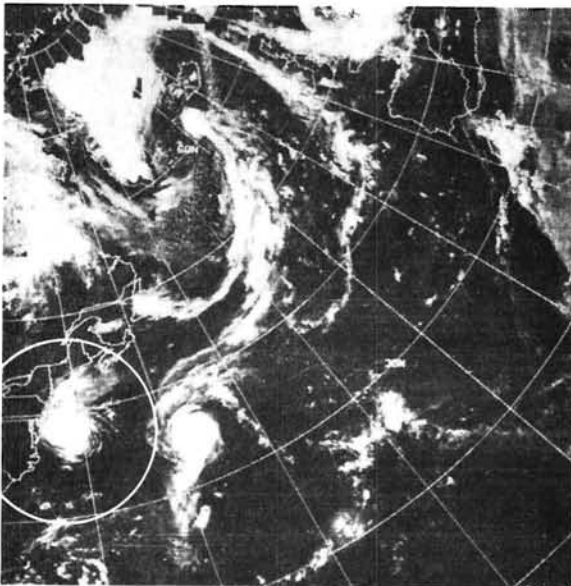
Hurricane Doria (38°N,72°W)
15 Sept 1967
Central Pressure ~973mb
Maximum Winds ~114kts
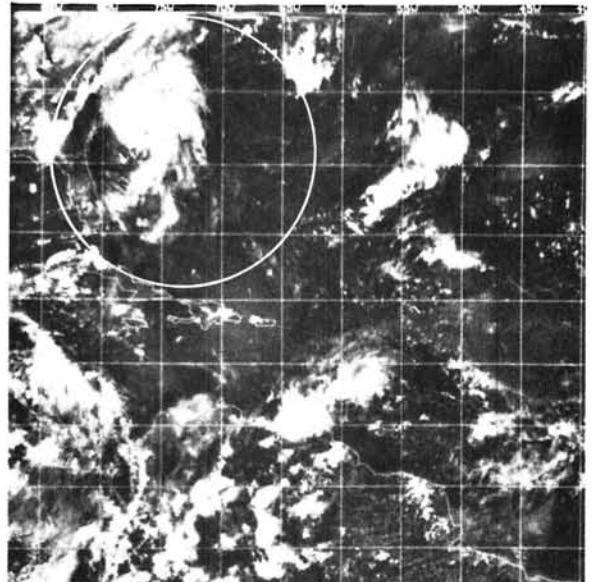
Hurricane Gerda (34°N,76°W)
8 Sept 1969
Central Pressure ~980mb
Maximum Winds ~80kts

Fig. 2-2. NOAA satellite pictures of typical hurricane and typhoon
cloud clusters.
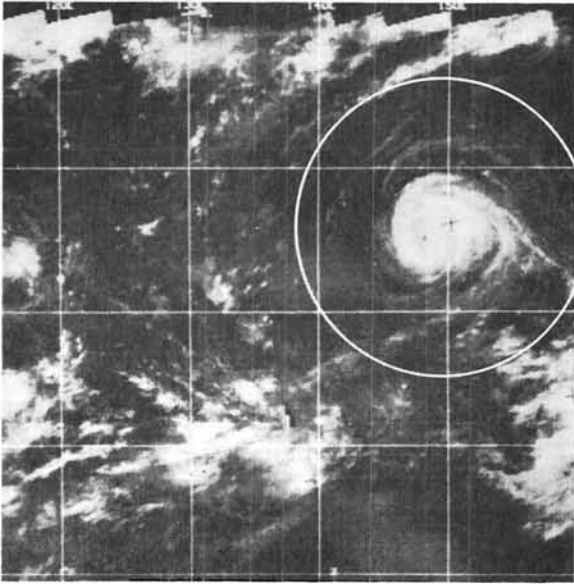
Typhoon Opal (22°N, 152°E)
5 September 1967
Central Pressure ~961mb
Maximum Winds ~115kts
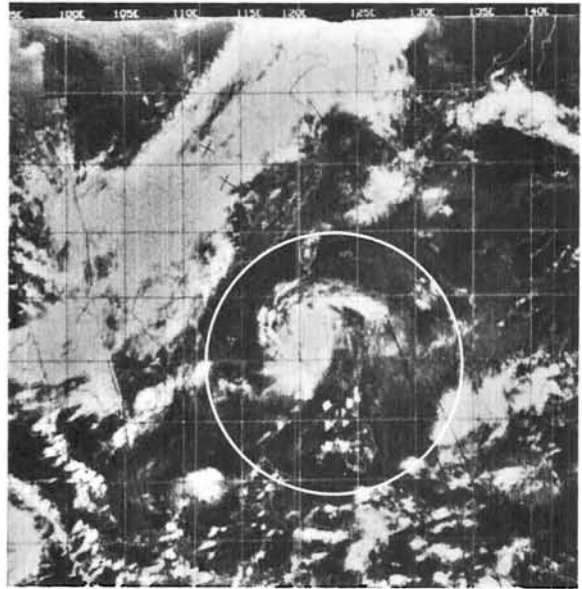
Typhoon Georgia (16°N,122°E)
10 Sept 1970
Central Pressure ~925mb
Maximum Winds ~130kts
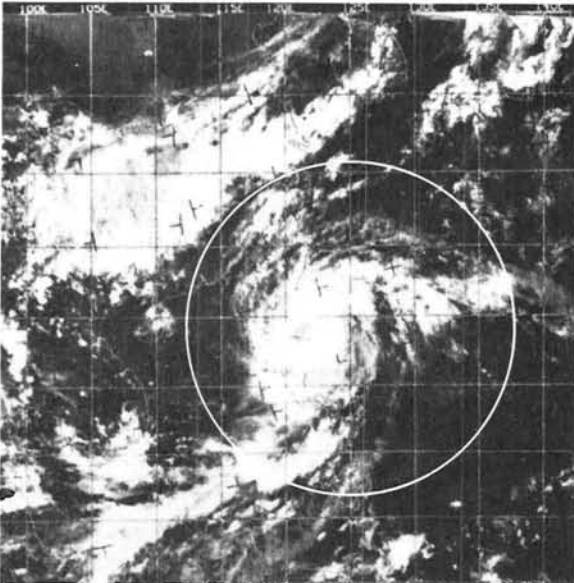
Typhoon Elaine (18°N,123°E)
27 September 1968
Central Pressure ~916mb
Maximum Winds ~145kts
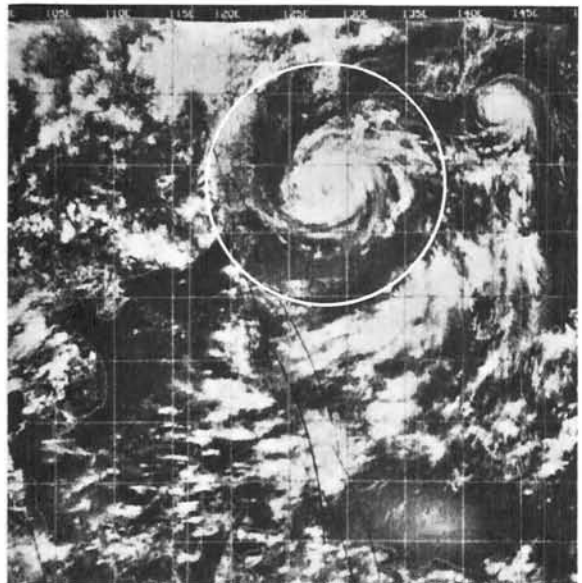
Typhoon Billie (28°N,139°E)
27 Aug 1970
Central Pressure ~945mb
Maximum Winds ~110kts

Fig. 2-2. Continued.
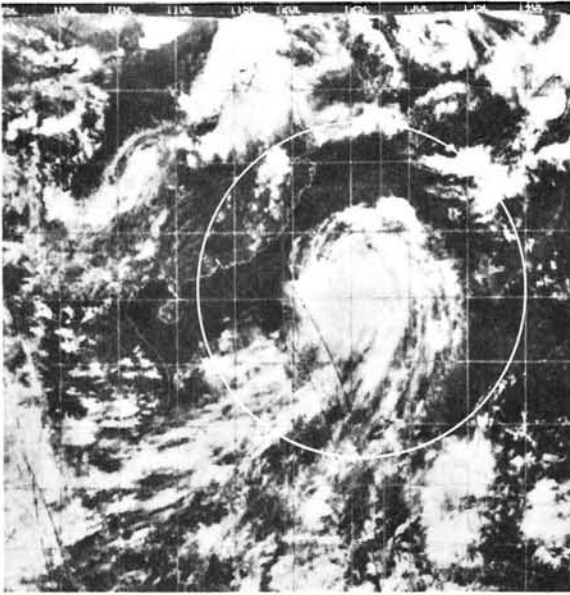
Typhoon Olga (20°N,126°E)
1 July 1970
Central Pressure ~908mb
Maximum Winds ~150kts
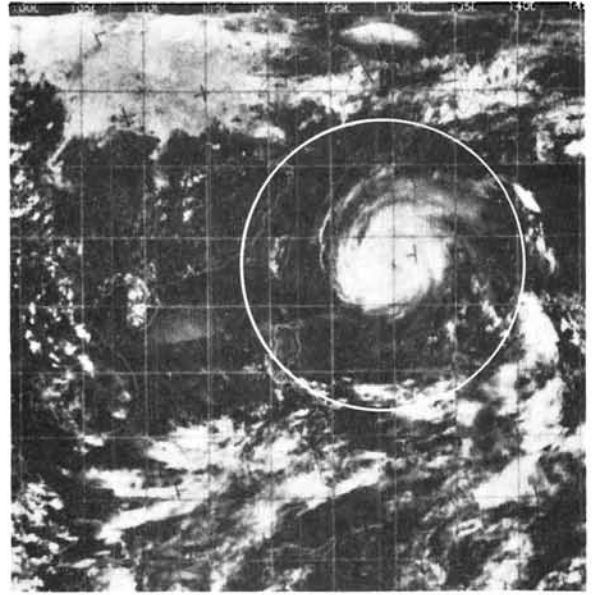
Typhoon Elsie (20°N, 138°E)
24 Sept 1969
Central Pressure ~891mb
Maximum ~145kts
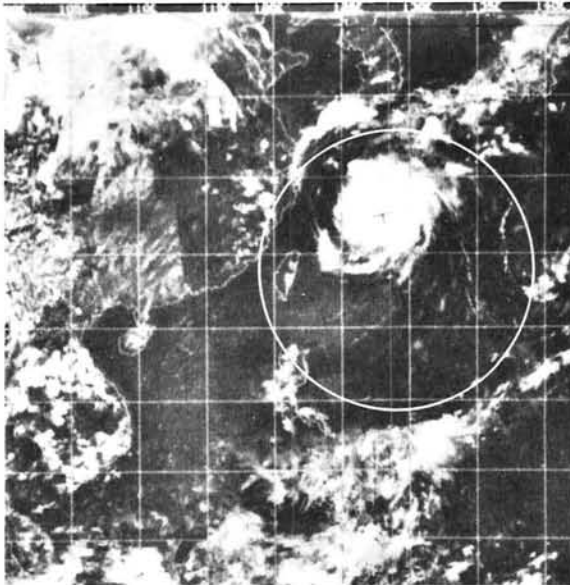
Typhoon Cora (25°N,127°E)
19 Aug 1969
Central Pressure ~935mb
Maximum Winds ~85kts
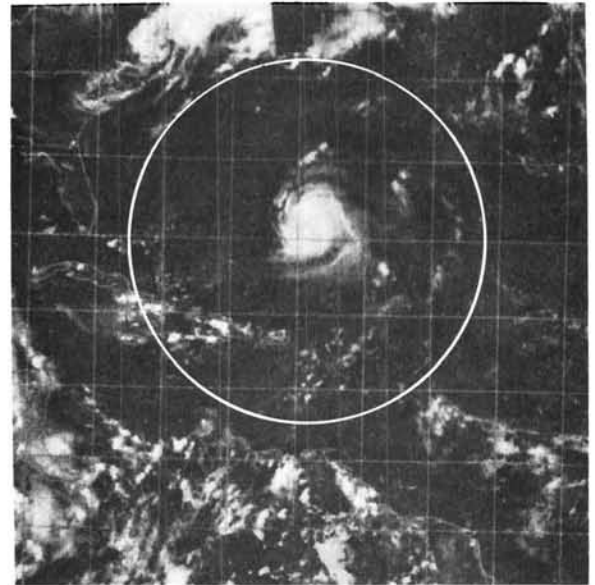
Hurricane Debbie (26°N,65°W)
20 August 1969
Central Pressure ~950mb
Maximum Winds ~110kts

Fig. 2-2. Continued.

X CAT. 1

POORLY ORGANIZED
SPIRAL BANDS

ILL-DEFINED CENTER OF
ORGANIZATION WITHIN
CENTRAL CLOUD MASS

X CAT. 2

WELL ORGANIZED BANDS

SPIRAL BANDS DEFINE
CENTER WITHIN CENTRAL
CLOUD MASS

X CAT. 3

MODERATE DEGREE OF
CONCENTRICITY TO
CLOUD BANDS

IRREGULARLY SHAPED EYE
WITHIN CENTRAL CLOUD
MASS

X CAT. 4

HIGH DEGREE OF
CONCENTRICITY TO
CLOUD BANDS

ROUND EYE NEAR CENTER
OF CENTRAL CLOUD MASS

OBSERVED MAXIMUM WIND (smoothed kt)

CATEGORY 4

CATEGORY 3

CATEGORY 2

CATEGORY 1

DIA. (units in deg. lat.=60 n. mi.)
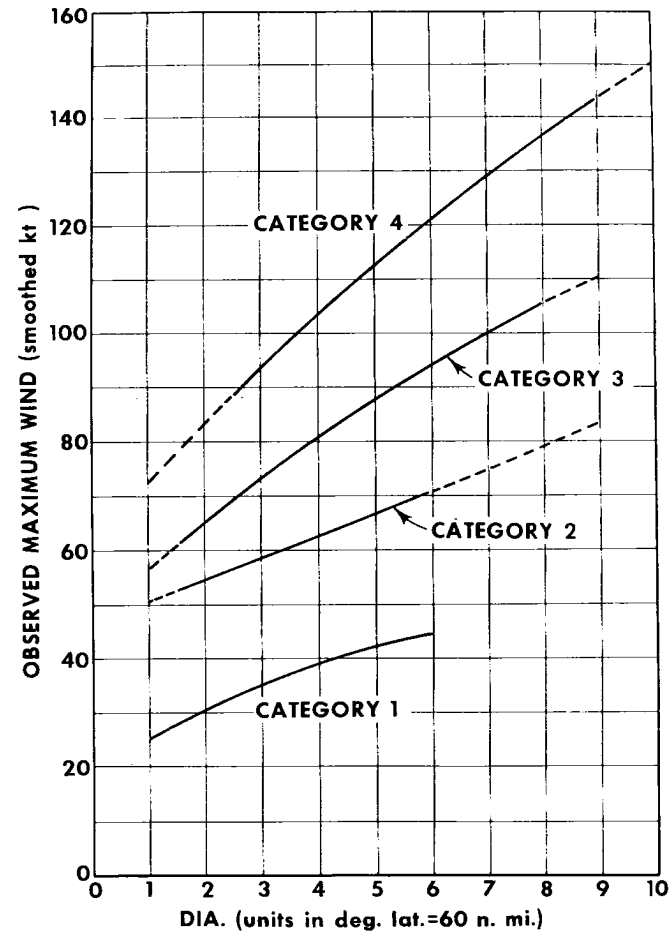
Fig. 2-3. National Satellite Laboratory determined relationship between hurricane maturity and satellite picture appearance at left, and diameter of hurricane cluster vs. maximum observed surface winds at right (from Fritz, Hubert and Timchalk, 1966).

12
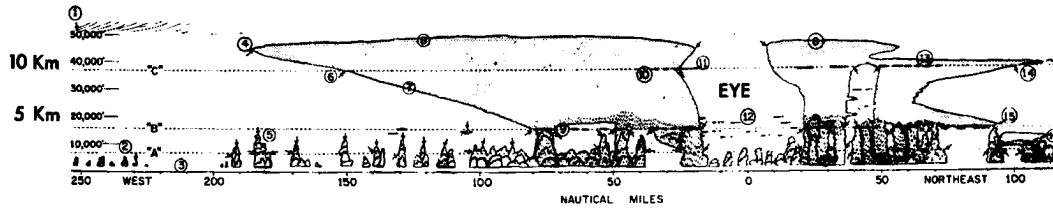
Fig. 2-4. Radial cross-section of cloudiness surrounding Hurricane Cleo on 18 Aug 1958 as the storm was moving rapidly north-ward in the Central Atlantic at 33°N latitude (from LaSeur and Hawkins, 1963).

cross-section of clouds surrounding a typical moderate intensity hurricane. Cloudiness extends out to 100-200 miles from the storm center.

Figs. 2-5 to 2-7 (from Rosenthal, 1971a) portray radial cross-sections of our best estimates of the typical tangential, radial, and vertical wind components extending out to 4° latitude from the center of the average intensity hurricane. Note the strong low level inflow that increases towards the storm center. This inflow is a fundamental feature of the inner storm region. Because of its large momentum loss to the ocean surface, the hurricane is continually running itself down. The low level kinetic energy and angular momentum losses must be continually replaced by inward transport of these quantities from larger radii. This inward mass transport, although weaker, is also present up to the middle tropospheric levels.

Fig. 2-8 is a portrayal of the mean radial wind distribution through the troposphere in two degree radial segments. This is believed to be
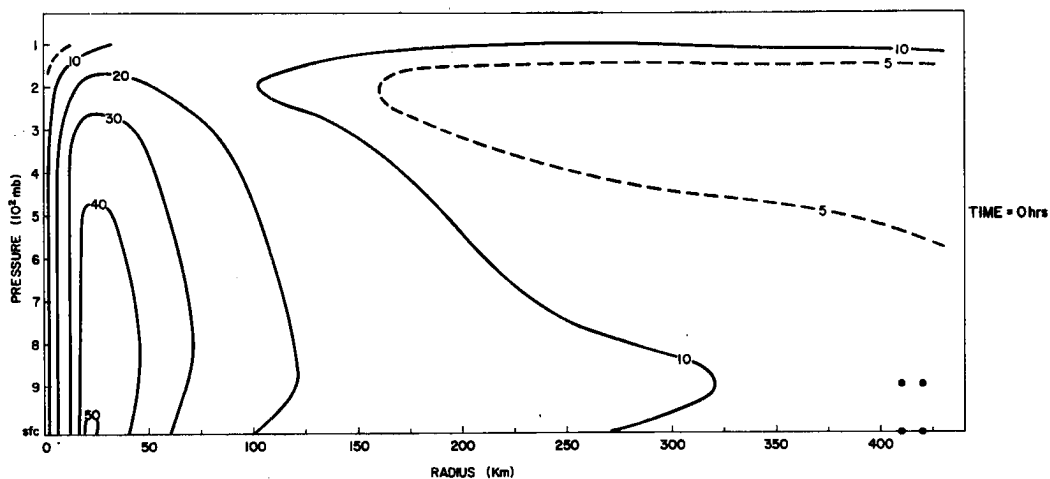
Fig. 2-5. Radial cross-section of typical hurricane total wind velocity in m/sec (from Rosenthal's 1971a storm model).
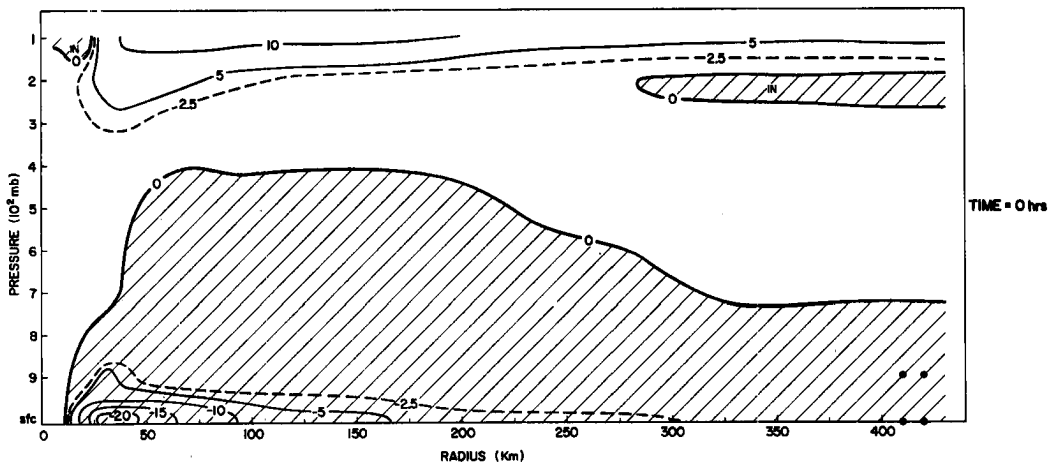
Fig. 2-6. Radial cross-section of typical hurricane radial wind velocity in m/sec (from Rosenthal's 1971a storm model). Minus values indicate inflow.
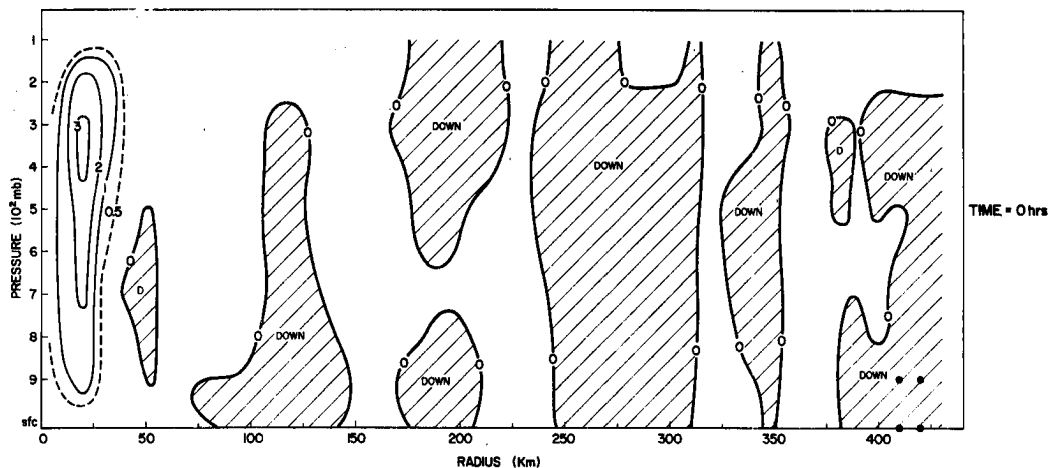
Fig. 2-7. Radial cross-section of typical hurricane vertical motion pattern in m/sec (from Rosenthal's 1971a storm model).
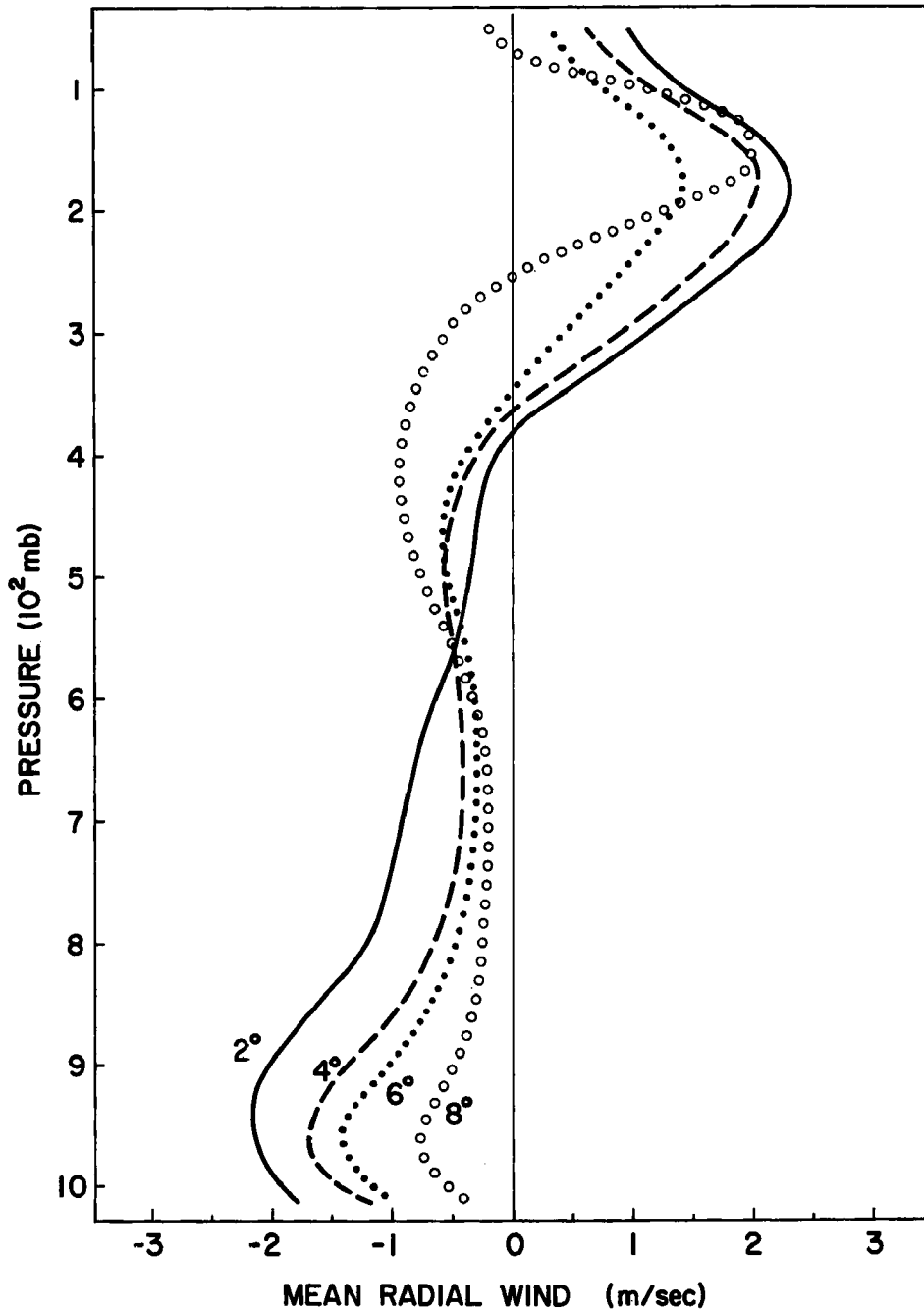
Fig. 2-8. Composite picture of observed tropospheric radial wind profiles at various latitude radii surrounding typhoons in the Western North Pacific as determined on the author's research project. Over 50 typhoons and over one thousand rawinsonde reports are involved in the data composite.

CLOUD RADAR COMPOSITE
From B-47 Flight into
Hurricane DAISY
Altitude 35,000 ft. (237 mb)
25 Aug. 1958
1800-2300 GCT

■ Intense Radar Echoes
☐ Radar Echoes of lesser intensity
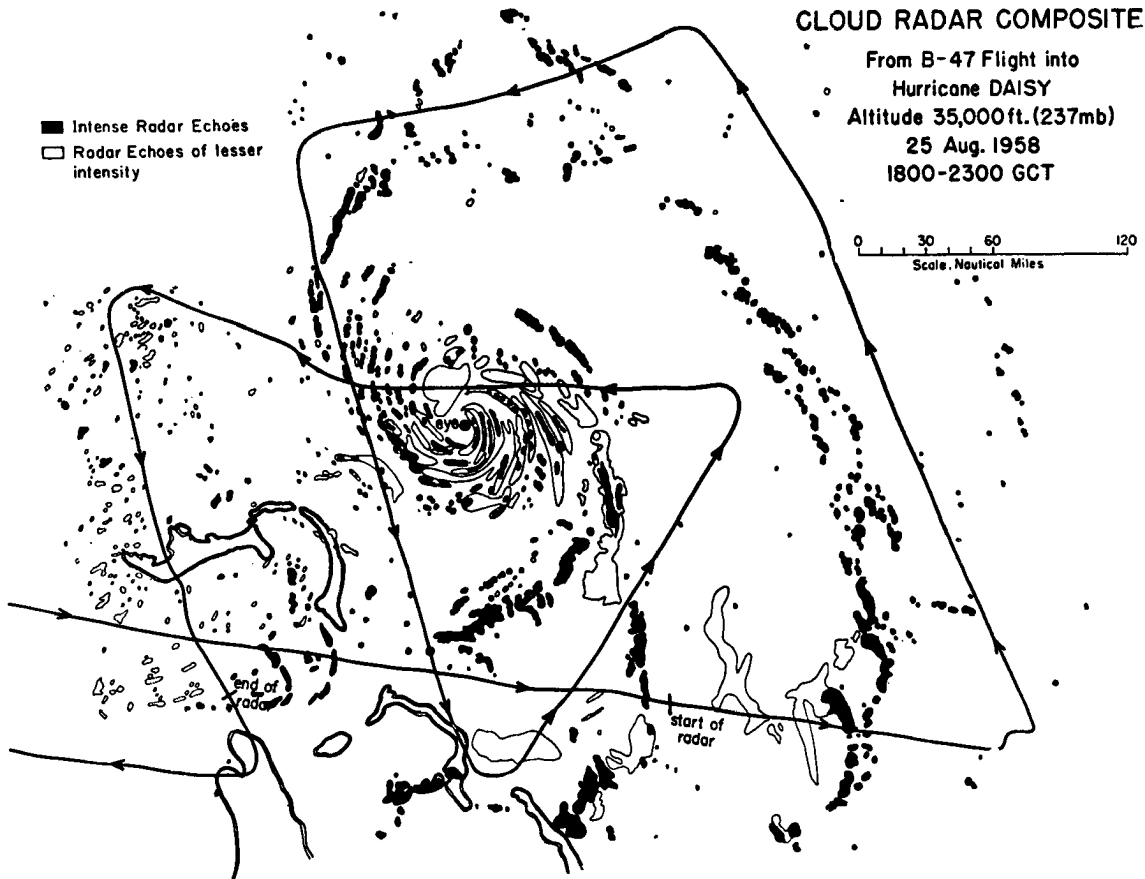
Fig. 2-9. Radar composite surrounding hurricane Daisy on 25 Aug. 1958 when it was located off the Florida coast.

typical of most hurricanes and typhoons. The information for this figure was obtained from compositing typhoon cloud clusters with respect to their surrounding rawinsonde data in the Western Pacific. Note that the inflow is concentrated in the surface layers, but smaller magnitude inflow still exists up to the 400 to 500 mb level. Outflow is concentrated at 150-200 mbs. The middle tropospheric and boundary layer inflows are not independent of each other. The role of the middle level inflow is to feed cumulus up-and-downdrafts (Gray, 1972b) which are initiated by the low level convergence.

Fig. 2-9 portrays a radar composite of hurricane Daisy on 25
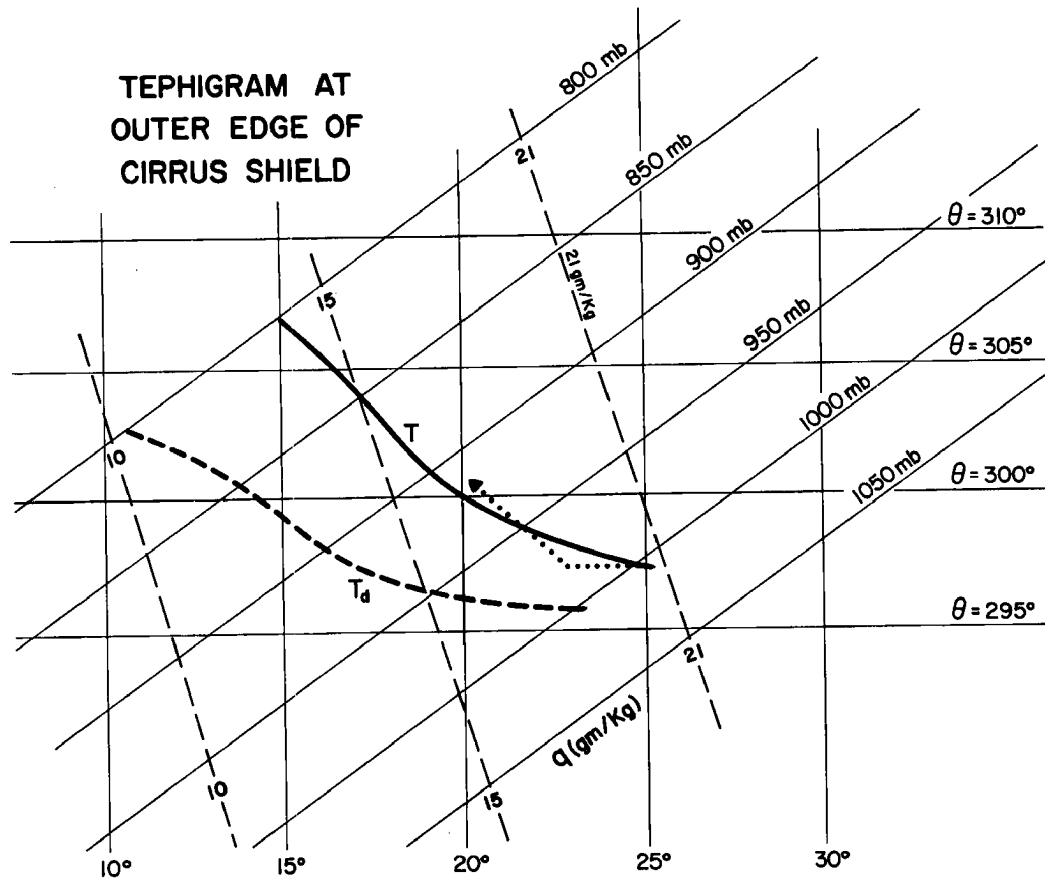
Fig. 2-10. Tephigram portrayal of typical temperature (T) and dew point (T_d) surrounding the edge of the typhoon's outer cirrus shield. The dotted curve shows the general lack of buoyancy of a parcel ascent curve from the surface in this region.

August 1958. This is typical of the type of convective cloud lines or feeder bands that exist around these storms. Although much of the inflowing air goes up in outer rain or squall bands before it reaches the storm's convective center, a large amount of the inflowing mass proceeds into the central eye-wall region. Note the general lack of radar echoes between 100 and 300 km radius.

Buoyancy at Outer Radii. It is difficult for the low level inflowing air at large radii to go up in outer rain bands because the convective

instability in the inflow layer is typically not very large. Fig. 2-10 shows a typical sounding (as determined by Bell and Tsui, 1972) of the temperature and dew points near the outer cirrus shields of typhoons. The dotted curve shows parcel ascent from the surface. Note that the surface air temperature averages only about 25 1/2^{O}C and that parcel ascent from the surface has little thermal buoyancy.[2] This boundary layer inflowing air can go up in outer rain bands only if it is acted upon by a substantial dynamic forcing. Thus, thermal buoyancy arguments dictate that for the usual hurricane or typhoon a significant portion of the low level inflowing air must penetrate into the convective eye-wall region. A sizable fraction of this low level inflowing air might have gone up in outer radius cloud bands if the outer region convective instability had been higher.

Inner Hurricane Wind Structure. A recent report by Shea (1972) has extensively discussed the inner core hurricane wind structure through analysis of 533 NOAA National Hurricane Research Laboratory (NHRL) radial flights in and out of hurricanes during the period of 1957-1967. Although most of these flights were above the boundary layer, over 60 low level missions were made between levels of 965 and 860 mb. Fig. 2-11 portrays the tangential and radial winds as measured by the Doppler wind equipment relative to the radius of maximum

---

[2]Daytime soundings from atolls give temperature values of 26.8^{O}C but nightime readings are only 25.5^{O}C. The nightime readings are believed to be typical of conditions surrounding hurricanes and typhoons over the open ocean.
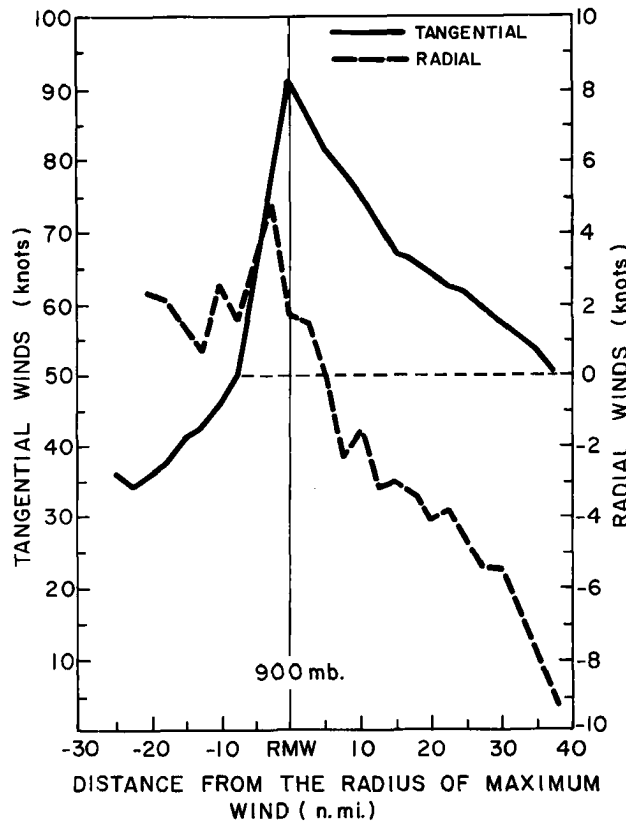
Fig. 2-11. Mean tangential and radial wind profiles averaged with
respect to the radius of maximum wind for all the avail-
able NOAA NHRL hurricane flight data between levels of
965 and 860 mb. Negative radial winds indicate inflow.
This figure shows the distinct inflow which takes place in
the upper boundary layer beyond the radius of maximum
winds (from Shea, 1972).

wind (RMW) at these lower levels. This is the best boundary layer

wind information available at inner hurricane radii. Note that the ra-

dial wind (dashed line, negative inward) penetrates to the radius of

maximum winds before it stops.

Large Variability of Hurricane Inner Core Wind Structure. If the

hurricane's destructive potential is related to its maximum sustained

surface winds, then the destruction potential cannot be specified by the

degree of outer circulation alone or by storm central pressure.
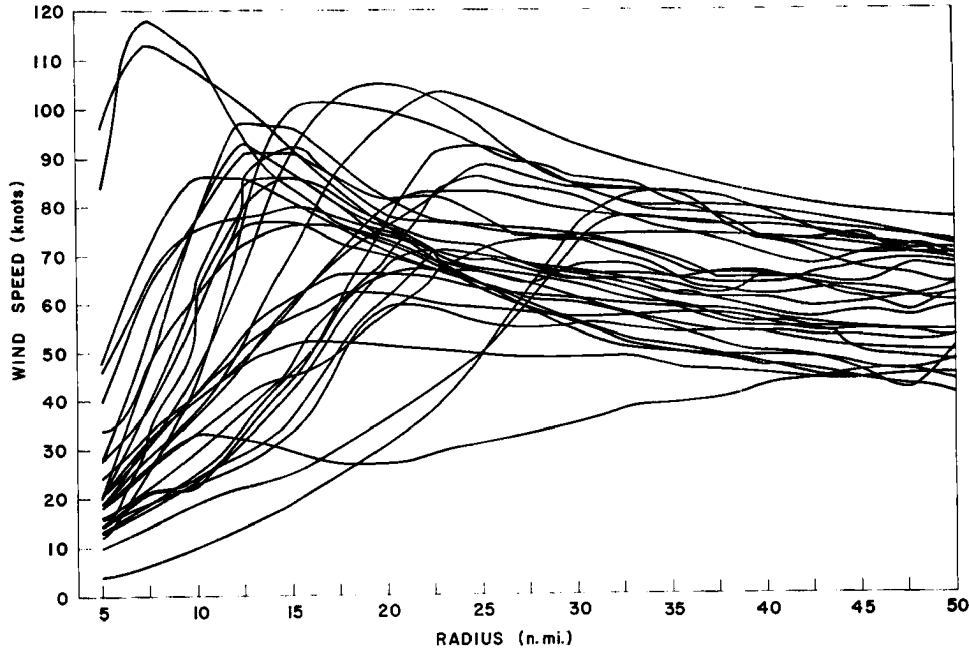
Fig. 2-12. A typical sample of the radial profiles of wind velocity as measured by the NOAA, NHRL. In general, the smaller the radius of maximum winds the higher the wind speed.

Hurricanes have variable relationships between their maximum winds, their radius of maximum winds, and their central pressures. Fig. 2-12 shows the typical variation of hurricane tangential wind profiles as measured by the NHRL aircraft. Note that some storms have their maximum winds at 30 and 40 nautical miles (n. mi.) from the storm center, whereas others have their maximum winds at only five to ten n. mi. radius. Assuming a similar outer storm circulation, the major determinant of a hurricane's inner core maximum winds is given by the radius to which the boundary layer air penetrates to the center. This figure shows that the radius of inward penetration varies a great deal between storms. As seen in Fig. 2-13, surface pressure is not a major determinant of hurricane maximum wind speed. Although a
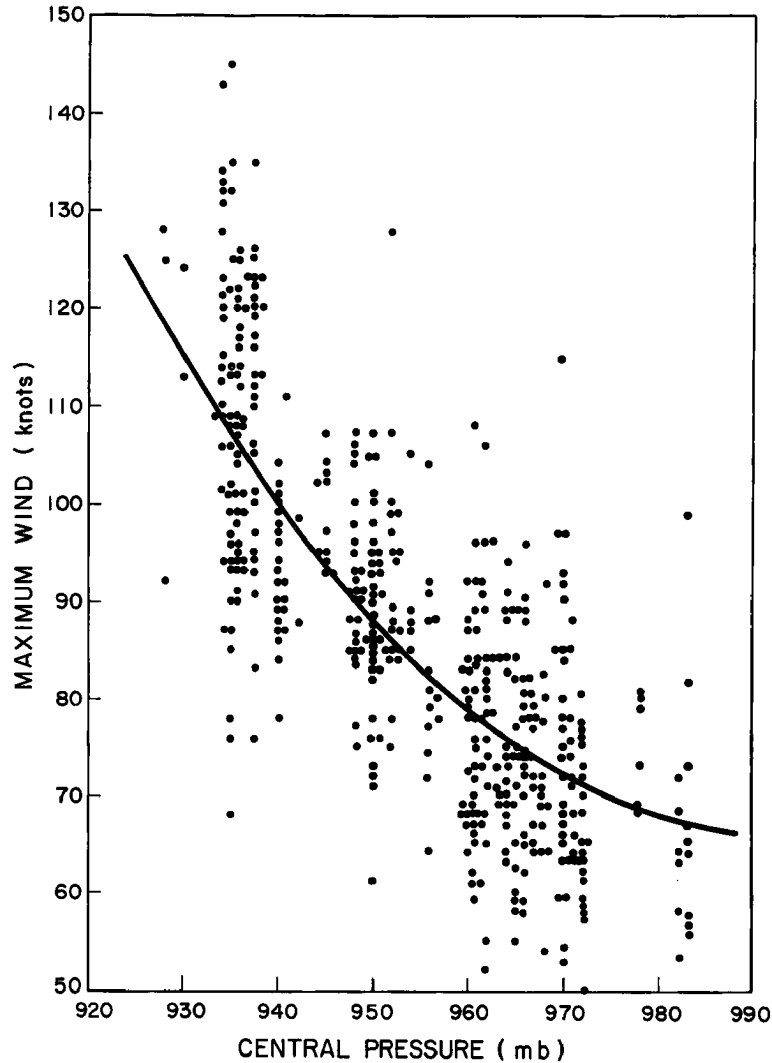
Fig. 2-13. Variation of the maximum wind with central pressure for all available lower tropospheric NHRL data. The curve of best fit is indicated by the heavy line (from Shea, 1972). Note the large spread of values.

statistical relationship of stronger winds with lower central pressure exists, there is a very large variation of maximum wind speed with hurricane central pressure. Large variations of maximum sustained surface winds are possible with similar hurricane central pressures.

Fig. 2-14 shows that the eye-wall cloud radius and the radius of maximum winds are very closely related, however. The inner eye-wall
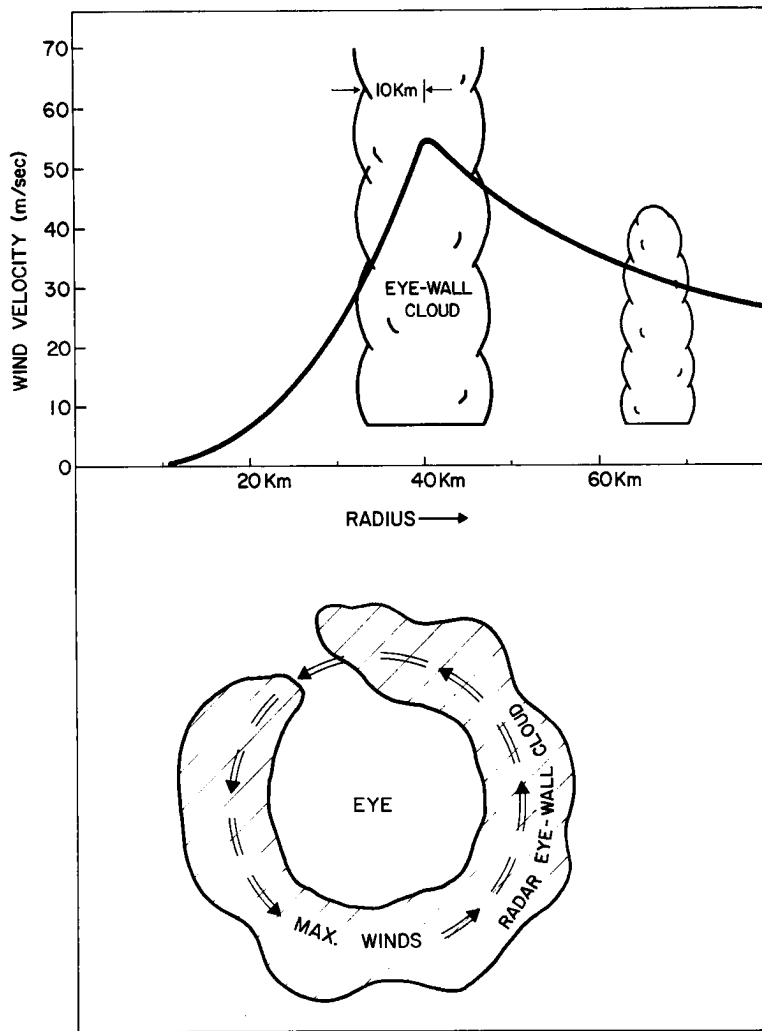
Fig. 2-14. Cross-section (top) and plan view (bottom) showing the typical location of the radius of maximum winds with respect to the eye-wall convective cloud. The inner eye-wall radius is typically 10 km inside of the radius of maximum winds (see Shea, 1972 for more discussion).

cloud radius is typically about 10 km inside the radius of maximum

winds. Given the same outer storm circulation, differences in maxi-

mum wind speed are primarily related to the radius of establishment

of the eye-wall cloud. The further inward the boundary layer air

penetrates, the closer in will be the eye-wall cloud and the stronger the surface winds.

Conclusion. Hurricane-typhoon maintenance is dependent upon a continuous frictionally forced low level mass convergence. The maximum velocity of the storm's surface winds is highly variable and (given a similar intensity outer circulation) is primarily dependent upon the distance to which the low level mass can penetrate into the center. This radius of inward penetration typically varies from 10 to 100 km. Beyond the radius of maximum winds the thermal buoyancy is small. This lack of strong buoyancy may explain why so much of the inflowing air typically penetrates to inner radii. The amount of inward mass penetration might be less if the outer radius (100-400 km) thermal buoyancy were larger.

3. BOUNDARY LAYER INFLOW RELATED TO HURRICANE INTENSITY

The radius to which the hurricane boundary layer inflow air penetrates into the storm center is related to the surrounding thermal buoyancy, and to the low level frictional veering angle (see discussion by author in paper by Shea, 1972, p. 111-116). Fig. 3-1 shows a frequency distribution from NHRL research flight data of the occurrence of maximum wind velocities at various radial intervals. Although a wide spread is present, the inverse statistical relationship of maximum wind velocity with Radius of Maximum Wind (RMW) is clearly evident.

Hurricane angular momentum and kinetic energy budget considerations as discussed by Riehl (1963), Palmén and Riehl (1957), Malkus and Riehl (1960), Gentry, Hawkins and Rosenthal (1970 Stormfury Report) and others dictate that the hurricane's maximum wind speeds will be related to the magnitude and distance of the low level inward mass penetration. This has also been verified by the symmetrical hurricane models of Ooyama (1969) and Rosenthal (1970b, 1971a, 1971b).

Angular Momentum Consideration. The absolute angular momentum (M_a) of a parcel when expressed in a cylindrical coordinate system

24
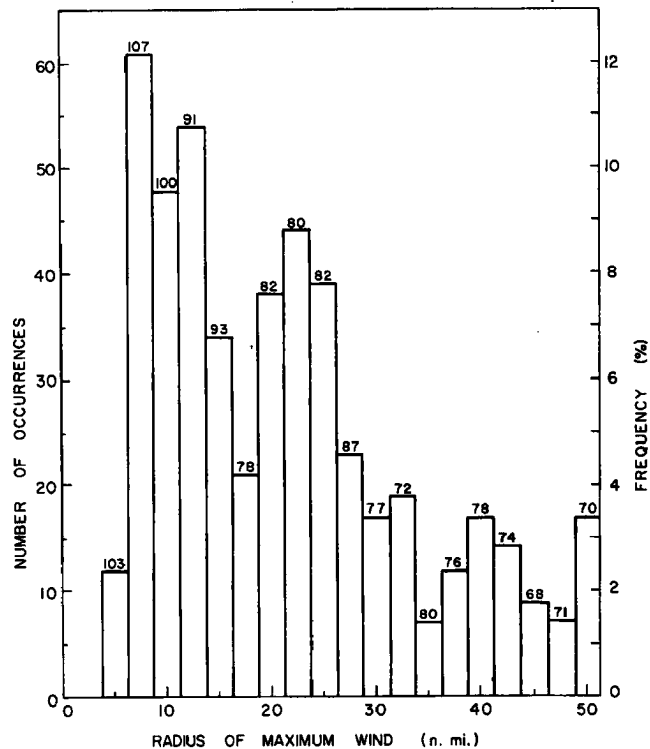
Fig. 3-1. Frequency distribution of the occurrence of hurricane maximum wind at various radii. The mean maximum wind (in kts) at each radii is indicated at the top of the radial band. Note again that the strongest winds are associated with conditions of maximum winds at small radius (from Shea, 1972).

with the origin at the hurricane center is given by,

$$M_a = ur + \frac{fr^2}{2} \qquad (1)$$

where r = the radial distance from the center of the vortex,
       u = the tangential wind velocity, and
       f = Coriolis parameter

A mean cross section of absolute angular momentum relative to the radius of maximum wind is shown in Fig. 3-2. Note how the absolute angular momentum decreases towards the storm center. This decrease is due to exchange of momentum between the air and the ocean.
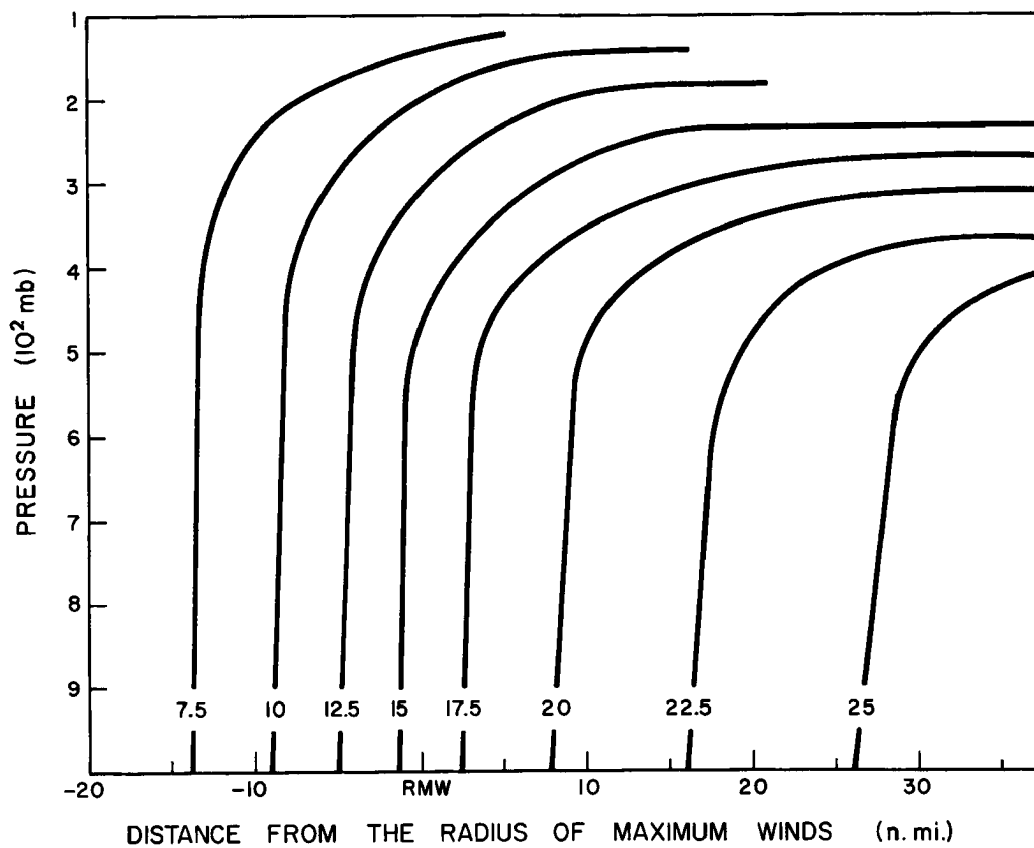
Fig. 3-2. Mean hurricane cross-section of absolute angular momen-
tum in units of $10^9 \, cm^2/sec$ relative to the Radius of Max-
imum Winds (RMW) as determined by Shea (1972) from
the NHRL aircraft data.

It shows that a hurricane represents a strong sink region of angular

momentum. At the upper outflow levels the lines of constant angular

momentum become more nearly horizontal. This is as it should be,

for no upper tropospheric momentum sinks are present.

Slope of Tangential Wind Profiles. Riehl (1954, 1963) and Hughes

(1952) have noted that hurricane radial profiles of tangential wind can

be approximated by an equation of the form,

$$ur^x = \text{constant} \tag{2}$$

where u = is the tangential wind
r = is radius from the storm center
x = is the exponent

Inside the Radius of Maximum Winds (RMW), x = -1 (solid rotation) is closely valid in an average of many storms. Outside the RMW, x = 0.5 has been shown by Riehl to give a good fit. Shea (1972) has recently assessed mean values of x inside and outside of the RMW for 492 lower tropospheric (500-900 mb) radial leg flight missions of the National Hurricane Research Laboratory and found results as shown in Table 3-1 . x inside = -1 and x outside = 0.5 are indeed very good approximations. When considering mean vortex data consisting of averages of 4-6 radial flight legs the standard deviation of $\pm$ 0.3 displayed by the individual radial legs is considerably reduced. Fig. 3-3 shows the variations of measured increase of mean vortex tangential wind starting at 50 n. mi. radius in comparison with the empirical $ur^{0.5}$ profile. Note that the scatter of these points is much reduced from that of Fig. 2-13 dealing with central pressure vs. maximum wind velocity.

Maximum wind velocity is related to only two basic parameters, 1) the wind velocity at outer radius and 2) the radius of maximum wind. Man's primary hope for beneficial modification must come from attempts to change one of these features. This could be accomplished if it were possible to artificially reduce the intensity of the storm's outlying boundary layer inflow.

Radial Distribution of Dynamic Parameters. Fig. 3-4 portrays the inward radial increase of wind velocity from boundary layer inflow

Table 3-1

Value of x exponent inside and outside the RMW from individual radial leg data.

Levels (mb)	Mean Exponent Inside RMW and Standard Deviation	Mean Exponent Outside RMW and Standard Deviation
900 to 500	$-1.05\,(\pm\,0.6)$	$0.47\,(\pm\,0.3)$
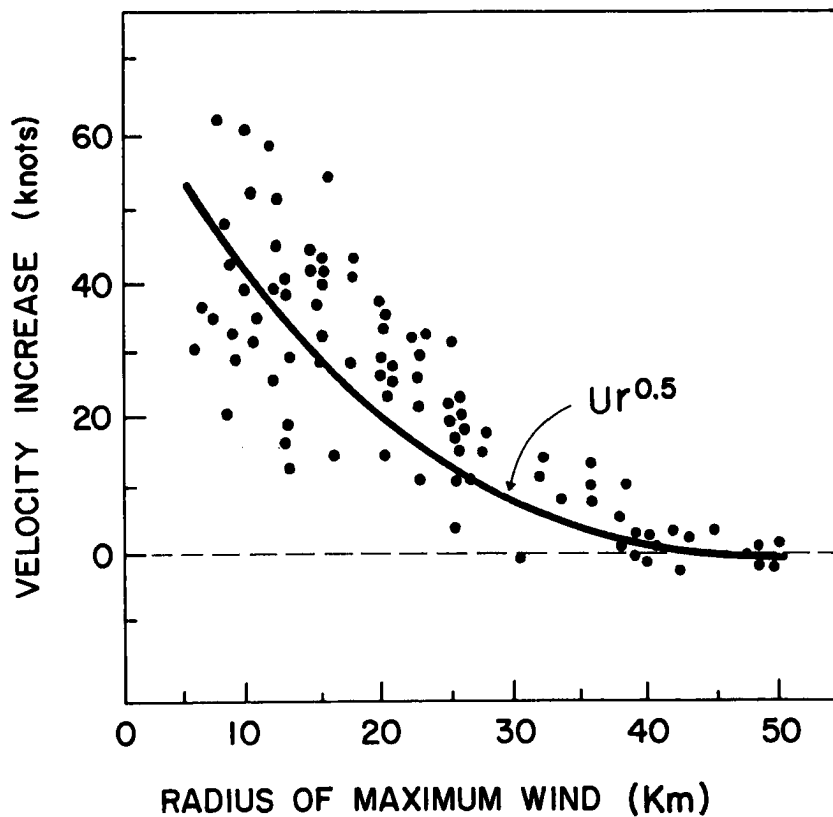
Fig. 3-3. Scatter diagram showing the variation of the radius of maximum winds vs. the wind velocity difference between this radius and the velocity of the wind at 50 n. mi. radius. The solid line shows the $ur^{0.5}$ curve of inward wind increase from 50 n. mi. radius. Information is from mean vortex NHRL flight data as analyzed by the author.
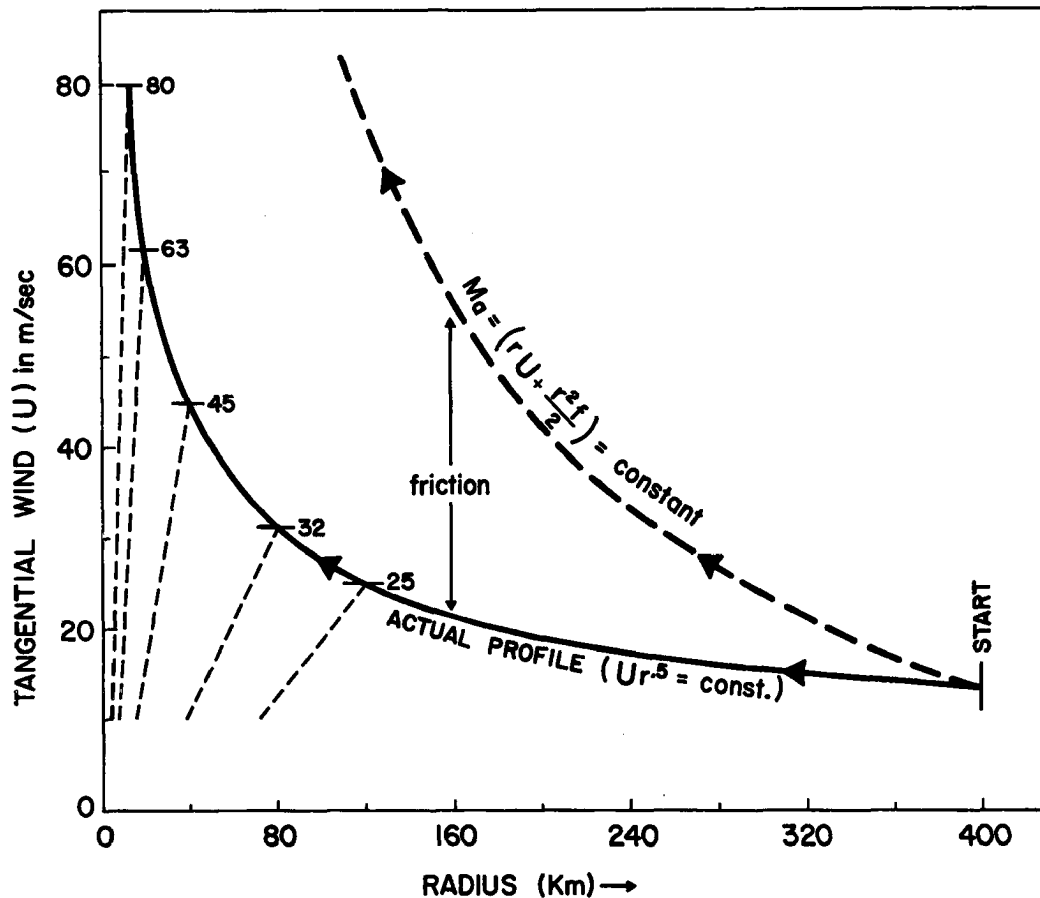
Fig. 3-4. Hurricane tangential wind profiles. Portrayal of increase
of tangential wind with inward penetration of boundary layer
air parcels assuming constant absolute angular momentum,
M_a, (top curve), and usual storm case where surface fric-
tion plays a large role (lower curve). The difference in
these curves is due to momentum transfer to the ocean.
Note how the maximum wind speeds are strongly related to
the distance of inward penetration of the boundary layer
air towards the storm center.

starting with a velocity of 15 m/sec at 400 km radius. A parcel con-

serving its angular momentum follows the top curve. The lower curve

represents the increase of wind in the real storm. The difference in

the two curves is due to the transfer of angular momentum to the ocean.

The tropical cyclone is the most inefficient of atmospheric systems.

It has its maximum winds in the lowest levels where contact with the
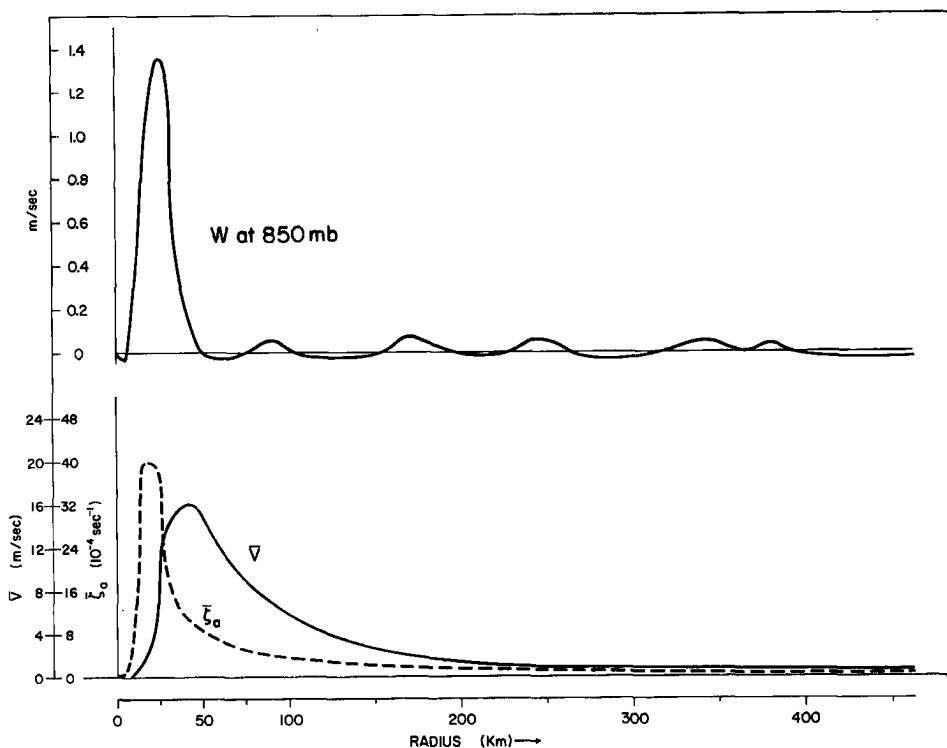
Fig. 3-5. Typical radial distribution of vertical motion (w) at 850 mb, and mean boundary layer radial wind velocity ($\bar{v}$) and absolute vorticity ($\bar{\zeta}_a$) in the typical hurricane or typhoon.

earth's surface creates large dissipation. Note how the wind velocities are dependent on the degree of inward radial penetration of boundary layer air. Parcels penetrating to a radius of 40 km will have velocities of 45 m/sec. Those penetrating to radii of 20 and 10 kilometers will have velocities of 63 and 80 m/sec respectively, etc.

Fig. 3-5 shows the typical distribution of vertical wind at 850 mb and the mean boundary layer radial profile of radial wind ($\bar{v}$) and absolute vorticity ($\bar{\zeta}_a$). Note the concentration of each parameter in the inner storm area, especially the vorticity.

Steady State Tangential Equation of Motion for Hurricane. An

examination will now be made of the terms in the symmetrical, steady-

state, cylindrical, tangential equation of motion with origin at the

hurricane center. This equation may be written as[3] (see footnote be-

low for derivation and symbols):

$$0 = -v\zeta_a - \omega \frac{\partial u}{\partial p} + F_\theta \tag{3}$$

Fig. 3-6 from Gray (1967) shows the typical inner core radial and ver-

tical average of the three terms of eq. (3) for conditions of an average

hurricane vortex with superimposed cumulus convection. The relative

magnitudes of these terms should also be about the same at larger

radii. A sizable magnitude of F_θ (due to cumulus induced vertical

momentum transfers) must prevail through the middle and upper tro-

posphere in order that acceleration balance prevail. The very small

---

[3] Neglecting small effects of the earth's curvature the tangential
cylindrical equation of motion can be written as:

$$\frac{du}{dt} + \frac{uv}{r} + fv = -\frac{1}{\rho r} \frac{\partial p}{\partial \theta} + F_\theta \quad .$$

where u, v, are the tangential and radial wind velocities, r is the ra-
dius, f the Coriolis parameter, ρ is density, p is pressure and F_θ
represents tangential friction. Expanding, we obtain:

$$\frac{\partial u}{\partial t} + \frac{u}{r} \frac{\partial u}{\partial \theta} + v \frac{\partial u}{\partial r} + \omega \frac{\partial u}{\partial p} + \frac{uv}{r} + fv = -\frac{1}{\rho r} \frac{\partial p}{\partial \theta} + F_\theta \quad .$$

where ω is vertical motion in mb per time unit. With steady-state
and symmetrical assumptions, terms $\frac{\partial u}{\partial t}$, $\frac{u}{r} \frac{\partial u}{\partial \theta}$, $\frac{1}{r\rho} \frac{\partial p}{\partial \theta}$ drop out.
Combining the terms with the coefficient v we obtain equation (3) with

$$\zeta_a(\text{absolute vorticity}) = (\frac{u}{r} + \frac{\partial u}{\partial r} + f) \quad .$$
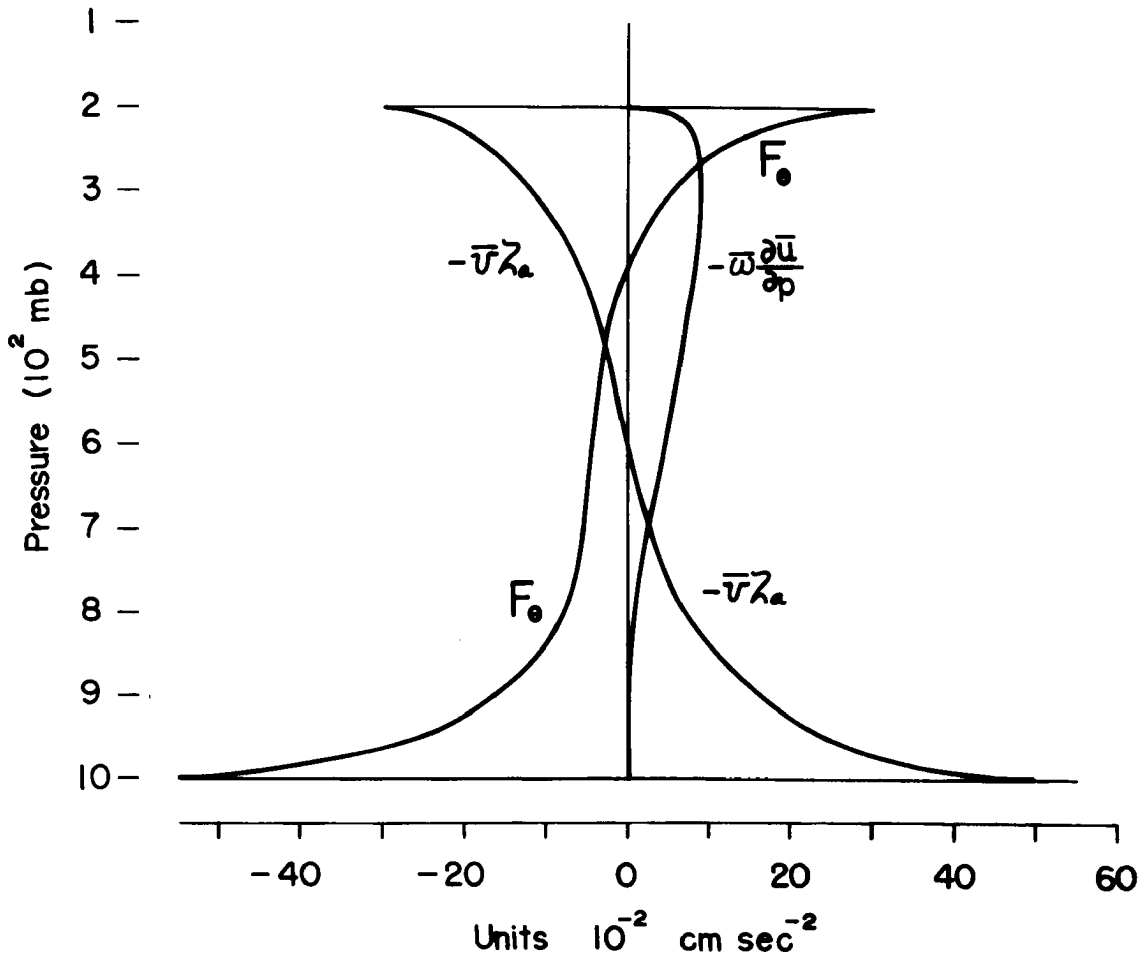
Fig. 3-6. Typical tropospheric distribution of the magnitudes of the three terms in the steady-state tangential equation of motion (eq. 3) which have been averaged over the inner eyewall cloud area. In the boundary layer F_θ is balance by the $-v\zeta_a$ term (from Gray, 1967).

vertical gradient of tangential wind in the lower levels (see Fig. 2-5) makes the $\omega \dfrac{\partial u}{\partial p}$ term negligible. The boundary layer steady-state, symmetrical tangential equation can thus be simplified to

$$0 = -v\zeta_a + F_\theta \tag{4}$$

Here the balance of tangential acceleration is only between terms F_θ and $-v\zeta_a$. The retarding influence of tangential friction is just balanced

by low level inflow. Thus, for steady conditions the magnitude of the boundary layer inflow ($-v$) is determined by the value of F_θ / ζ_a. F_θ may be represented by $\dfrac{\partial \tau_{\theta z_0}}{\rho \partial z} \sim \dfrac{\Delta \tau_{\theta z_0}}{\rho \Delta z}$, where $\tau_{\theta z_0}$ is the surface stress, ρ is density, and Δz is the thickness of the layer over which the gradient of stress is applied. Normally the "turbulent gust" induced stress decreases to a small percentage of its surface value at ~ 1 km level. Surface stress is typically represented as

$\tau_{\theta z_0} = C_D \rho u_0^2$ where C_D is the surface drag coefficient and u_0 the wind at 10 m height. The drag coefficient has been estimated by Palmén and Riehl (1957) and Miller (1964) to be approximately 1.5 - 2.5×10^{-3} in the hurricane circulation beyond the RMW. Accepting empirical estimates of C_D and Δz and disregarding vertical variations of ρ and u, the boundary layer frictional acceleration can be represented in terms of the low level tangential wind alone, thus

$F_\theta = -k u^2$ where $k = C_D / \Delta z$.

The $ur^{0.5}$ relationship implies that the rotational component of the vorticity ($\frac{u}{r}$) is twice the magnitude of the negative shearing component ($\frac{\partial u}{\partial r}$). In this case the absolute vorticity (ζ_a) can be represented as $(\frac{u}{r} + \frac{\partial u}{\partial r} + f) = (\frac{1}{2} \frac{u}{r} + f)$.

With these substitutions for F_θ and ζ_a, the boundary layer radial wind in eq. (4) can be expressed as

$$v \approx -k \frac{u^2}{(\frac{u}{2r} + f)} \tag{5}$$

For given values of r and f the steady state mean boundary layer

radial wind ($\bar{v}$) and tangential wind ($\bar{u}$) are directly related to each

other. At radii greater than the RMW this relationship turns out to be

approximately

$$\bar{v} \approx -\bar{u} / 10 \tag{6}$$

Thus, for every m/sec change of sub-cloud layer inflow, the new

adjusted steady tangential velocity to satisfy eq. (5) must take on a

value 10 m/sec less than its previous value.

Influence of Alteration of Boundary Layer Radial Wind. Fig. 3-7

portrays model specified and observed mean sub-cloud layer (surface

to 600 m) values of radial wind and divergence plus resulting mean

vertical motion at the top of this layer. Values are given in 200 km

segments. The top drawing shows these parameters as they result

from a hurricane sub-cloud layer model assuming $\bar{u}r^{0.5}$ = constant

and $v = -\bar{u} / 10$ — with the constant determined from the lower

curve of Fig. 3-4. The bottom drawing is determined from data com-

posites surrounding typhoons as discussed in Fig. 2-8. Although the

observed divergences and vertical motions of the bottom drawing are

not very accurate their magnitude is correct.

Note the small mean divergence of $1-2 \times 10^{-6} \sec^{-1}$ and the small

mean upward vertical motion at cloud base (~ 600 m) of only 6 and 10 mb/

day ($\sim.05$ to 0.1 cm/sec) between 400-600 km radius. It would not take

a great deal of extra cumulus convection to substantially increase this

SUB-CLOUD LAYER (sfc-600m) CONDITIONS

$$
\begin{pmatrix}
\overline{U}r^{0.5} = \text{Const.} \ \& \\
\overline{U} = -\overline{u}/10 \\
\text{Model Specified}
\end{pmatrix}
$$

$-\overline{\omega}$ mb/day	↑95	↑18	↑6	↑3	
$-\overline{U}$ m/sec	←2.0	←1.5	←1.2	←1.0	
$\overline{\text{DIV.}}$ 10^{-6}sec^{-1}	-20	-3.3	-1.2	-0.6	

RADIUS
(AREA WEIGHTED)

Center 200Km   400Km   600 Km   800Km

OBSERVED	$-\overline{\omega}$ mb/day	↑(95)	↑~15	↑~10	↓~10	
	$-\overline{U}$ m/sec	←(2.0)	←1.5	←1.3	←0.6	
	$\overline{\text{DIV.}}$ 10^{-6}sec^{-1}	(-20)	~-3.0	~-2.0	~+2.0	
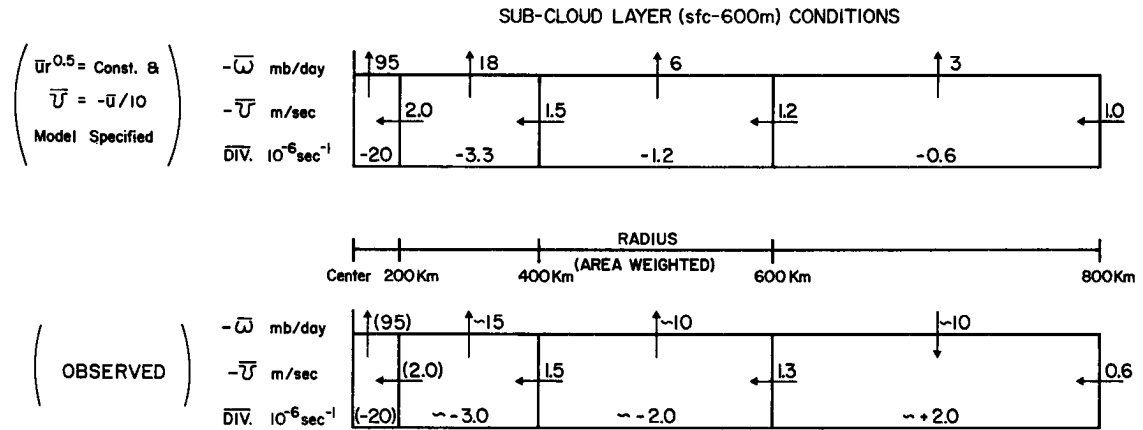
Fig. 3-7. Radial distribution in 200 km segments of mean sub-cloud layer radial wind ($\overline{v}$) and mean divergence (Div.). The resulting mean vertical motion ($\overline{\omega}$) at the top of the sub-cloud layer is also shown. The data accuracy of the bottom drawing is such that the divergence and vertical motion values shown are only accurate to about $\pm$ 50 percent. The small magnitude of these values at outer radii is to be noted.

mean vertical motion at cloud base. If this were to occur a substantial reduction in the mean sub-cloud layer inflow at radii inside of this extra cumulus convection region would occur.

Fig. 3-8 portrays the equilibrium sub-cloud layer u profiles which would result if the mean vertical motion at radii between 400 and 600 km were arbitrarily increased by 50 percent ($\sim$3 mb/day) and 100 percent ($\sim$7 mb/day) — curve C. Vertical motion changes of this amount result in an increase of boundary layer convergence of $\sim$ 0.7 and $1.5 \times 10^{-6}\text{sec}^{-1}$, respectively. These are not large convergence changes[4], yet their influence would be to reduce the 400 km radial

---

[4]The average convergence in a typical trade wind cloud cluster is about $3-5 \times 10^{-6}\text{sec}^{-1}$ (Williams, 1970).
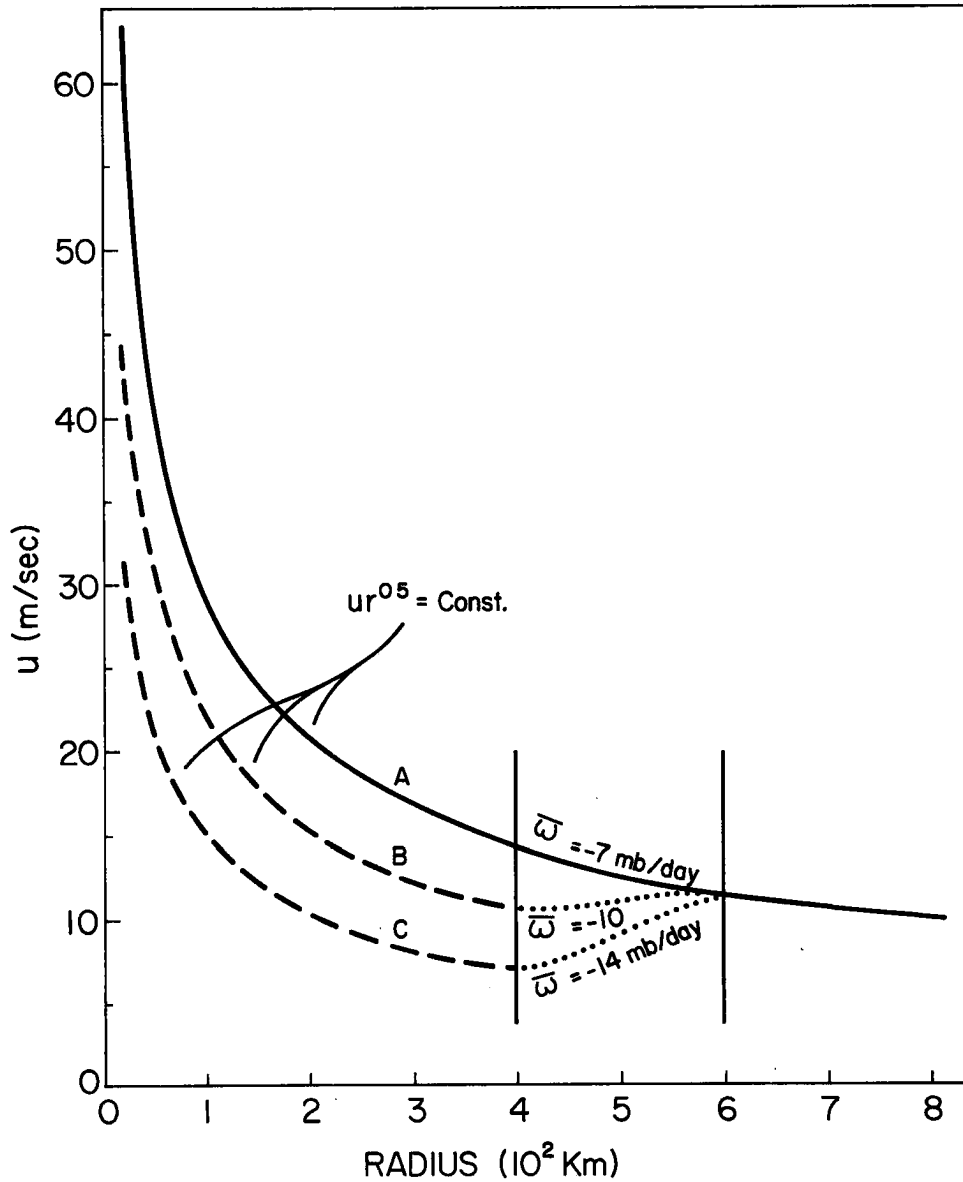
Fig. 3-8. Radial profile of equilibrium tangential wind (u) at the top
of the sub-cloud layer which is present in the normal hur-
ricane (curve A). Mean vertical motion between 400-600
km radius is - 7 mb/day. Curves B and C show the same
equilibrium u profiles which results if the mean vertical
motion between 400-600 km were increased to values of
−10 and −14 mb/day, respectively. This would lead to a
25 (curve B) and 50 (curve C) percent reduction of the sub-
cloud layer radial wind at 400 km and a consequent reduction
of the inner equilibrium wind profiles as shown.

inflow by 25 and 50 percent. For balanced acceleration in eq. (6) a consequent reduction of the tangential winds by the same percentages must also occur. For the relationship $u\, r^{0.5} = \text{constant}$ to apply at inner radii, a reduction of the tangential wind at 400 km by 25 and 50 percent requires that the radial profile of u follow curves B and C — a substantial reduction of the inner core winds from curve A. The fundamental influence to inner storm wind reduction of increasing the top of the sub-cloud layer vertical motion at outer storm radii is clearly evident.

The above discussion applies to boundary layer steady state conditions when $-v\zeta_a$ is balanced by F_θ. We will now investigate the situation when $-v\zeta_a$ and F_θ are not equal and unsteady conditions exist.

Rate of Decrease of Boundary Layer Velocity with Radial Wind Alteration. The boundary layer, symmetric, cylindrical, tangential equation of motion for the intensifying vortex may be written as:

$$\frac{\partial u}{\partial t} = -v\zeta_a - \omega\frac{\partial u}{\partial p} + F_\theta \tag{7}$$

Here again the $\omega\dfrac{\partial u}{\partial p}$ term can be neglected as very small. Eq. (7) can then be simplified to

$$\frac{\partial u}{\partial t} = -v\zeta_a + F_\theta \tag{8}$$
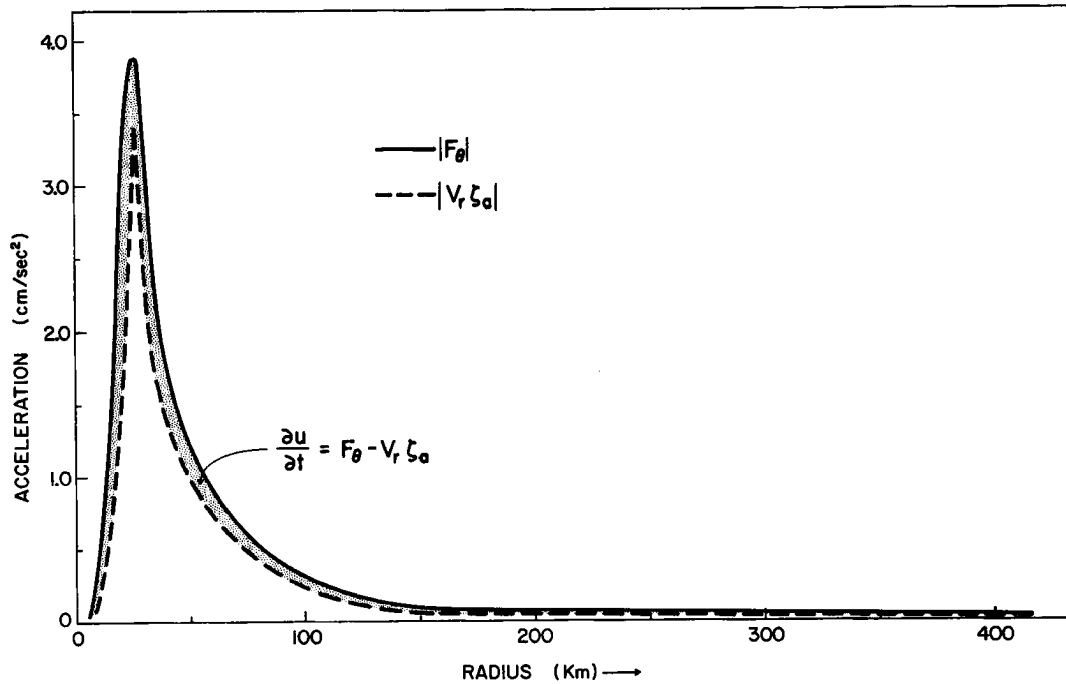
Fig. 3-9. Radial portrayal of typical values of terms F_θ and $-v\zeta_a$ and resulting $\frac{\partial u}{\partial t}$ wind deceleration (shaded area) for a ratio of $v\zeta_a / F_\theta$ of 0.9.
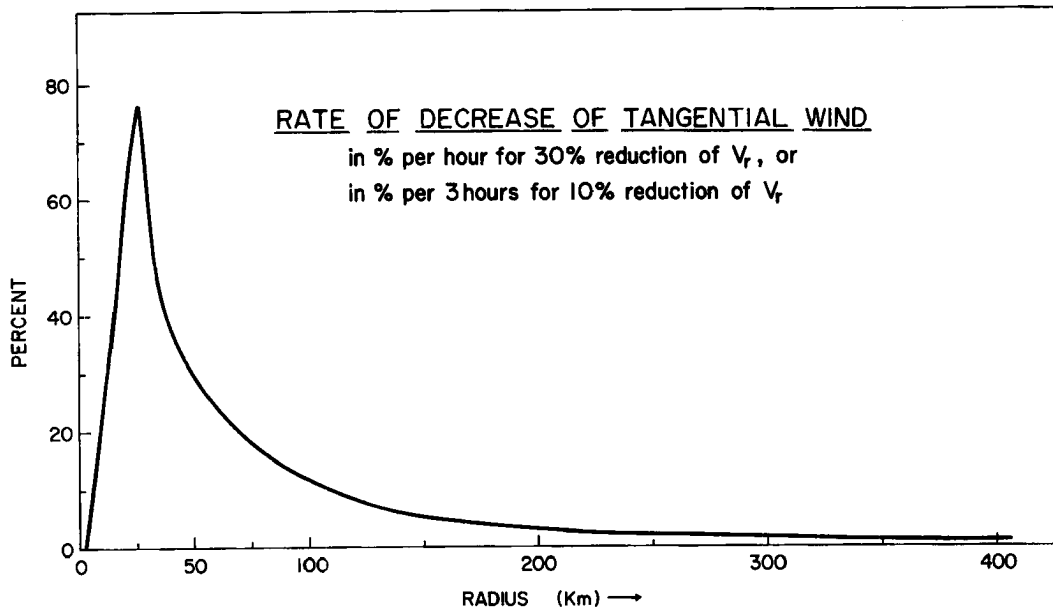
Fig. 3-10. Rate of decrease of low level tangential wind for various percentage initial impulsive reductions in low level radial inflow with all other conditions being held constant. Note how large and rapid these wind reductions are and how they are concentrated around the radius of maximum winds.

One sees immediately the tremendously powerful influence that varia-
tion of the inward radial wind has on the rate of tangential wind
changes.

Fig. 3-9 portrays the typical radial distribution of the magnitudes
of the F_θ and $-v\zeta_a$ terms and the resulting negative acceleration
which results from a $\left|v\zeta_a\right| / \left|F_\theta\right|$ ratio of 0.9. Note that the u wind
deceleration is only a small difference between these two terms but as
seen in Fig. 3-10 this small difference, if resulting from radial wind
decrease, produces very large percentage rates of change in the tan-
gential wind. Were the low level radial wind to be impulsively de-
creased by 30 percent, an initial rate of decrease of u at the RMW
would be as large as 75 percent per hour. This is an amazingly large
deceleration rate. If 10 percent of the boundary layer inflow were
suddenly stopped the initial rate of tangential wind decrease at the RMW
would be about 25 percent per hour. At further out radii the decelera-
tion rates are considerably less. Nevertheless, the point is made
strongly that any interruption of the low level radial inflow will cause
very rapid and profound changes in the boundary layer wind structure.
The influence of these boundary layer wind changes will be rapidly
propagated to upper levels and will very soon lead to basic alteration
of the entire storm central wind structure.

Conclusion. Hurricane intensity is crucially dependent on the ra-
dius to which the boundary layer inflow penetrates and upon the magni-
tude of the radial inflow. Rapid and sizable reductions in the hurricane

inner core wind structure would occur if the boundary layer inflow could be artificially reduced by but 5 to 10 percent.

The current Stormfury modification hypothesis (as discussed in Section 11) is now based on the idea of an artificial interrupting of a portion of the boundary layer inflow at a radius beyond the eye-wall cloud by silver iodide seeding of outer rainbands.

4. MODIFICATION GOAL

Modification attempts should be directed toward reduction of the hurricane's low level inflow. This might be accomplished through a stimulation of the boundary layer convective buoyancy at outer radii. As discussed in Section 2 the convective buoyancy beyond the eye-wall radius to the outer moat region is not very great. Surface temperatures are but 25-26°C. The weak potential buoyancy and negative horizontal wind shear inhibit a portion of the boundary layer air from rising at outer radii. Much of the inflow must penetrate into the storm center and rise in the inner eye-wall cloud.

If there were some way to add buoyancy to the outlying air beyond the eye-wall radius then more cumulus convection might occur at outer radii. This extra convection would take additional mass out of the boundary layer and reduce the normal amount of inflowing mass that would reach the radius of maximum winds at the eye-wall cloud. By previous arguments, this would lead to a reduction of the inner wind structure. The hurricane modification goal must thus be concentrated on ways of increasing the natural cumulus convection at outer radii. Carbon black dust interception of solar radiation at outer radii is thought to be the best agent for accomplishing this.

Modification Hypothesis. If the outer boundary layer surrounding the hurricane cirrus shield can be artificially warmed at a rate of about 1/2 to 1°C/hr for a period of ten hours, a significant stimulation

41

will be given to cumulus convection at radii beyond the eye-wall cloud so as to cause a noticeable decrease in the low level inflow to the radius of maximum wind. This will lead to a decrease in the inner core maximum wind velocities. A significant decrease in storm damage will result.

By artificially warming the atmospheric boundary layer to the point where absolute instability occurs (as over land areas in the afternoon) additional cumulus convection should be inititated. This extra cumulus convection may occur directly at the places of carbon dust seeding or take place later as the warmed inflowing air is carried for a number of hours underneath the cirrus shield. The extra outer radius heating increases the likelihood of the inflowing air being convected up and out of the boundary layer before it reaches the radius of maximum winds. A reduction of the inner core wind structure will follow.

5. CARBON BLACK DUST AS AN ARTIFICIAL HEAT SOURCE

Artificial Interception of Solar Radiation. About 80 percent of the
incoming solar radiation (I_o) in the cloud free areas of the tropics rea-
ches the earth's surface. As pictorially shown on the left portion of
Fig. 5-1 the larger part of the incoming solar energy is absorbed by
the oceans. Most of this energy subsequently goes into evaporation.
Because this evaporation energy transport from the ocean is not directly
dependent on solar radiation, but goes on during both the day and night,
the oceanic boundary layer does not experience a daily heating cycle as
is common over land.

If a significant portion of the incoming solar energy over the oceans
could be absorbed in the atmospheric boundary layer during the day-
light hours, an artificial stimulation of cumulus convection would occur.
This might be accomplished by aerosol interception of solar radiation
as shown on the right side of Fig. 5-1. Fig. 5-2 compares the extra
boundary layer short wave solar heating rate which is possible in 10
hours due to 15 percent extra absorption of incident solar radiation
with the usual 10 hour net long and short wave radiation of the tropical
troposphere as determined by Cox (1969), Cox and Suomi (1969), and
Cox and Hastenrath (1970).

Carbon Black Dust as an Artificial Atmospheric Heat Source. The
characteristic of carbon dust which makes it so attractive as an atmo-
spheric heat source is the extraordinarily large amount of solar

$$I_0 \left(\begin{array}{c} \text{INCIDENT SOLAR RADIATION AT TOP OF} \\ \text{TROPICAL ATMOSPHERE} \sim 800 \text{ Cal/cm}^2 \text{ per day} \end{array} \right)$$

~20% of I_0 absorbed
or scattered &
reflected back
to space

~20% of I_0 absorbed
or scattered &
reflected back
to space

extra ~15% of I_0 (120 calories/day)
absorbed by 10% carbon black coverage

OCEAN SURFACE

~80% of I_0
absorbed by Ocean

~65% of I_0
absorbed by Ocean
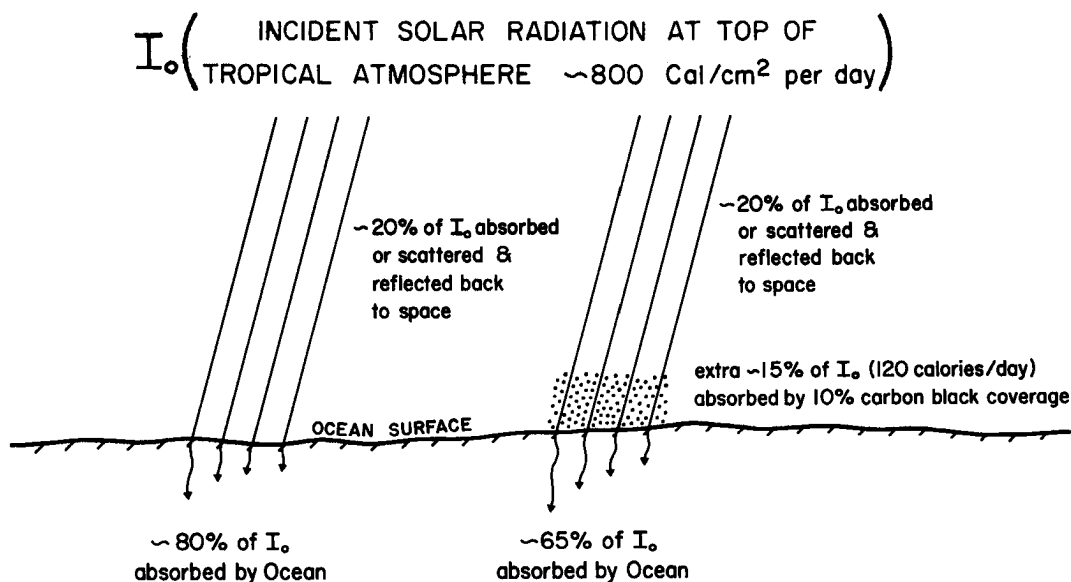
Fig. 5-1. Contrast of clear air tropical condition with normal solar
absorption by atmosphere-ocean (on left) with extra solar
absorption with 10% aerosol coverage in boundary layer
(on the right).

RADIATION INDUCED
TEMPERATURE CHANGES

LONG WAVE

SHORT WAVE

SHORT WAVE HEATING IN 10 HOURS
WITH 15% EXTRA I_0 ABSORPTION

PRESSURE (10^2 mb)

°C/10 hr
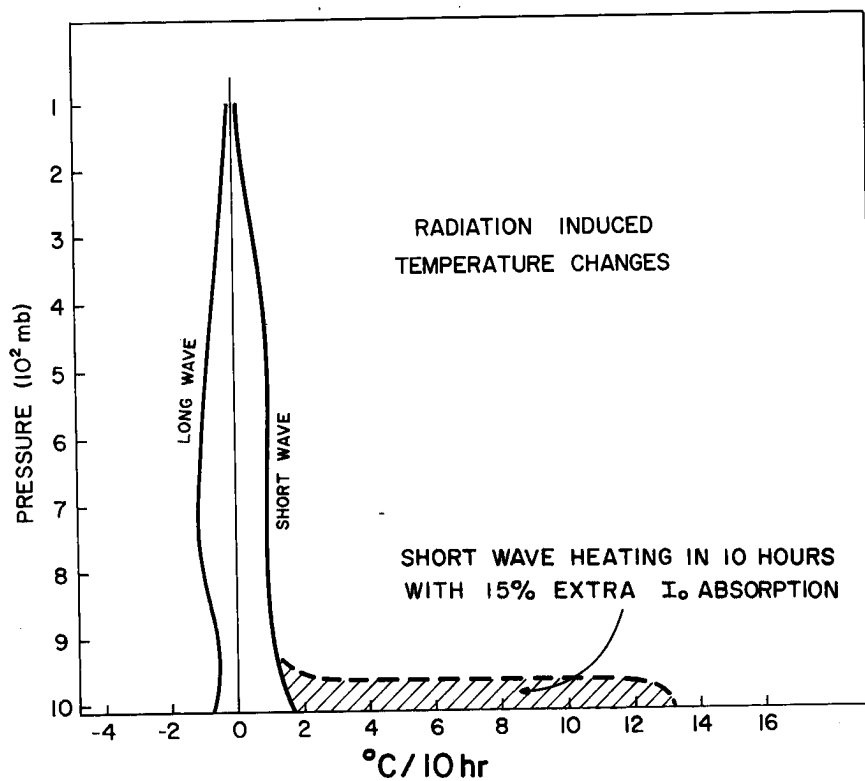
Fig. 5-2. Comparison of 10 hr heating-cooling rates due to long and
short wave radiation in clear regions with the extra bound-
ary layer induced heating (shaded area) which is possible
in 10 hours from 15 percent artificial solar absorption.

radiation which can be absorbed per unit mass of carbon. In a companion paper to this report, Frank (1973) has extensively discussed the characteristics of carbon black dust as an atmospheric absorber of solar radiation from the method of estimating aerosol solar absorption developed by Korb and Möller (1962). The reader is referred to Frank's paper for a thorough discussion of this subject. For the purpose of discussing the use of carbon black dust as an artificial energy source for hurricane modification the following information summarizes the pertinent facts on carbon black dust:

1) Carbon black dust consists of fine spherical particles composed of 95-99% pure carbon, the remainder being made up of volatile materials. It is formed by the controlled incomplete combustion of fossil fuels (usually natural gas) according to a variety of processes depending upon the size and purity of the particles desired. Carbon black is commercially available in sizes from .01μ to .25μ in diameter. The uniformity of size of any class of particles is generally good. Most particles are close to spherical in shape. If put out in sizes less than a few microns it has negligible fall velocity. Most carbon blacks can be purchased in quantity for about $.05 to $.07 per pound.

2) The density of carbon black particles is $2 \, gm/cm^3$ while the packing densities range from about 0.3 to 0.6 gm/ cm^3. The high radiation absorptivity, and low heat capacity (about .125 cal/g°C) of carbon black make it an ideal agent for interception of solar radiation and transfer of this heat to the surrounding air molecules by conduction. Turbulent mixing carries the heat further. Being hydrophobic, carbon dust does not readily absorb water vapor. If put out in small size it will not act as a condensation nucleus. Sub-cloud layer relative humidity is always < 100%.

3) Particles of 0.1 micron radius maximize the solar absorption per unit mass but (as discussed by Frank, op. cit.) the size is not critical. Solar absorption to weight is not greatly altered by variations in size from

.01 μ to 0. 20 μ radius. Individual particles of 0.1 μ radius weigh but 10^{-14}gm. It takes 3×10^{13} particles or about 0.3 gm of carbon to solidly cover a horizontal cross-section of 1 m^2.

4) Carbon black dust particles heat the surrounding air primarily by direct solar energy absorption and rapid molecular (i. e., conduction) transfer (~94%) of this heat to the surrounding air particles. About 6% of the heat transfer from the carbon to the air is accomplished by long-wave radiation.

5) The maximum efficiency of solar radiation to weight and cost requires that the percentage area coverage of carbon black be in the range of 0-30%. Higher carbon areal coverage rates cause redundancy in solar absorption and lower energy to weight and cost ratios.

6) Absorption rates for areal coverage percentages of 0-20% are little affected by zenith angle changes up to 65-70°. This allows for 9 to 10 hours of nearly constant absorption rates during daylight hours.

7) One pound of carbon black dust can absorb more than 20 billion calories of solar radiation in a single 10 hour period. On the other hand, coal, currently the cheapest of conventional combustable fuels, provides on complete combustion about 4 million cal per lb or about 1/6000 as much heat per unit mass as the carbon. The relative costs of energy availalbe from carbon black and coal are shown in Table 5-1. The cost of complete combustion coal heat is about 200 times greater than the cost of carbon heat per 10 hr. period. Among energy sources normally used by man only nuclear energy compares with carbon black as a source of accumulation of energy per unit mass, and no known substance compares as a source of heat per unit cost. A 20 Kiloton nuclear explosion produces about the same amount of thermal energy as can be obtained from 2,000 lb of carbon dust in 10 hours of solar heating. In addition, the carbon dust is not consumed during the heat absorption process and might be used again on following days. Silver iodide seeding in super-cooled clouds can also liberate tremendous amounts of energy per unit mass but the energy from this source does not locally accumulate unless the mass compensation for the stimulated convection occurs near and on a time

Table 5-1

RELATIVE WEIGHTS AND COSTS OF COAL AND CARBON
BLACK DUST ENERGY

Fuel	Cost (dollar/lb)	Heat (cal/lb)	Heat per Unit Cost (cal/dollars)
Coal	$.002	$4 \times 10^6 \frac{cal}{lb}$	$1.2 \times 10^9 \frac{cal}{dollar}$
Carbon Black	$.05	$2 \times 10^{10} \frac{cal}{lb}$ per 10 hrs.	$4.0 \times 10^{11} \frac{cal}{dollar}$ per 10 hrs.
Ratio $\frac{(Carbon\ Black)}{Coal}$	$\sim \frac{25}{1}$	$\sim \frac{6000}{1}$	$\sim \frac{200}{1}$

scale of the seeding. This is rare. As the seeded cloud dies out the suspended frozen particles melt and re-evaporate.

8) Table 5-2 lists the short wave absorption by carbon dust in the tropical boundary layer (surface to 960 mb) which would result from various carbon dust equivalent area coverages. The concentration of 0.1μ radius carbon particles per cm^3 is also shown. For carbon dust area coverages of 10 and 20 percent, only ~ 50 and ~ 100 pounds respectively of carbon dust are needed to cover an area of one km^2. At purchasing rates of but 5 cents/lb this amounts to but $3 and $6 per one km^2 coverage. One U. S. Air Force C-5A can dispense 200,000 lbs of carbon black, causing a 10% carbon dust coverage (and 120 extra calories absorption per cm^2 per 10 hours) over an area of 4000 km^2. In clear conditions this amounts to no less than 4×10^{15} calories of artificial absorbed energy per aircraft. Ten percent areal coverage of carbon dust provides heat to increase the mean temperature of the air within the boundary layer (surface to 960 mb) at a rate of about $1^\circ C$/hr for a 10 hour period.

Table 5-2

SHORT WAVE ABSORPTION BY CARBON BLACK DUST IN THE
TROPICAL BOUNDARY LAYER

Cloud Height = sfc. - 960 mb

Percent Area Coverage:	0	9%	18%	26%	35%	53%	70%
Concentration (Particles/cm^3):	0	5,000	10,000	15,000	20,000	30,000	40,000
Carbon Dust mass (pounds/km^2):	0	45	90	135	180	240	360
Net Absorption by Carbon (ly/10hrs):	0	111	198	268	325	412	473

Cost of Dispersal. The major expense to be expected when attempt-

ing to utilize carbon black as an atmospheric heat source is the cost of

air dispersal. Preliminary cost analysis (below) indicates that the cost

of air dispersal of large amounts of carbon black from aircraft, such as

the U. S. Air Force C-5A (see Appendix B for listing of capability of

this aircraft) would be 2-3 times the price of the carbon black itself. A

rough estimate of the cost of operating one C-5A for one 200,000 lb

carbon black mission is given as:

C-5A Operating Costs ($ dollars/hr)	
Consumables:	$1000 - $2000
Support:	$1000 - $2000
Crew:	$100
Total:	$2100 - $4100

The best guess is that total operating costs would be approximately $3,000/hr. For one 8-10 hour mission:

C-5A Operating Costs (8-10 hrs): $30,000

2×10^5 lb carbon black $0.05/lb: $10,000

TOTAL $40,000

Hence, neglecting project expenses and all development costs, the cost of one C-5A flight with a full load of carbon black is about $40,000. The C-5A is the most economical aircraft in service at the present time with respect to pay-load-miles per unit cost. The minimum cost of dispersal, therefore, will be approximately equal to the cost of operating a C-5A aircraft. The required time and area flexibility of operational dispersal make aircraft use indispensible.

Dispersion of Carbon Black Away From Aircraft Track. Based on atmospheric diffusion estimates by Turner (1969), particles dispersed from a C-5A in winds greater than 5-10 m/sec can be assumed to diffuse at least 1 km in distance from the flight path in a few minutes to an hour or two. Flying at 300-400 knots a C-5A could conservatively disperse a carbon dust cloud of about 1000 km² horizontal area per flight hour. Choosing a representative horizontal area coverage of 10%, a C-5A flying at 300-400 kts could lay out an areal coverage of carbon dust of about 4,000 km² (10% coverage) in 4 hours. This would expend all of its 200,000 lb carbon dust load.

Tropical Boundary Layer Heating Rates vs. Percent Carbon Coverage. Table 5-3 (from Frank, op.cit.) gives the boundary layer heating

Table 5-3

TYPICAL TROPICAL BOUNDARY LAYER CARBON DUST INDUCED

HEATING RATES FROM ONE C-5A AIRCRAFT FLIGHT

Total carbon mass = 1×10^5 kg (1 C-5A full load)

Seeding Depth = 0.55 m

Area	% Area Coverage	Net Heat Absorbed $(\frac{cal}{cm^2 \, 10hrs.})$	Temperature Change ($^\circ$C/10hrs.)
7200 km^2	5%	60	4
4000 km^2	9%	110	8
2000 km^2	18%	200	13
1500 km^2	26%	270	18
1000 km^2	35%	325	22
680 km^2	53%	410	27
510 km^2	70%	470	31

rates that can be accomplished for various percentage carbon black

coverages which are possible with one C-5A aircraft.

These enormous area coverages open the possibility of large scale

weather modification. Fig. 5-3 portrays comparative areas which can

be covered by various numbers of C-5A aircraft at 10 percent carbon

dust coverage in contrast with the typical size of the hurricane cloud

cluster. This would cause an artificial increase of the mean bound-

ary layer temperature of 1°C/hr for 10 hours over the dotted area

shown.
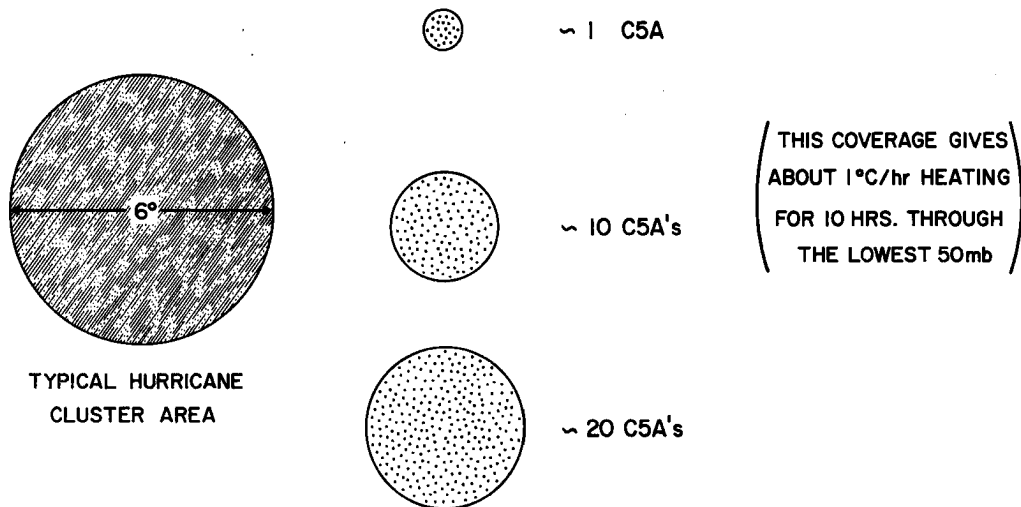
Fig. 5-3. Comparison of typical hurricane cluster area (6°latitude diameter) with the area (dotted) of 10 percent carbon black coverage which is possible with various numbers of C-5A aircraft.

Particle Clumping. Carbon black particles tend to agglomerate into clumps many times their original size when stored in bulk or in a liquid suspension. This clumping could have effects upon the radiation characteristics of the carbon particles since the particle size ($r = .1\mu$) was chosen to maximize absorption of incident solar light. Fig. 5-4 depicts the absorption coefficient per unit mass ($\frac{E}{\alpha}$) of a carbon black dust cloud as a function of particle size and size parameter (α) for a given wavelength of $\lambda = .72\mu$ (median for the solar spectrum). Maximum cloud extinction per unit mass occurs for particles of $r = .11\mu$. However, particles as small as $r = .01\mu$ or as large as $r = .20\mu$ could be used with a loss of efficiency of 15% or less. Since these values encompass a particle size range of a factor of 20, it may be possible to put out very small particles ($r \leq .01\mu$) and allow them
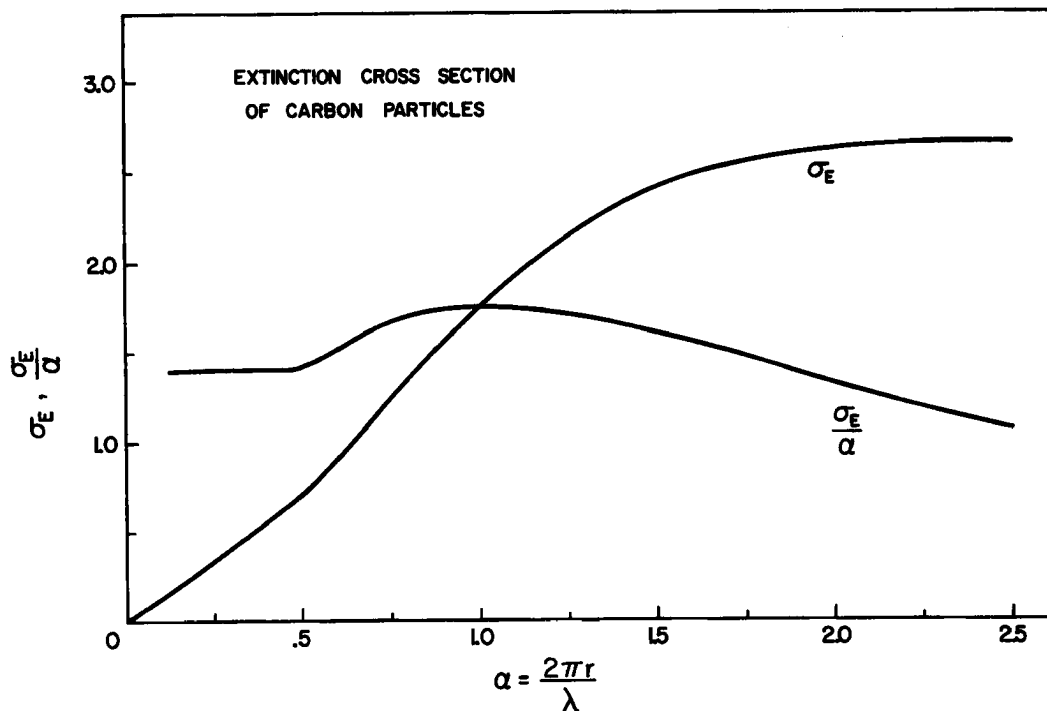
Fig. 5-4. Solar energy extinction (σ_E) and extinction per unit mass (σ_E / α) as a function of size parameter (α) where $\alpha = \frac{2\pi r}{\lambda}$, r is the carbon particle radius, λ the wavelength of maximum solar energy (from Frank, 1973).

to clump to various sizes within the acceptable size range without

seriously decreasing cloud absorption.

If it were deemed desirable to work with carbon particles of rela-

tively uniform and exact size, there are two basic methods for dispers-

ing the particles to avoid agglomeration. The first method requires

the use of a chemical dispersing agent, the second is a mechanical

method.

     1) Chemical Method. At the factory carbon black is broken
       down into individual particles by mechanical mixing and
       suspending the particles in a mixture of water and dis-
       persing agent. The dispersing agent coats the surfaces
       of the carbon particles. This prevents agglomeration

(Cabot, 1969). The mixture can then be sprayed into the air leaving the individual carbon particles as the water evaporates. For carbon particles of radius $= .1\mu$, the maximum loading of carbon (percent of entire mixture which is carbon) is about 65%. Approximately 2% of the mixture would be made up of a dispersing agent (not a toxic chemical) and the remainder would be water. This method results in an increase in air dispersal costs due to the cost of dispersing the inactive mass (primarily water) and the cost of the dispersing agent. There is also some question as to the effects of residues from various dispersing agents upon the radiative properties of the carbon particles.

2) <u>Mechanical Method.</u> Clumps of carbon particles can also be broken down by thrusting them against a barrier or by injecting them into an air stream, and then subjecting the air to strong shear forces. The former method is the typical one used. The breaking up by shear forces is usually done by forcing the air stream through a nozzle under pressure (Marteney, 1965). This method does not involve dispersal of excess mass or the use of a dispersing agent. At present, however, this method has only been used with very small nozzles and low mass flow rates. Nevertheless, it is felt that it would be possible to disperse large numbers of individual carbon particles using aerodynamic shear to break down natural occurring clumps by dispersing the particles from a 400 knot aircraft with large wake turbulence or by blowing the particles out the exhaust of the jet engines. The higher wind speeds and turbulence occurring in the boundary layer plus the heating influence should further reduce any clumping tendency.

It is believed that present engineering technology can find methods to overcome any possible clumping problems which might be encountered.

Conclusion. Carbon black dust can be employed to obtain a remarkably high ratio of artificial solar energy absorption per unit mass and per unit cost. Very high boundary layer heating rates can be obtained from areal coverages of but 50 lb/km^2. It appears that massive

areal dispersion of carbon dust by cargo aircraft such as the C-5A is economically feasible. Clumping and dispersion of the carbon dust away from the aircraft track do not appear to be major obstacles.

6. PROPOSED METHOD OF BENEFICIAL MODIFICATION

It is hypothesized that if sizable areas surrounding the hurricane cluster can be seeded in the boundary layer with carbon black dust the effect will be to stimulate additional cumulus convection either at the place of the carbon seeding or, if turbulence and large boundary layer mixing occurs, then at radii inside the carbon seeding but beyond the radius of maximum winds. The effect of the carbon dust seeding will be to enhance the cumulus buoyancy by increasing the low level temperatures and evaporation rates.

Fig. 6-1 shows where the proposed carbon black dust would be placed at radii beyond the edge of the cirrus shield and how this might interrupt part of the low level inflowing mass through enhancement of cumulus convection beyond the eye-wall radius. Fig. 6-2 more explicitly shows the typical regions around the hurricane cirrus shield in the clear moat area where the proposed carbon black seeding would be accomplished. Fig. 6-3 shows the cirrus shield and a radar composite of hurricane Daisy (25 August 1958) along with the desirable location of the carbon dust material to accomplish modification objectives.

Fig. 6-4 compares the area of a 6° latitude wide hurricane cluster with the area of 10 percent carbon dust seeding that can be accomplished by ten C-5A aircraft. Each C-5A aircraft can lay a 10 percent carbon dust coverage over the area shown by the individual numbers. As the right quadrant of the storm usually has the largest inflow it might be
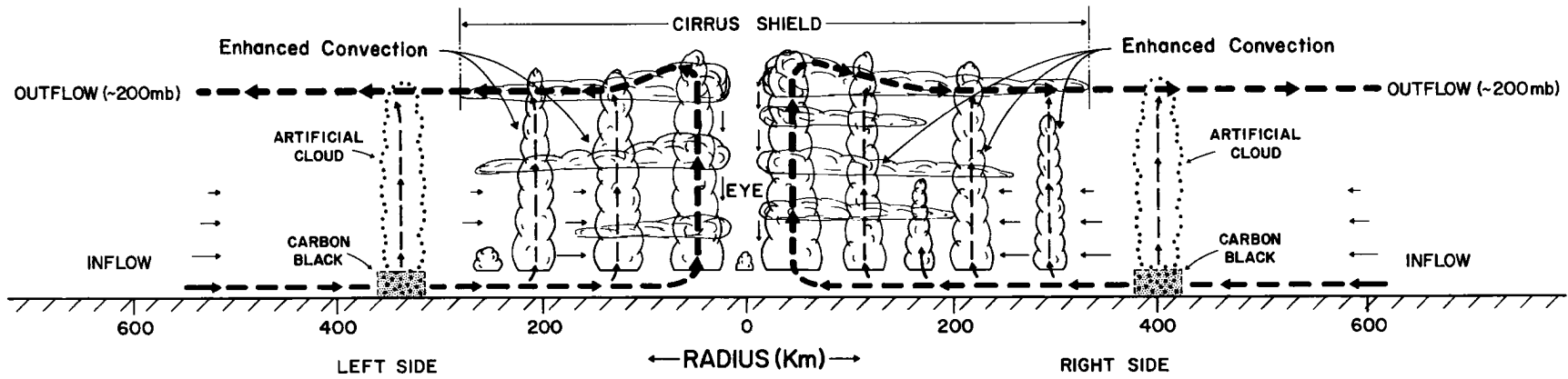
55

Fig. 6-1. Idealized portrayal of typical hurricane radial circulation and how carbon black dust seeding of the boundary layer just beyond the cirrus shield might lead to enhanced cumulus convection and reduction of low level inflow which penetrates to the eye-wall cloud.
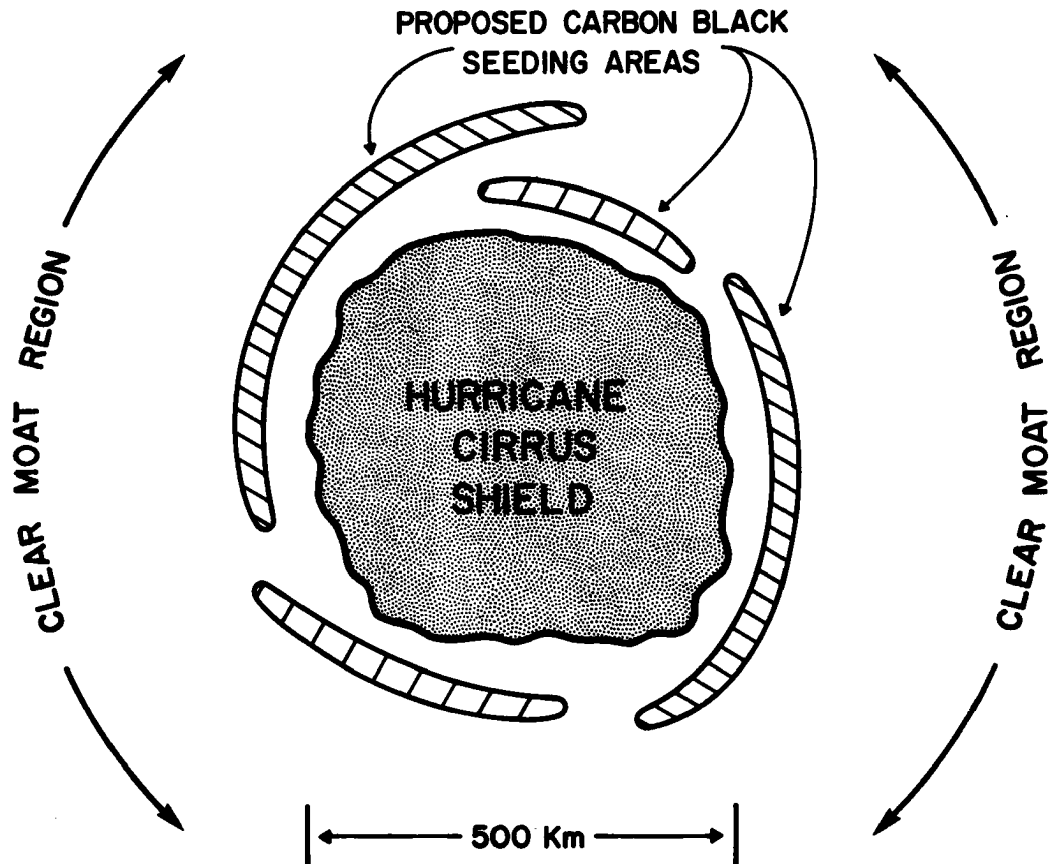
Fig. 6-2. Long hatched areas show where the boundary layer seeding of carbon black dust should be accomplished in the clear area moat region 8-10 hours upward from the hurricane cirrus shield.
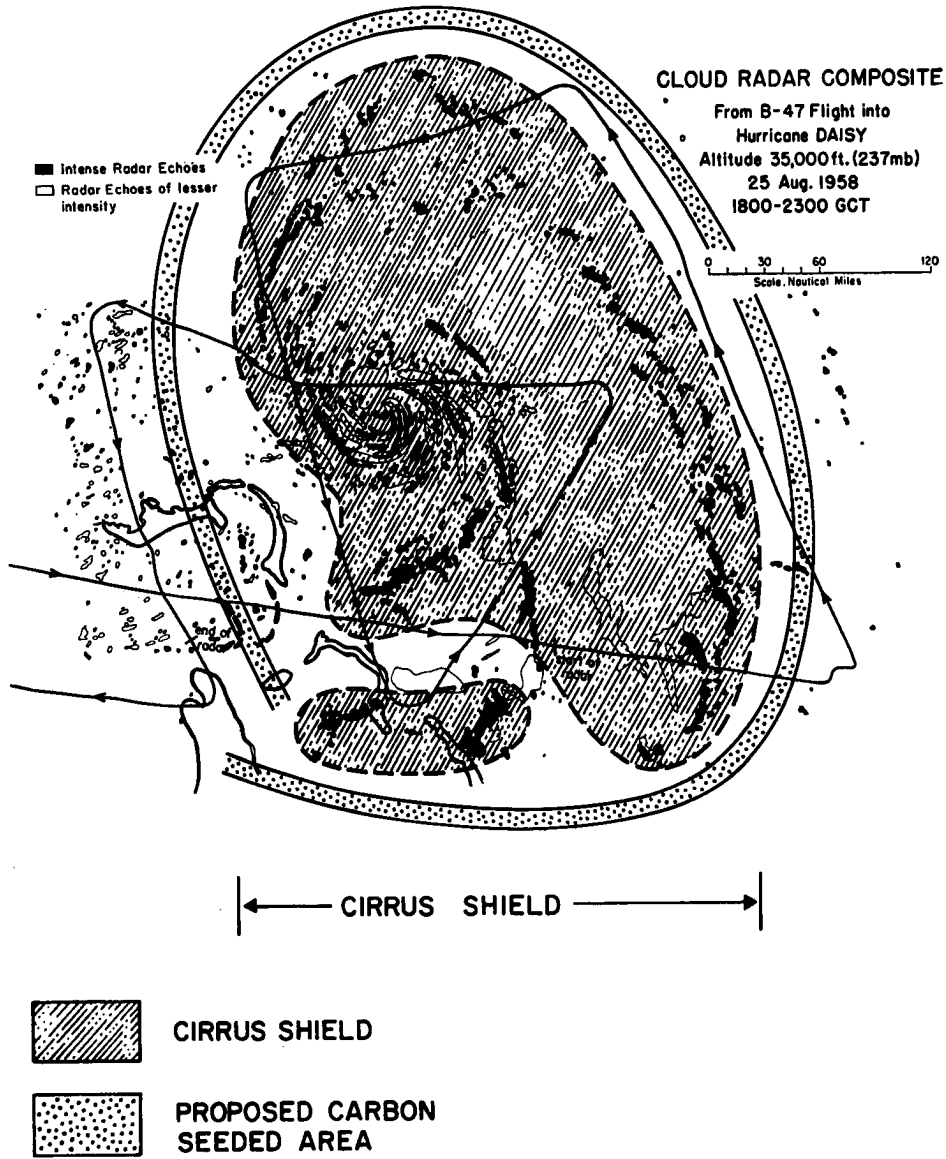
Fig. 6-3. Cirrus shield of hurricane Daisy of 25 August 1958 and hypothesized likely area for carbon dust seeding to reduce storm's intensity.
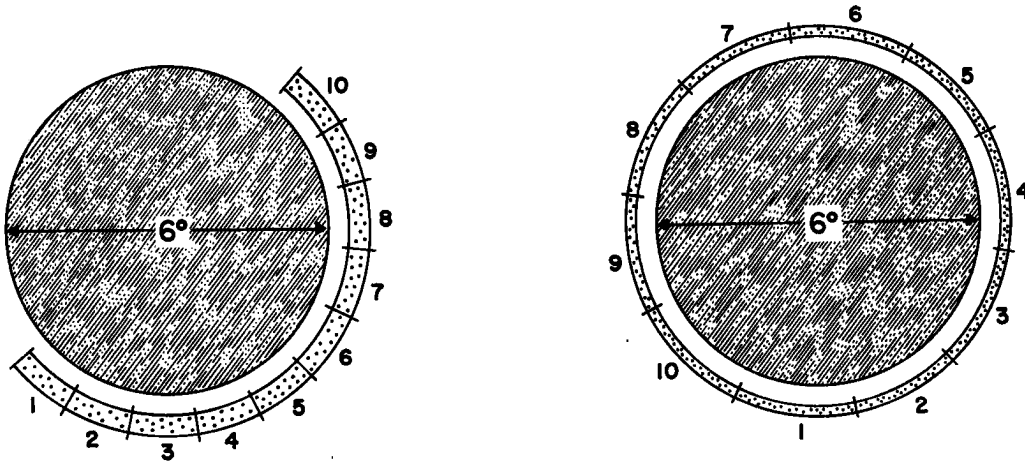
Fig. 6-4. Area comparison of number of C-5A aircraft (10 in all) that are required for 10 percent carbon black dust coverage surrounding the typical hurricane cluster of 6° latitude width. Each aircraft can lay a 10 percent carbon dust coverage over the area shown by the individual numbers.

more desirable to concentrate the seeding in the right semi-circle as shown in the left portion of this figure for a storm moving northward. If not, the seeding can be spread around the entire cluster as seen in the right portion of the figure. In very intense storms which have larger cluster areas, 15-18 C-5A aircraft may be required.

The carbon dust must be placed sufficiently upstream in the moat region such that it does not flow underneath the cirrus shield before its 10 hour heating can be accomplished. In some intense hurricane cases where the moat region is very large it may be desirable to place the carbon dust 36 hours travel away from the cirrus shield and obtain two days of solar heating. In these cases it would probably be advantageous to spread the dust in areal concentrations of only 3 to 5 percent — equivalent boundary layer heating of about 1/3 to 1/2°C/hr. for 10 hours. These lower concentrations would allow for a larger areal

coverage and result in less cumulus convection the first day. This would help maintain more of the dust in the boundary layer for second day utilization.

Logistics of Putting Out Carbon Black. It is envisaged that a national or international body will maintain a fleet of aircraft available for this modification work on a year around basis. The aircraft could shift oceans with the changing seasons, and/or be on call to fly to storm regions. Warning of the potential of intense tropical storms striking land areas can (with the help of the satellite) often be made three-four days in advance to allow time for an empty jet aircraft to fly in from distant locations and load on carbon dust. Carbon black could be stored in a variety of locations such as Miami, Norfolk, San Juan, Bermuda, Guam, Manila, Hong Kong, Tokyo, Madras, Darwin, Brisbane, Diego Garcia (S. Indian Ocean), etc., to meet rapid demand when a storm materializes. Storms would be seeded when they are one to two days upwind from populated coastal areas.

Conclusion. It is hypothesized that if two to three million pounds of carbon black dust can be spread around the outer cirrus shield of a hurricane that this will stimulate extra cumulus convection at outer radii and lead to substantial reductions of storm maximum winds within 18-24 hours.

7. LIKELY EFFECTS OF CARBON DUST SEEDING

Carbon dust spread in areal coverage amounts of 10 percent will cause artificial heating amounts of about $120 cal/cm^2$ per 10 hours. This will lead to extra low level warming as portrayed in tephigram form in Fig. 7-1. Dry adiabatic ascent can then occur from the surface to 860 mb. A decided buoyancy advantage would be gained for cumulus convection as shown by the tephigram curves in Fig. 7-2 which compares the parcel ascent "after $120 cal/cm^2$ heating" curve with the "before heating" parcel curve.

Extra Evaporation. The solar absorption by carbon dust is but one influence. This extra heating should also stimulate an increase of evaporation. The increased surface warming will stimulate an extra downward mixing of upper level dryer air to the ocean. This dryer air will increase the water vapor difference between the ocean and the air and lead to increased evaporation rates. Evaporation rates may perhaps be double or triple their normal amounts. Priestly (1959) has quoted a number of references indicating that ocean evaporation rates can be approximated by the formula:

$$\text{Evaporation} \sim \rho_o C_e u_o (q_s - q) \tag{1}$$

where
$$\rho_o = \text{surface air density}$$
$$C_e = \text{coefficient of evaporation, equal to } \sim 2 \times 10^{-3}$$
$$u_o = \text{low level wind speed}$$

TEPHIGRAM PLOT OF MAGNITUDE OF ENERGY INPUT
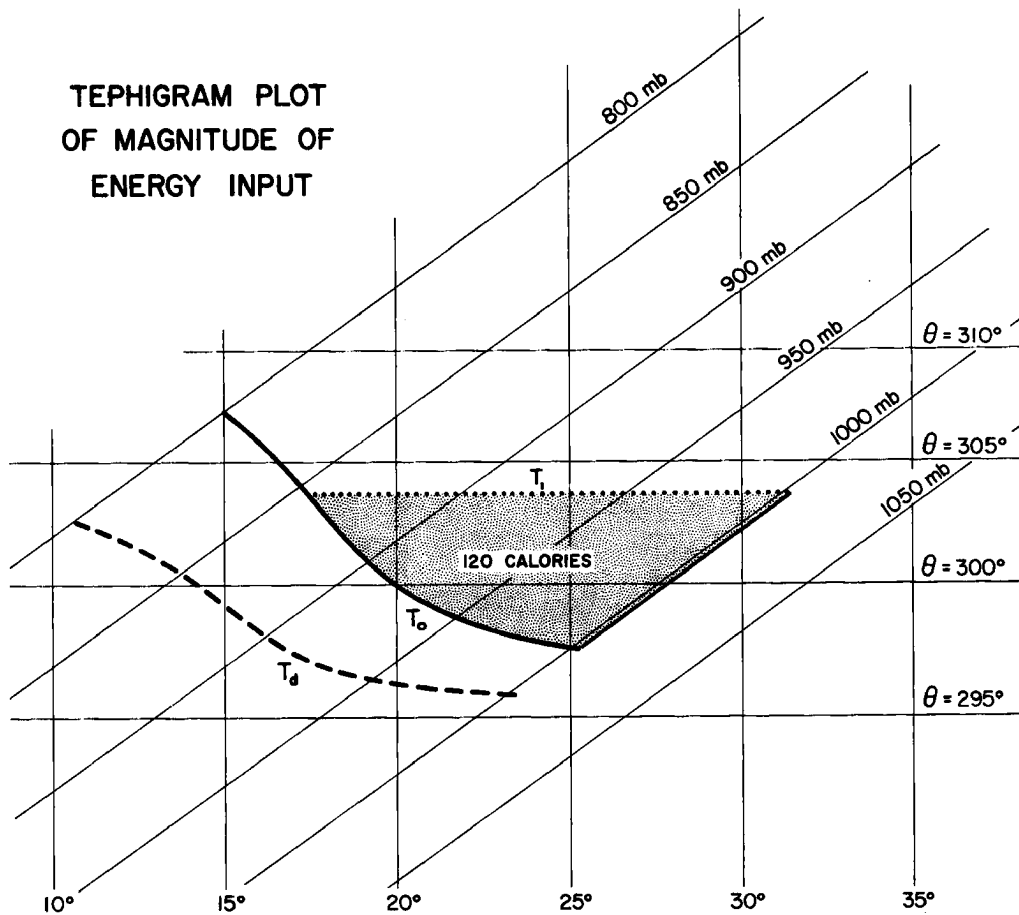
Fig. 7-1. Typical tephigram plot of temperature (T_o) and dew point (T_d) for a typical low level sounding just beyond the hurricane's outer cirrus shield. The extra energy input (shaded area) to the low levels in ten hours $(120\,\text{calories}/\text{cm}^2)$ that results from solar absorption due to 10 percent areal coverage of carbon dust is shown. This heating should lead to a dry adiabatic temperature curve as shown by line T_i.

$q_s - q$ = difference in specific humidity between the saturated value equivalent to the ocean temperature (q_s) and the air value (q).

It is seen in Fig. 7-3 that the Δq or $q_s - q$ difference between air at 860 mb and the ocean is about four times larger than the difference
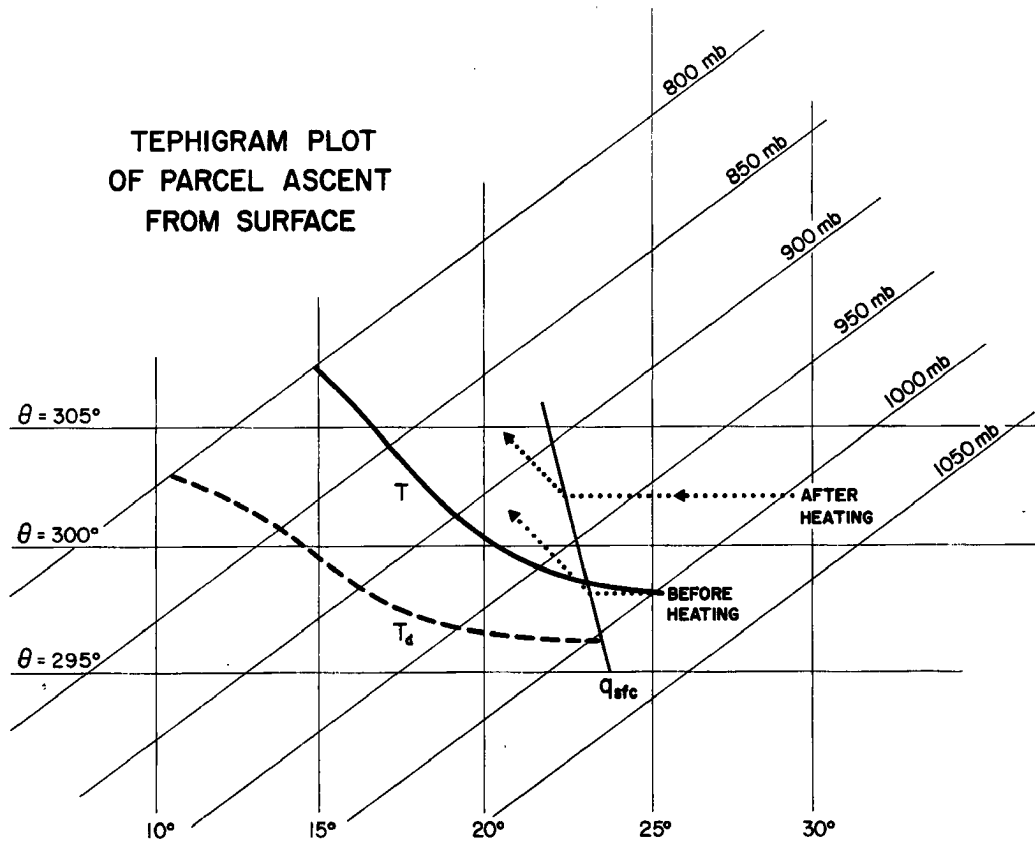
Fig. 7-2. Tephigram plot of parcel ascent from the surface for the region just beyond the hurricane's cirrus shield for condition before and after an artificial solar heating of 120 calories/cm^2 in 10 hours.

between surface air and the value representing saturation at the ocean temperature. Any mixing down of upper level air should substantially increase the evaporation rates. The energy for this increased evaporation, however, will come largely from the ocean and not the air. Thus, it may be possible for the carbon dust solar heating to extract extra energy from the ocean that would not naturally occur. This extra evaporation will occur a number of hours after warming as the air moves inward underneath the cirrus shield. The potential buoyancy of the low levels will be enhanced by the extra water vapor content of the artificial
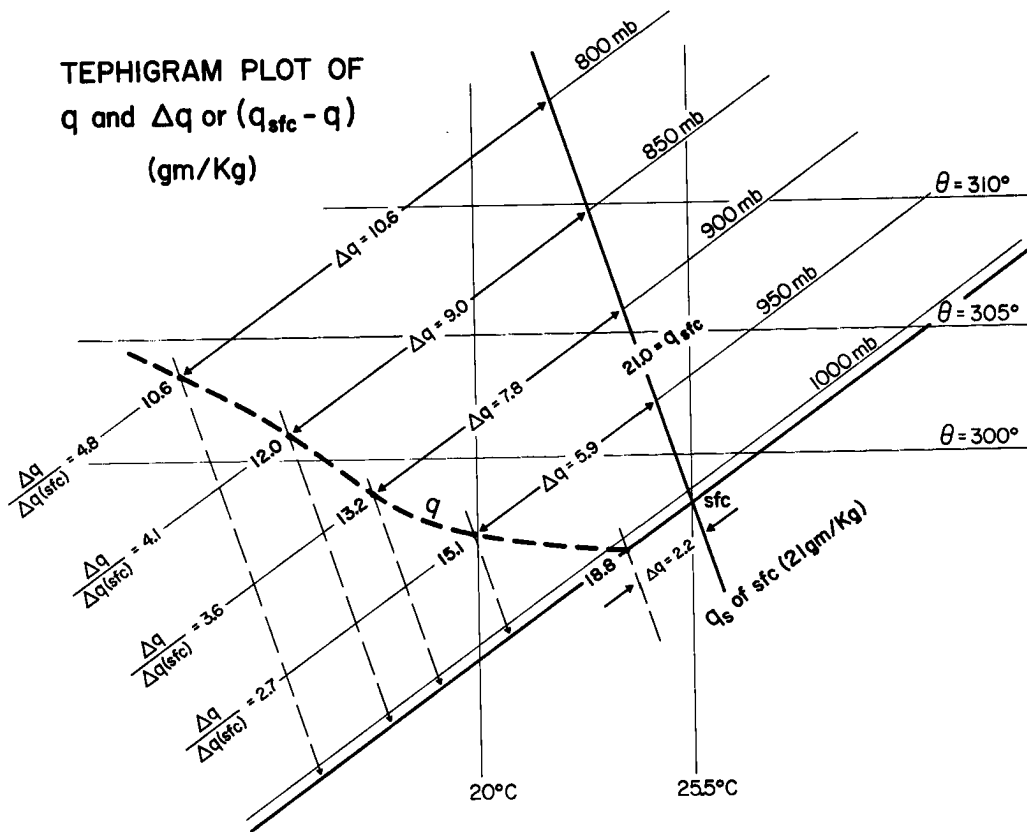
Fig. 7-3. Portrayal of specific humidity difference of upper layer air with surface saturated specific humidity of the ocean (q_S) and how extra mixing downward of dryer air would greatly enhance the q_S - q values.

evaporation. An increase of water vapor content of one gram per kilogram increases the boundary layer θ_e by no less than $2\text{-}1/2^{\circ}\text{K}$.

M. Garstang[*], E. Zipser, and E. Ruprecht[*] have discussed with the author the typical extra dryness of "disturbed" vs. "undisturbed" boundary layer air due to downdraft mixing from higher levels. During boundary layer flights in the BOMEX project the author has also observed extra dryness in the boundary layer surrounding active cumulus convection. See reports of Garstang (1967) and Zipser (1967) and Garstang and Warsh (1970) for more documentation.

---

[*]Personal communication.
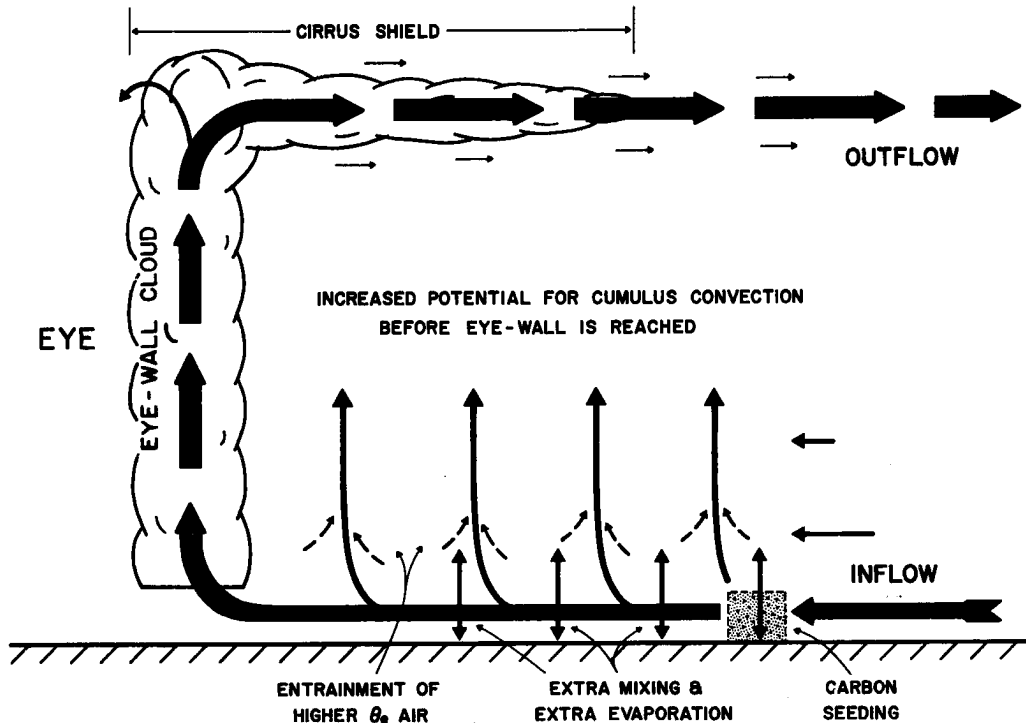
Fig. 7-4. Idealized view of how an increase of low level temperature-moisture through carbon dust interception of solar radiation would lead to extra enhancement of deep cumulus convection at outer radii, and tend to cause less low level mass penetration to the eye-wall cloud region.

Therefore, the extra solar heating at outer radii is expected to lead to an increase not only of outer radii thermal buoyancy but also of buoyancy due to extra water vapor content as well. Even though the extra evaporation influences may not be felt at the place of carbon seeding they are expected to take place in the air before it reaches the eye-wall radius 18-36 hours later. Fig. 7-4 attempts to show how enhancement of buoyancy from extra heating and evaporation will lead to more artificially induced cumulus convection at radii beyond the eye-wall cloud and lessen the inflow to the inner storm region. Fig. 7-5 is an idealized portrayal of the expected artificial increase of low level θ_e from extra solar absorption and evaporation.

66
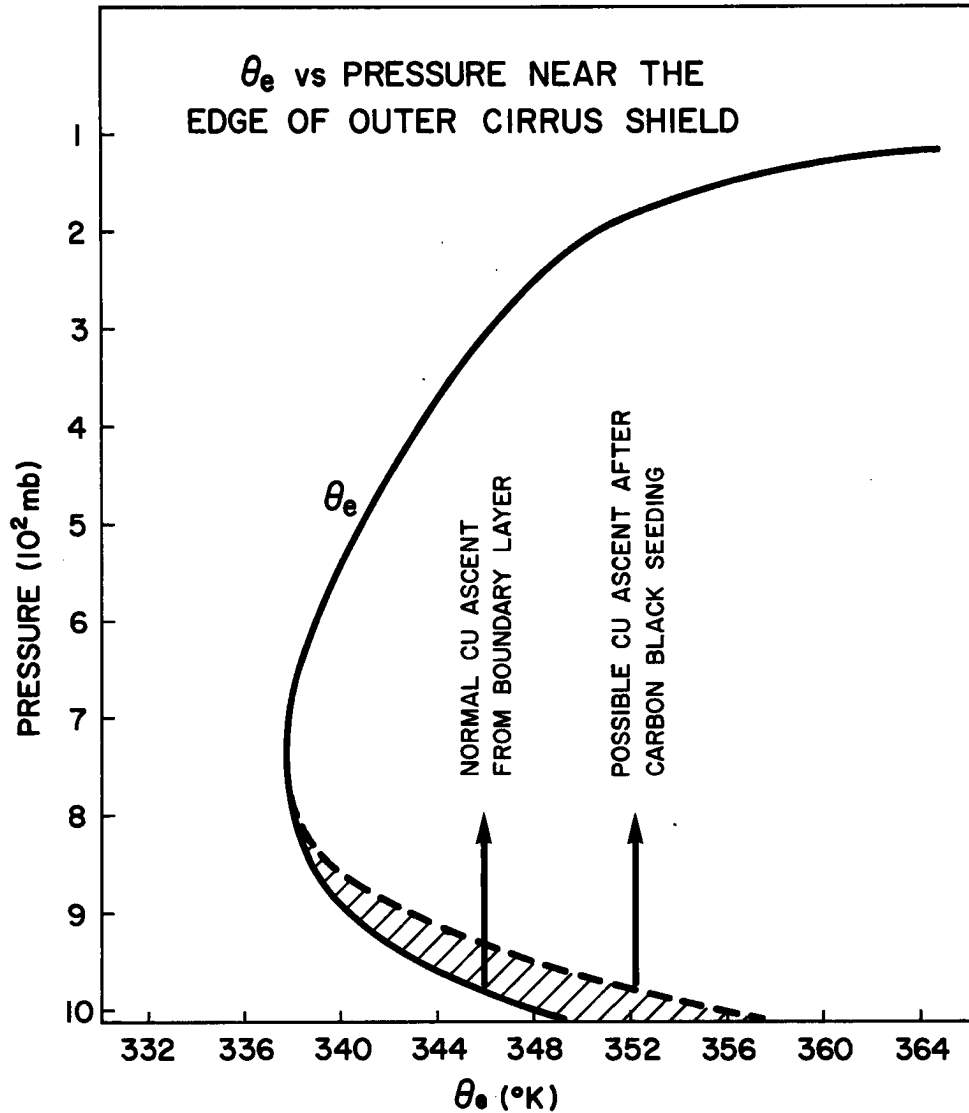
Fig. 7-5. Portrayal of expected influence of increased low level tem-
perature and moisture (shaded area) due to extra carbon
absorption on alteration of the tropospheric θ_e profile.

Testing of Extra Buoyancy in a Cumulus Cloud Model. The whole

life cumulus cloud model of Lopez (1972) has been used to attempt an

evaluation of the extra buoyancy influences of increased temperature

and moisture on the boundary layer air.

Fig. 7-6 shows a cloud top vs. time diagram of different cumulus

clouds that have had their boundary layer temperature increased by

various amounts. Cloud (a) is the null case. The other clouds which
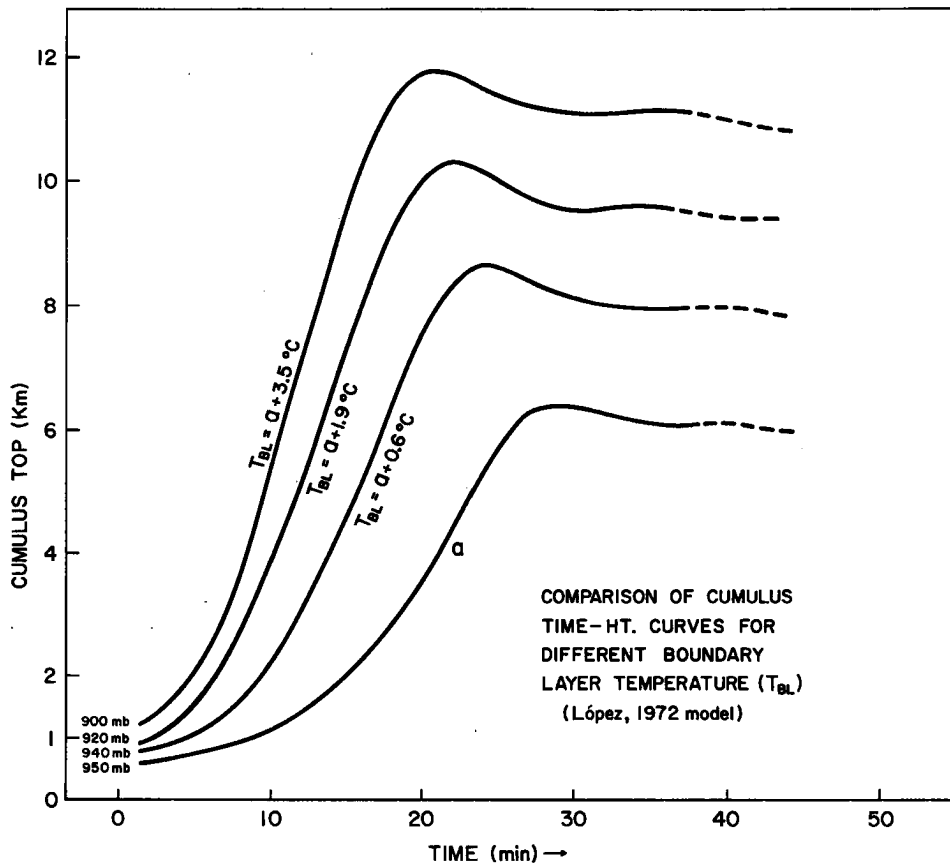
Fig. 7-6. Time vs. height diagram of cumulus growth for a towering cumulus (a) of López's (1972) whole life cloud model. The other curves portray the increased growth rates and heights of this same cloud if the boundary layer temperatures are increased by the amounts shown and all other parameters remain the same.

grow higher and more rapidly have had their boundary layer temperature values (T_{BL}) increased by the amount specified. Note that temperature increases of but 1 or 2 degrees in the boundary layer can lead to significantly more intense cumulus convection (with all other factors held constant).

Fig. 7-7 shows a similar influence for a two gram per kilogram increase in the boundary layer specific humidity with all other influences held constant. Here again the cumulus convection is much more intense.
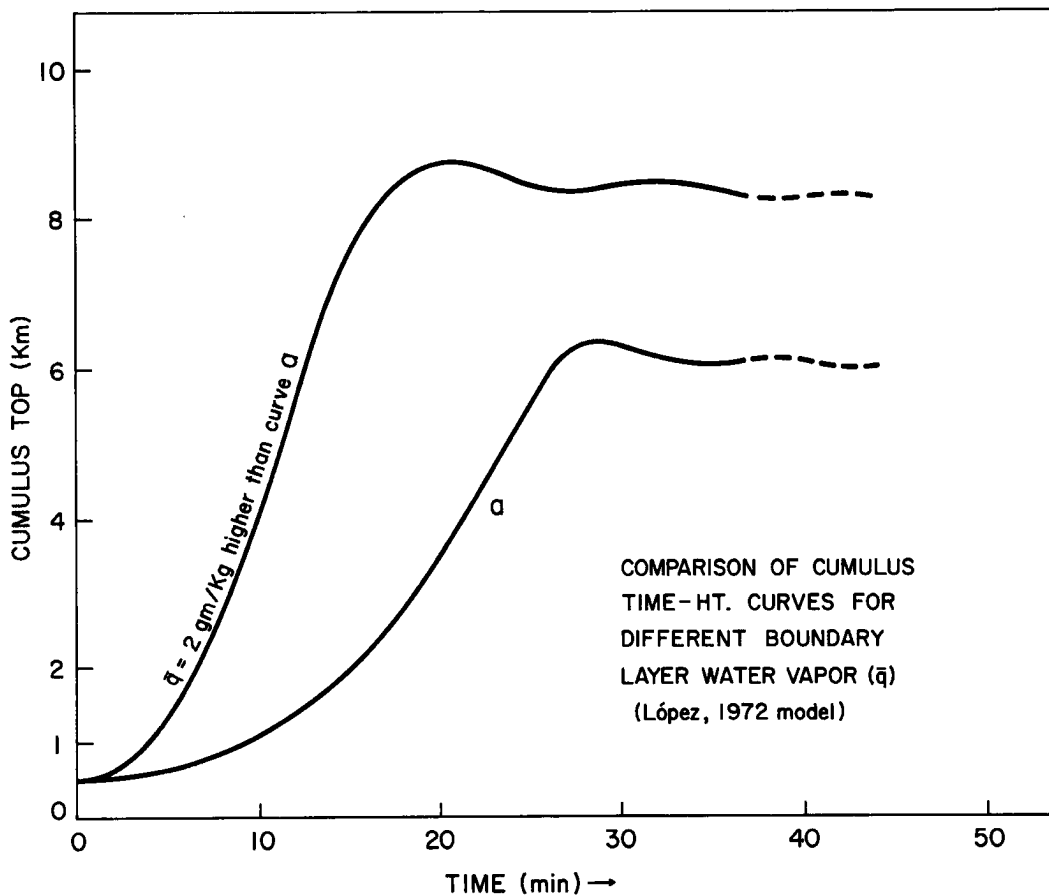
Fig. 7-7. Time vs. height of cumulus growth for a towering cumulus (a) of Lopez's (1972) whole life cloud model and the increase growth time and height of the same cloud if it had an extra boundary layer water vapor content of 2 gm/kg.

Residence Time of Carbon in Boundary Layer. Not all of the carbon dust will remain in the low levels during the ten hour heating period. Some of it will be advected upward and out of the sub-cloud layer. If spread evenly over large areas, however, the carbon loss in 10 hours through upward advection should not lead to massive dust depletion.

Fig. 3-7 showed that the theoretical and observed mean divergence in the sub-cloud layer between 400-600 km radius is but 1 to 2×10^{-6} sec^{-1}. This gives 600 meter level mean vertical motion of only

~ 7 mb/day (.05 to 0.1 cm/sec). Over a ten hour period of 3.6×10^{4} sec this leads to an upward advection of but 18 to 36 meters, or evacuation of 3-6 percent of the sub-cloud layer depth.

When the carbon stimulates extra convection, the normal situation will be altered. During periods of active convection the mean motion is not representative of the actual vertical motion. As previously discussed by Gray (1972b) for tropical cloud clusters the mean vertical motion at cloud base is but a fraction of the actual up-and-down local circulation. If the carbon dust stimulates a situation of very active cumulus convection, then it is likely that an extra up (moist and dry) and down (moist and dry) circulation perhaps 5 to 10 times the mean vertical circulation will occur. In a 10 hour period this extra upward circulation may advect as much as 25-50 percent of the sub-cloud layer mass to higher levels and largely replace it by descending motion surrounding the cumulus. This extra vertical recycling of mass will lead to further enhancement of the mean vertical motion out of the boundary layer. All convective areas have upward positive circulation.

A large portion of this sub-cloud layer heating loss by upward carbon advection will be made up by compensating heat gain at levels just above the boundary layer. Much of the carbon dust to leave the sub-cloud layer will be carried upward by small cumulus or stratocumulus and will remain within the lower troposphere. These smaller cumulus have lifetimes of but 10-20 minutes. As they die out the carbon they captured from lower levels should again be liberated for solar absorption, although drop agglomeration (see Section 10) will reduce the high energy

absorption to mass ratios. Some of the upward advected carbon particles

will later sink back into the sub-cloud layer in downdrafts. Only the carbon

carried upward in tall cumulus or that scavenged by raindrops during

the 10 hour solar heating period will be lost from the lower troposphere.

Some additional loss of heating will also result when the artificially

developed clouds shelter the boundary layer carbon dust for solar ab-

sorption. Also, some of the carbon dust may be concentrated in selec-

tive up-and-down roll and/or isolated convective circulations which

depend on the local boundary layer stability.

Despite these losses of optimum sub-cloud layer heating it is ex-

pected that most of the theoretical energy gain of $10^{\circ}C/10$ hours per

50 mb for 10% carbon coverage will be received by the atmosphere be-

low 600-700 mb--the level of minimum total energy. (The majority

of solar energy gain will still be felt in the sub-cloud layer). Energy

gain at levels below 600-700 mb should enhance cumulonimbus con-

vection by increasing the low level total energy or θ_e values as seen

in Fig. 7-5. Much of the carbon heating influence will be felt in con-

densation energy gain from the extra rainfall.

Upper Level Moisture at the Radius of the Cirrus Shield. The mid-

dle tropospheric relative humidities at the radius of the outer cirrus

shield appear to be high enough to support Cb convection if the bound-

ary layer buoyancy can be increased. This extra buoyancy increase

should also lead to additional low level dynamic forcing. Table 7-1

shows the relative humidities at various levels as determined by Bell

and Tsui (1972) in areas surrounding typhoons. The surface pressures of the soundings are shown. Surface pressures of around 995 to 1005 should subscribe to the pressures around the outer edge of the typhoon cirrus shield. Values of 60-80 percent relative humidity appear to be high enough to support deep cumulus convection if an extra increase in boundary layer buoyancy can be accomplished.

Table 7-1

Relative humidity at mandatory pressure levels for soundings taken with various surface pressures surrounding typhoons (from Bell and Tsui, 1972).

Surface Pressure (mb) at sounding time	850 mb	700 mb	500 mb	400 mb
990-994	88	85	83	78
995-999	89	88	78	67
1000-1004	90	80	71	60
1005-1009	88	86	71	62

Conclusion. The likely effects of the outer carbon dust seeding will be to warm the boundary layer and enhance the evaporation rates. Energy for the evaporation will come largely from the ocean. This artificially enhanced warming and extra evaporation are expected to lead to significant extra man induced cumulus convection at radii beyond the eye-wall cloud region. Some of the theoretical boundary layer heating will be lost through upward advection of carbon dust. Most of this boundary layer loss will be made up by extra energy gain at levels just above the boundary layer. This above the boundary layer heating should enhance the likelihood of cumulonimbus convection.

8. TESTING OF MODIFICATION HYPOTHESIS IN NUMERICAL MODEL

This outer heating modification scheme has recently been tested in the Rosenthal (1970b, 1971a, 1971b) circular symmetric tropical cyclone model and has been found to verify the physical hypothesis to a high degree.

The model is a seven level primitive equation model containing the water vapor cycle and parameterized cumulus convection. The radial interval is 10 km and the time step is 2 minutes. In an overall sense it appears to handle the basic dynamics of the hurricane quite well.

The model is initialized with a symmetric vortex with maximum winds of 7 m/sec at 250 km radius. The model is then integrated in time. It slowly builds up a moist layer during the first seventy hours of integration and then intensifies rapidly to a hurricane vortex with maximum winds of ~50 m/sec at a radius of 25 km in another 80-100 hours. The vortex then stops intensifying and remains in an approximate steady state for several days. It is the latter steady-state that is used for experimentation. Appendix I describes the model in more detail.

The steady state total wind, radial wind, and vertical motion patterns of this model are portrayed in Figs. 8-1 to 8-3. Note the concentration of winds at the inner radii of 25 km.
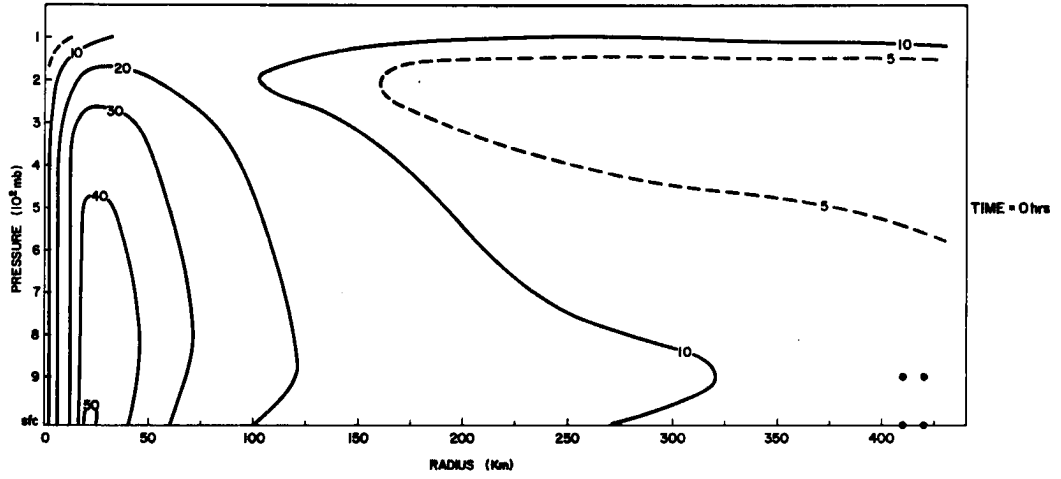
Fig. 8-1. Steady State Total Wind m/sec.
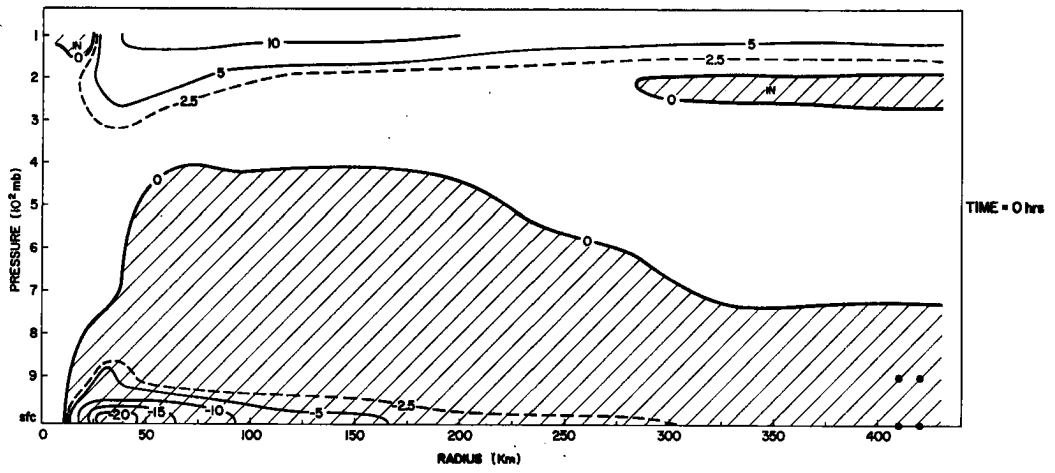
Fig. 8-2. Steady State Radial Wind m/sec.
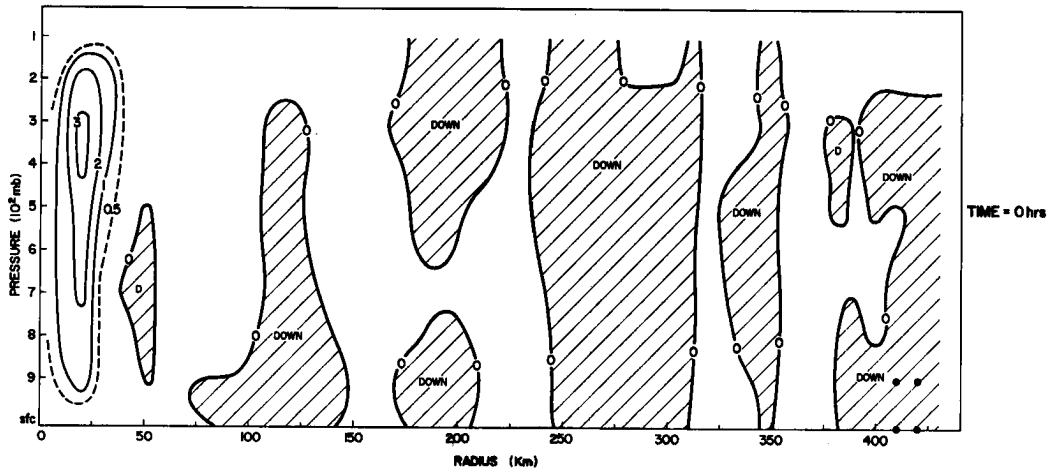
Fig. 8-3. Steady State Vertical Motion m/sec.

To this steady-state hurricane model artificial heating values are applied at the <u>four</u> black dots shown at radii of 415 and 425 km and at the levels of the surface and 900 mb. Heating rates are applied at these grid points for a ten hour period to simulate solar heating. They are then discontinued for 14 hours. When the integration goes beyond 24 hours, the heating rates are reapplied for the period between 24 and 34 hours and cut off again. Two heating rates have been used at the 4 grid points shown. These are:

1) $1/2^{\circ}$C per hr for 10 hours, no heating after this but integration of the model to 24 hours.

2) $1/4^{\circ}$C per hour for 10 hours, no heating for 14 hours, then a second rate of $1/4^{\circ}$C per hour from 24-34 hours. The model is integrated out to 34 hours in this latter case.

The maximum artificial heating influences are felt about 24 hours after integration is started. It takes 12-24 hours for the effects of this outer heating to manifest itself with changes in the inner core of the hurricane.

Figs. 8-4 to 8-9 are vertical cross-sections showing the influence after 10 and 24 hours of an artificial heat source of $1/2^{\circ}$C/hr applied at the four black dotted grid points for the first 10 hours. Note that the maximum reductions in the horizontal and vertical winds occur where these values are highest. Such changes would be beneficial in terms of storm damage reduction. After 24 hours the wind at the surface at the radius of maximum winds <u>is reduced by</u> 15 m/sec (30% reduction from the original value). The surface kinetic energy at the radius of maximum winds has been reduced to but 40% of its initial value. The
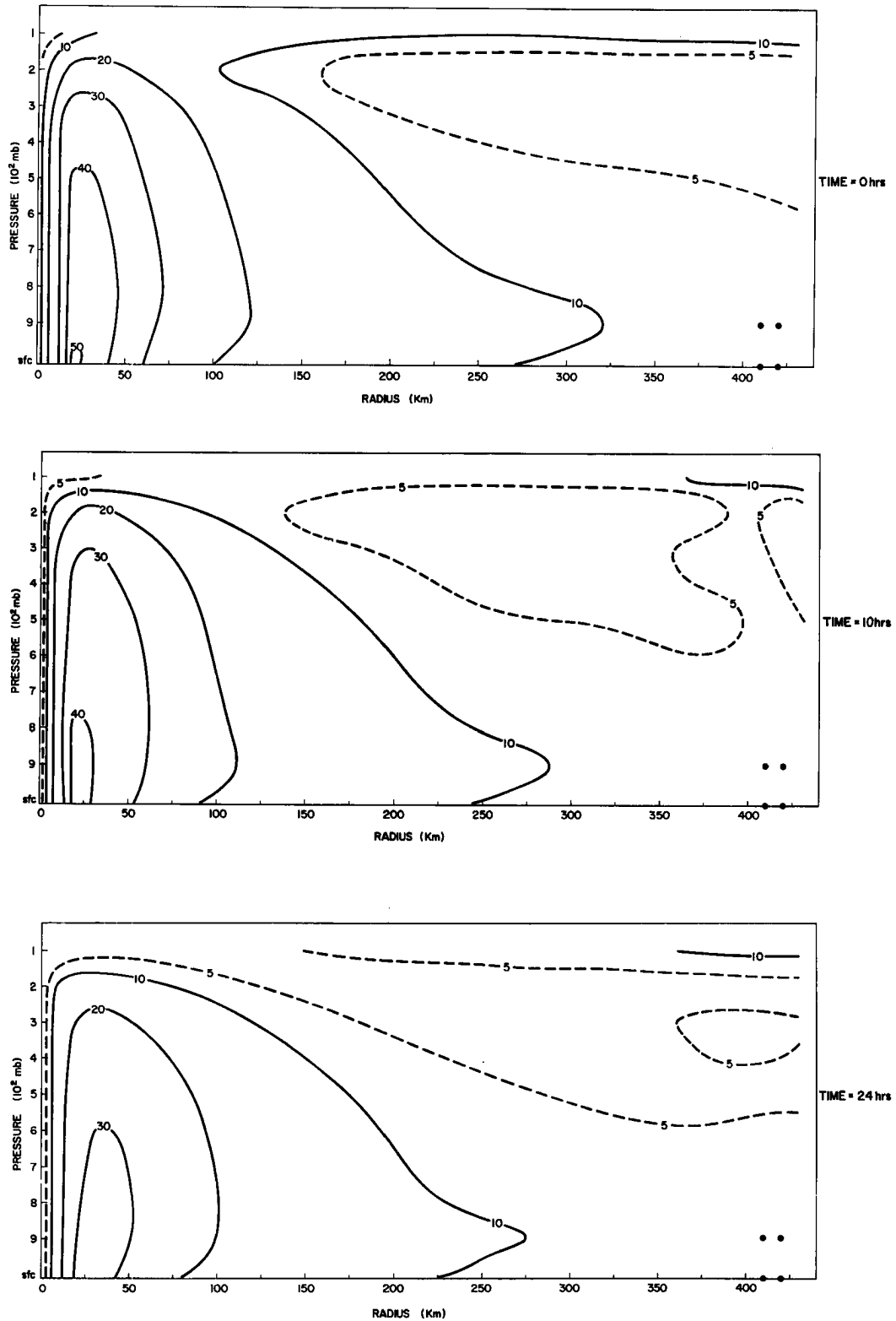
Fig. 8-4. Total wind speed (in m/sec) at various time periods as a
result of artificial heating rate of $1/2^{\circ}C/hr$ for the first
10 hours applied at the four grid points shown at the lower
right.
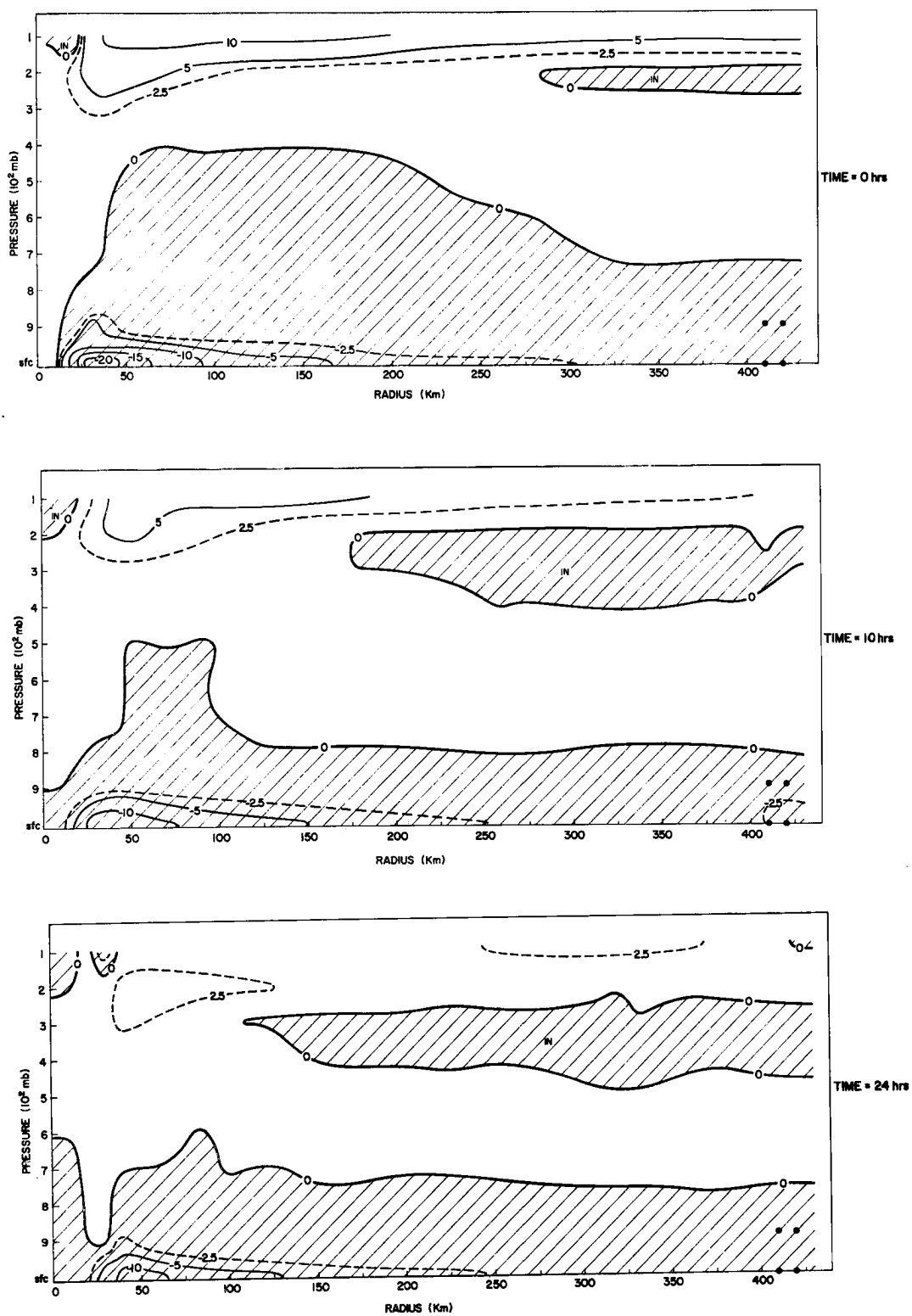
Fig. 8-5. Radial wind (in m/sec) at various time periods as a result of artificial heating rate of $1/2^\circ C/hr$ for the first 10 hours applied at the four black dot grid points shown at the lower right.
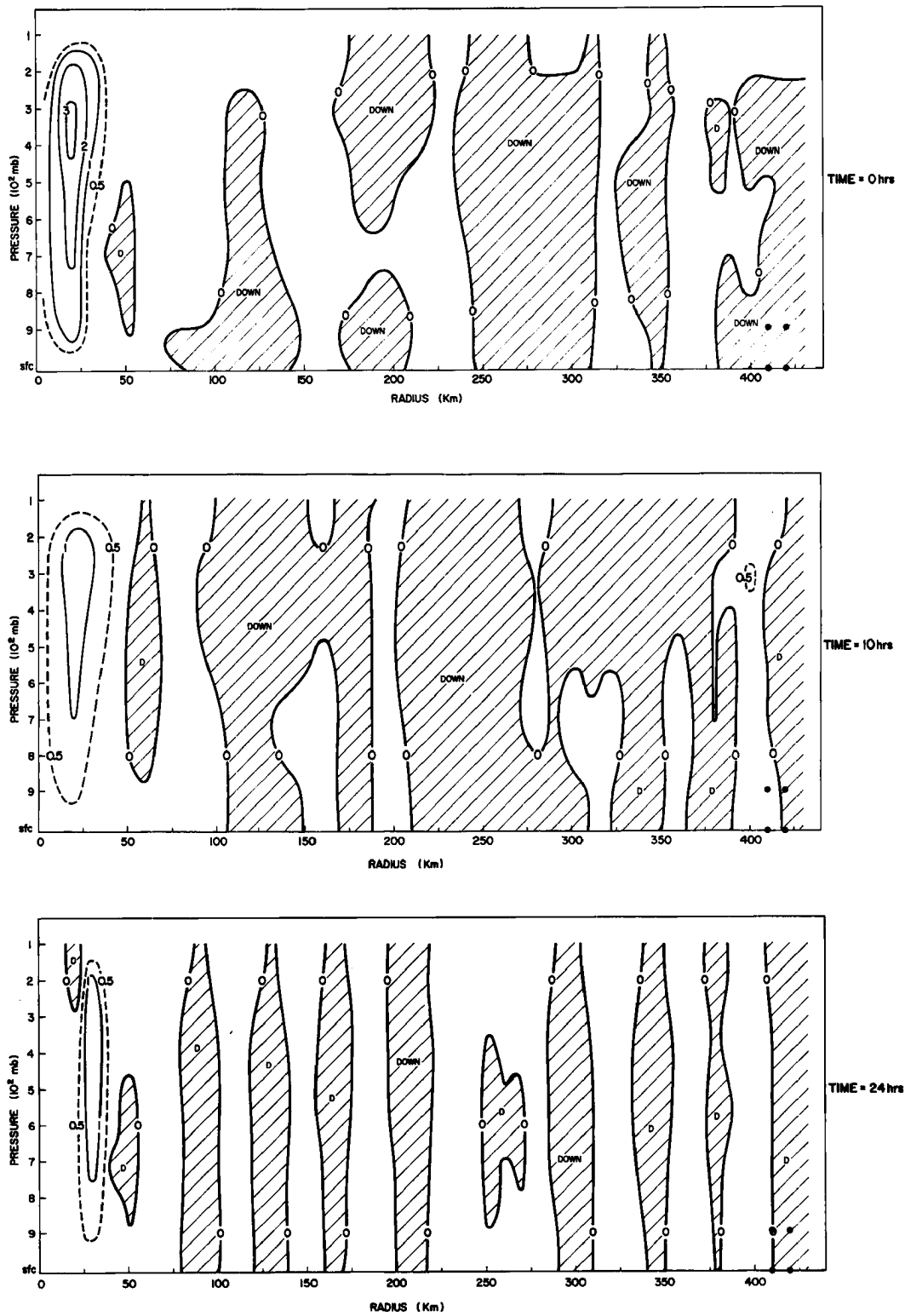
Fig. 8-6. Vertical wind (in m/sec) at various time periods as a result of artificial heating rate of $1/2^{\circ}C/hr$ for the first 10 hours applied at the four black dot grid points shown at the lower right.
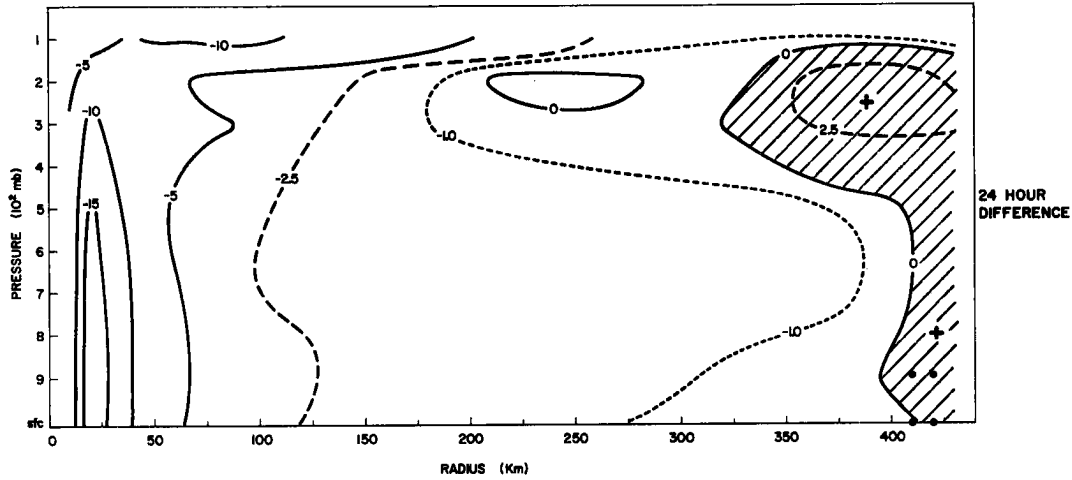
Fig. 8-7. Total wind difference in 24 hours for 1/2°C/hr artificial heating rate for the first ten hours at the four black dot grid points shown.
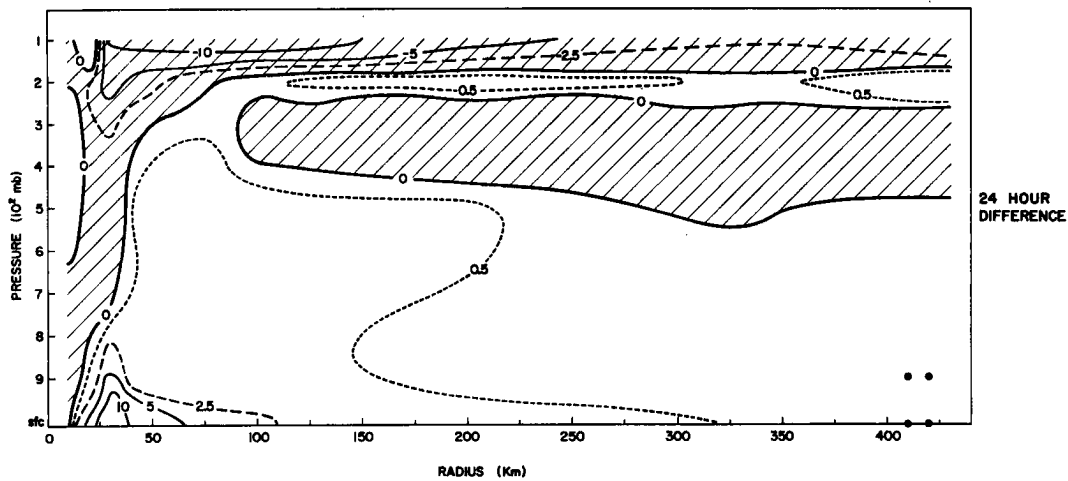
Fig. 8-8. Radial wind difference in 24 hours for artificial 1/2°C/hr heating rate for first ten hours at four black dot grid points shown.
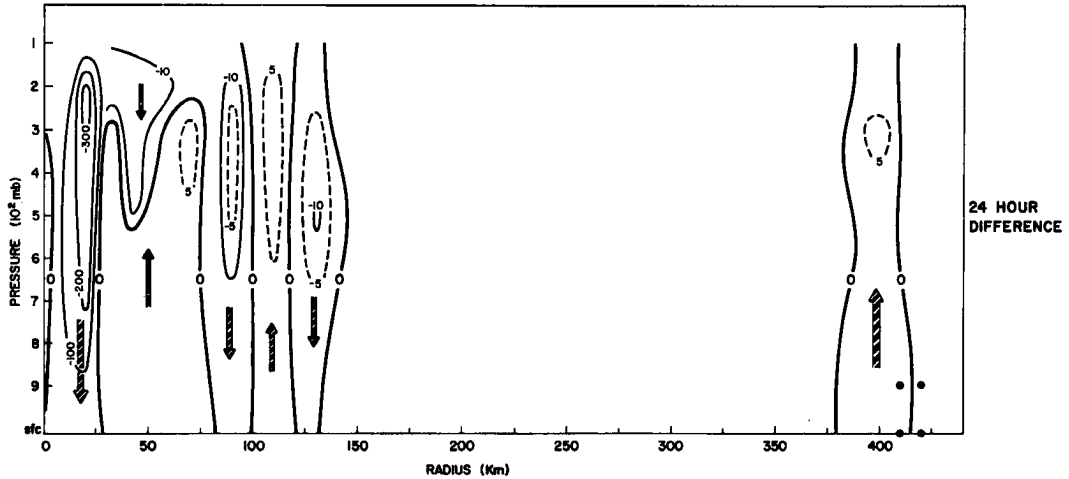
Fig. 8-9.   24 hour difference of vertical wind (in m/sec) for artificial 1/2°C/hr heating rate for first ten hours at the four black dot grid points shown.

radial winds and vertical motion pattern at the inner core radii have likewise been greatly altered.

Figs. 8-10 and 8-11 show similar vertical cross-sections for artificial heating rates of 1/4°C/hr at the four black grid points for ten hours, no heating for 14 hours, and then a heating rate again of 1/4°C/hr for ten hours. The model is integrated for a total of 34 hours. These two ten hour heating rates at 0-10 and 24-34 hours produced about the same influence as that of the 1/2°C/hr artificial heat applied at 0-10 hours. Again, the surface winds and kinetic energy at the radius of maximum winds are reduced by about 30 and 60 percent.

Increase of Winds Beyond the Radius of Artificial Heating. Although not shown here, the winds for these and other experiments
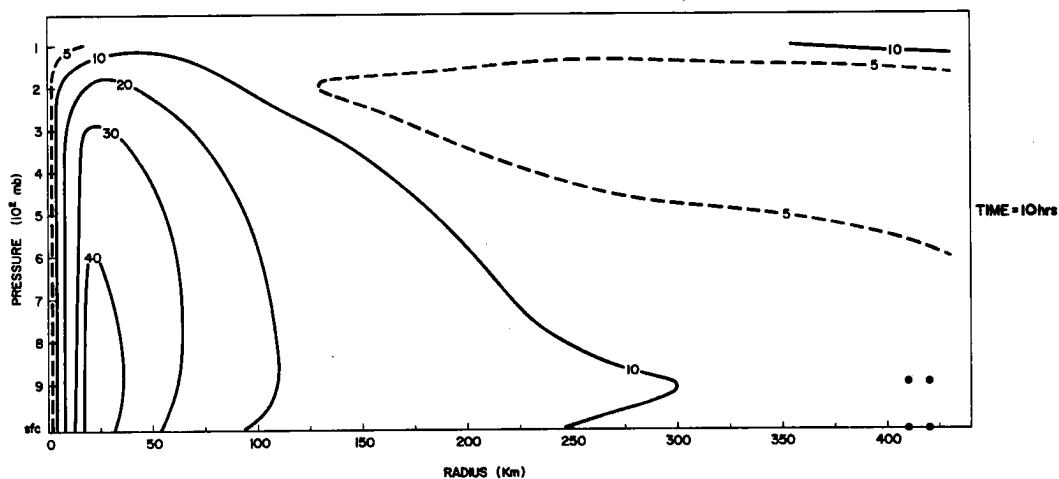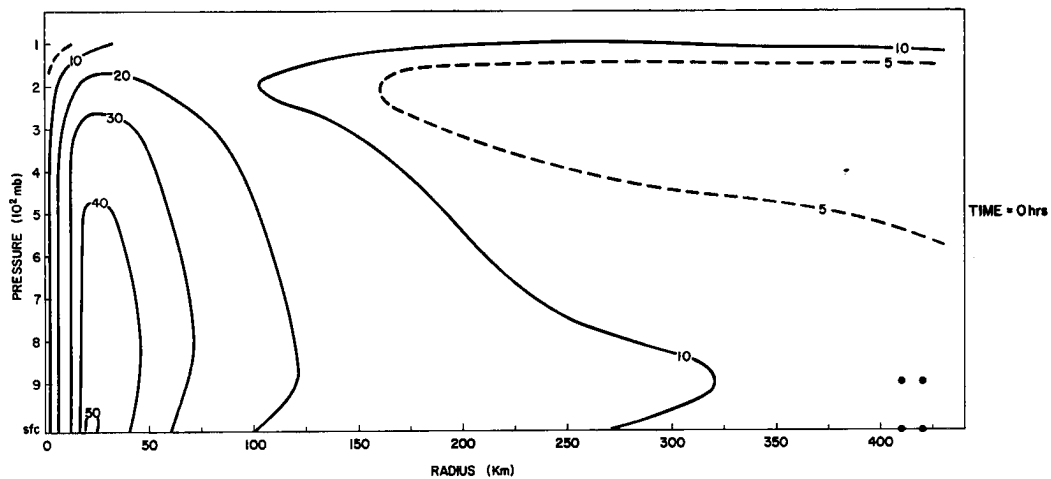
Figs. 8-10a-d. Total wind (in m/sec) at various time periods as a
result of artificial 1/4°C/hr heating rate for 10 hours,
no heating for 14 hours and again 1/4°C/hr heating
for 10 more hours. Heating is applied at the four
grid points shown.
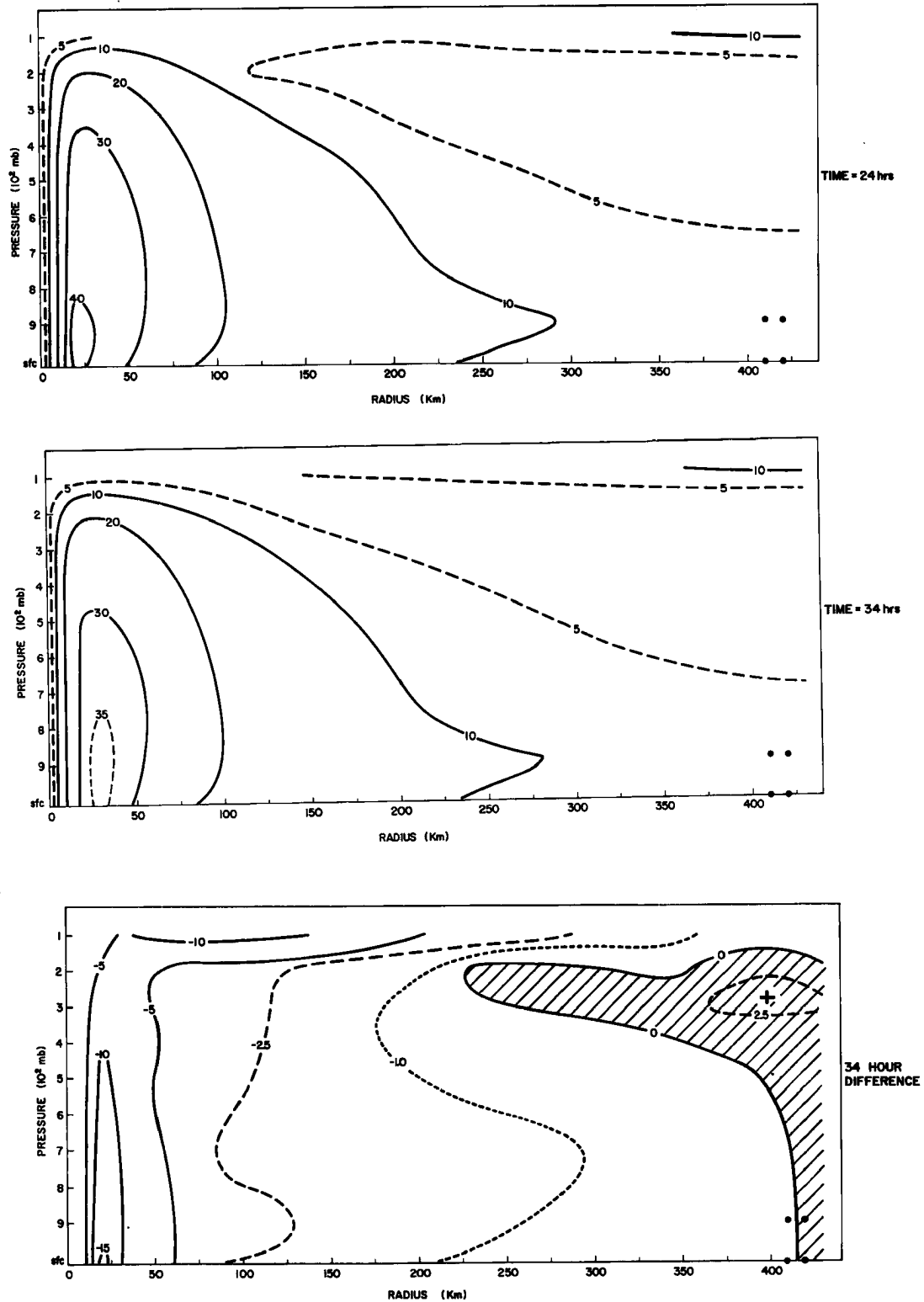
Fig. 8-11. Total wind difference in 34 hours for 1/4°C/hr artificial heating rate for 10 hours, off for 14 hours, and on again for 10 hours applied at the four black dot grid points shown.

where the heating is applied at closer-in-radii show that the winds increase at radii beyond the radius of artificial heating. This results from the increased transverse circulation at the outer radii due to the artificial heating and the extra convection. An increase of radial winds at outer radii would lead to extra water vapor convergence and a slight increase of the overall cyclone rainfall. Rather than being concentrated in the center, however, the rainfall is more uniformly spread throughout the vortex. Severe flooding would be reduced but the overall beneficial influences of the cyclone rainfall to a broad area would be maintained.

Conclusion. The Rosenthal symmetric hurricane model shows that substantial reduction of the winds at the inner core radii occur after 24-34 hours for artificial heating rates of $1/4$ and $1/2^\circ$C for ten hours applied at outer boundary layer grid radii. Reduction of winds at inner radii and increases at outer radii would lead to a more even rainfall distribution and perhaps slightly increased rainfall amounts. As discussed earlier, these artificial heating rates can be accomplished from carbon black dust seeding with 5-10 Air Force C-5A aircraft. Heating rates many times larger than the $1/4$ and $1/2^\circ$C per hours specified in this model can be accomplished for heavier carbon dust seeding.

Even though the Rosenthal model may have certain limitations in correctly representing all the physical processes occurring with the real hurricane, it is very probable that the influences of interest are correctly represented.

9. ECONOMIC CONSIDERATIONS

Fig. 9-1 shows the global regions where tropical storms occur and gives the average annual number of storms which form in each region. The Western North Pacific is by far the most active region with an average of 30 tropical cyclones per year. Military aircraft reconnaissance from Guam since World War II has given us a reasonably solid statistical sample of tropical cyclones in the Western Pacific (see Gray, 1971) which is not available for the other tropical storm regions, except for the Western Atlantic where the sample size is much smaller. The 26-year Western North Pacific data (available from U. S. Navy tropical storm data tapes of Navy Environmental Prediction Facility, Monterey, Ca., and from the Joint Typhoon Weather Center, Guam annual reports) allows for the stratification of storms by intensity.
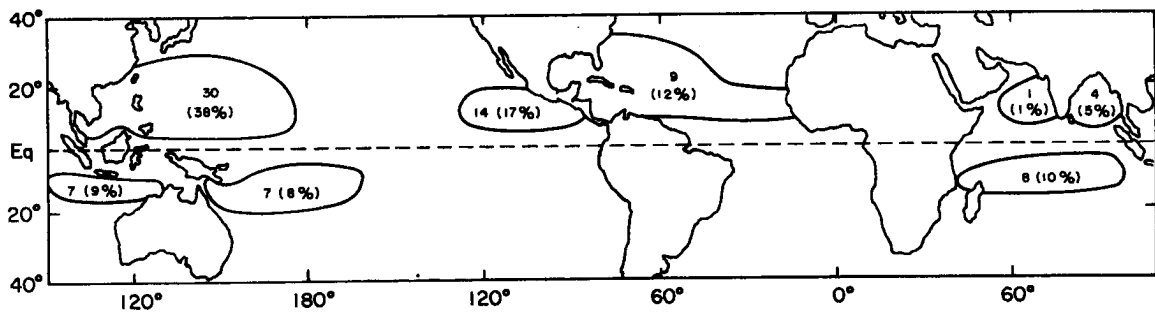
Fig. 9-1. Portrayal of global regions where tropical storms occur. The numbers in each region give the annual number of storms with maximum sustained surface winds greater than 25 m/sec. The relative number of storms in each region in percentage of the global total is also shown (from Gray, 1968--updated by Atkinson (1971).

83

If we assume that the intensity stratification of storms for the Western North Pacific is approximately valid for the other regions, then, with information of Fig. 9-1 we can estimate the number of storms of various intensities in the other regions. Table 9-1 gives this estimate by annual number of cyclones with maximum sustained surface winds of various intensities.

TABLE 9-1

Estimate of Annual Number of Storms With Maximum Sustained
Surface Winds of Various Intensities

Max. Sustained Surface Winds m/sec	In Western N. Pacific ~40% of Global Total	Other Regions ~60% of Global Total	Global Total
> 80	~ 2	~ 3	~ 5
60-80	~ 5	~ 8	~ 13
40-60	~ 11	~ 18	~ 29
25-40	~ 12	~ 21	~ 32
Total	~ 30	~ 50	~ 80

Storm Damage Estimates. With global information on the number of storms of various intensities it may be possible to estimate tropical cyclone damage if a relationship between maximum sustained surface winds and storm damage is available. Fig. 1-1 from Howard, Matheson, North (1972) as discussed in Section 1 gives a recent estimate of property damage (in 1969 U.S. dollars) as related to maximum sustained hurricane surface wind speeds. This estimate applies only to the U.S. It shows property damage increasing in relation to approximately the forth power of the maximum sustained

surface winds. For individual storms with maximum sustained surface winds of 200 mph (their highest estimate) they estimate property damage of about 400 million. These estimates do not seem exaggerated. Although annual U.S. property damage from tropical storms is about 500 million, individual hurricanes such as Betsy (1965) and Camille (1969) have each caused property damage of about 1.5 billion. Betsy's and Camille's maximum sustained surface winds could not have been much more than 200 mph ($\sim$ 90 m/sec). The damage relationship of Howard, Matheson, and North does not appear to be an exaggeration. If anything, their relationship may underestimate the destruction caused by the very intense storms.

In order to obtain an estimate of the economic impact of these storms and the potential for damage reduction, Fig. 9-2 has been constructed from the information of Howard, et al. in Fig. 1-1. This new figure shows damage reduction vs. percentage reduction of maximum sustained surface winds. For 10% wind reduction of a cyclone with maximum sustained surface winds of 70 m/sec, the damage reduction would be, according to this figure, about $50 million. This figure only allows estimates of individual storm damage, however. In order to make an estimate of the potential for annual U.S. and global damage reduction it will be further assumed that

   (1) only one-quarter of all tropical storms in each intensity
       category of Table 9-1 strike land where it is desirable to
       reduce their intensity

DAMAGE REDUCTION vs PERCENT
REDUCTION OF MAXIMUM SUSTAINED
SURFACE WINDS   (data from
study of Howard, Matheson,
and North, 1972)
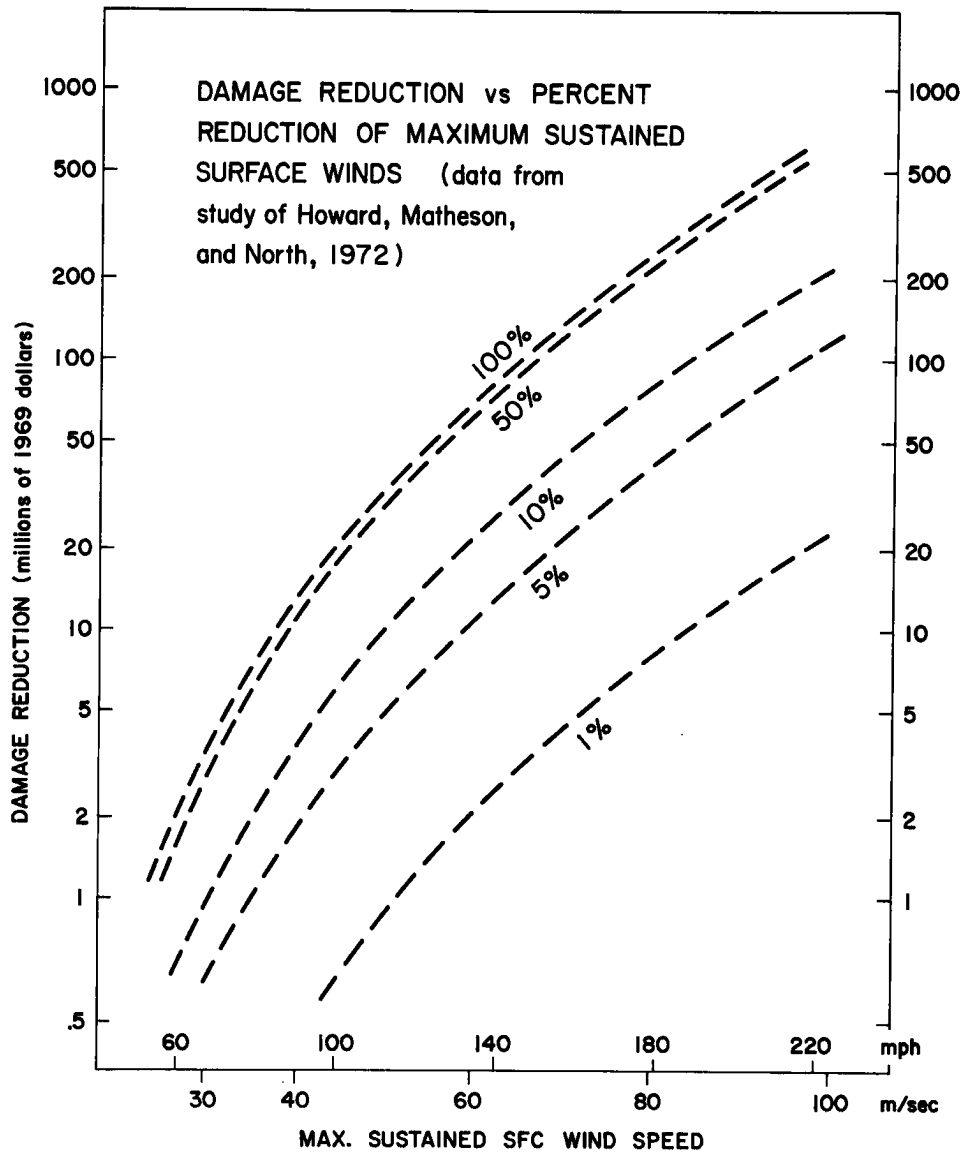
Fig. 9-2.   Information of Fig. 1-1 portrayed in terms of
storm damage reduction vs. reduction of maxi-
mum sustained surface winds in percent.

(2) the wind speed damage relationship of Fig. 9-2 for the
U.S. is, in the average, applicable to other global
locations, and

(3) it is possible to artificially reduce the maximum sustained
surface winds of storms as they strike land by 20 percent

Admittedly, the above assumptions are crude but as accurate informa-
tion is not available, they seem to be reasonable estimates based on
the best information we have at this time.

Table 9-2 shows the annual damage reduction estimates for the
U.S. and the globe based on the above assumptions and with the tropi-
cal storm frequencies and intensities of Table 9-1. For 20 percent
reduction of maximum sustained surface winds, the estimated annual
reduction in U.S. and global damage is about 100 and 800 million
dollars respectively.

The individual storm damage reduction for other percentage arti-
ficial maximum surface wind decreases is shown in Table 9-3.
Damage reduction is very strongly correlated with storm intensity.
The damage reduction figures would hardly be changed if storms
with maximum sustained surface velocities less than 40 m/sec were
not considered. If we consider only one-quarter of the storms with
maximum sustained surface velocities greater than 40 m/sec, then
the annual damage reduction estimates for various percentages of
maximum surface wind reduction are given in Table 9-4.

TABLE 9-2

No. of Storms and Estimate of the Annual Damage Reduction Potential From Carbon Black Seeding if 20 Percent Maximum Sustained Wind Speed Reduction is Possible for One-Quarter of all Storms
(In Millions of 1969 U.S. Dollars)

Max. Sustained Surface Wind (m/sec)	Damage Reduction of Each Storm for Max Wind Decreases of 20%	Annual No. of Treatable Storms	Total Damage Reduction in Millions of Dollars	
		For U.S.	For Globe	
>80 (avg. 90)	250	0.2/50	1.25/310	
60-80 (avg. 70)	90	0.4/28	3.2/300	
40-60 (avg.50)	20	1.0/20	7.2/144	
25-40 (avg.33)	4	1.0/4	8.0/32	
	Annual Total	2.6/~100	16/~800	

TABLE 9-3

Individual Storm Damage Reduction in Millions of 1969 Dollars by Storm Intensity and Percent that the Maximum Surface Winds are Reduced

Max. Sustained Surface Wind (m/sec)	Percentage Wind Reduction					
	1	5	10	20	33	50
> 80 (avg.90)	15	70	140	250	330	400
60-80 (avg.70)	5	25	50	90	115	140
40-60 (avg.50)	1	5	10	20	25	30
25-40 (avg.33)	0	1	2	4	5	7

TABLE 9-4

Annual Damage Reduction (in Millions of 1969 Dollars) for Various Percentage Reductions of Storm Maximum Sustained Surface Winds. Only one-Quarter of Tropical Cyclones with Maximum Surface Winds Greater than 40 m/sec have been considered

Percent Reduction of Maximum Sustained Surface Winds	For U.S. (1.6 Treatable Storms per year)	For Globe (12 Treatable Storms Per year)
1	~5	~35
5	~30	~220
10	~60	~450
20	~100	~800
33	~140	~1050
50	~170	~1300

Cost Estimates of Storm Modification. In Section 5 it was estimated that the cost of operating a U.S. Air Force C5A for 8-10 hours with regular maintenance, etc., is about $30,000. This aircraft can carry 200,000 lbs of carbon black which costs about $10,000 (at $0.05/lb). A single C5A carbon black flight costs about $40,000. Allowing for multiple additional expenses such as:

1) depreciation of aircraft
2) transportation to modification area
3) loss of flight missions during inactive storm periods
4) accidents
5) all supporting research and personnel costs, etc.
6) all administrative, inter-governmental activity, etc.

it might be safely estimated that all additional expenses would be no more than about one and a half times the cost of operating the aircraft with maintenance plus the cost of the carbon black. We might safely

estimate that all aspects of a total modification program would be no more than \$100,000 per one C5A flight mission. 10 and 20 flight missions would thus cost one and two million dollars, respectively. These estimates are probably on the high side. Were the military to lease its C5A aircraft free of charge, the modification costs would be only about 25-50 percent of this estimate. Nevertheless, we will maximize the cost of modification and use the \$100,000 per one C5A flight mission figure.

Assuming that 15 and 20 C5A aircraft missions are required to significantly reduce the intensity of storms with sustained maximum surface winds of 60-80 m/sec and >80 m/sec, and that 5 and 10 C5A aircraft are required to significantly reduce storms whose intensity is in the <40, and 40-60 m/sec class[5], we might estimate the damage reduction to modification cost ratio of implementing such a program. This is portrayed in Table 9-5 for all four classes of storm intensity. The economic gain for all classes of strong storms and for nearly all percentage wind reductions is clearly evident. Large economic gains of 10-100 to 1 are possible with 10-20 percent artificial wind reduction.

Table 9-6 portrays the annual potential damage reduction to modification cost for various percentage maximum sustained wind decreases. Only one quarter of those storms whose maximum sustained surface winds are greater than 40 m/sec have been considered.

---

[5]More intense storms typically have larger cirrus shields and require more aircraft to surround them with carbon dust.

TABLE 9-5

Ratio of Damage Reduction to Modification Cost for Different Intensity
Storms and Percentage Maximum Wind Decreases

Maximum Sustained Surface Wind (m/sec)	Percentage Reduction of Maximum Sustained Surface Winds					
	1	5	10	20	33	50
>80 (assume 20 C5A aircraft)	7/1	35/1	70/1	120/1	160/1	200/1
60-80 (assume 15 C5A aircraft)	3/1	15/1	35/1	60/1	75/1	95/1
40-60 (assume 10 C5A aircraft)	1/1	5/1	10/1	18/1	25/1	30/1
25-40 (assume 5 C5A aircraft)	0	2/1	4/1	6/1	10/1	14/1

TABLE 9-6

Ratio of Yearly Average of Damage Reduction to Modification Cost in
Millions of 1969 Dollars for Different Percentages of Wind Decrease.
Only One-Quarter of Storms with Intensity Greater than 40 m/sec are
Included.

Percentage Wind Reduction	Damage Reduction/Modification Cost	
	For U.S.	For Globe
1	5/3	30/14
5	30/3	180/14
10	60/3	450/14
20	100/3	800/14
33	140/3	1050/14
50	170/3	1300/14

The large economic gain is clearly evident. This, of course, does not consider the other uncalculable beneficial influence of reduction in loss of life. In storms such as Audrey (1957) in the U. S. and the Bay of Bengal storm of November 1970 prevention of loss of life would be a dominant consideration.

Indirect Economic Benefits. The above individual storm economic discussion vastly underestimates the potential economic gain that would accrue if a substantial success and reliability in storm maximum wind reduction could be demonstrated. If man could confidently reduce the inner core wind speeds by 25 to 40 percent (and thus reduce inner core destruction by 50 percent or more) then extra building industry construction costs to meet hurricane damage and extra government anti-hurricane construction for sea-walls, flood conduit channels, etc. could be reduced. These potential construction cost reductions would be enormous.

It is much more economical to reduce the destructive force of individual hurricanes whose inner core areas may strike a coastal area only once every 20, 50, or 100 years than to build expensive hurricane protection into all buildings along all coasts which may be affected. The likelihood of utilization of hurricane protection facilities at any one location is always small.

Conclusion. The storm damage reduction to cost of modification ratios for storm wind reduction of but 10-20 percent are very large. From both an economic and fatality point-of-view, the carbon dust modification scheme appears to be well justified.

10. POLLUTION AND HEALTH CONSIDERATIONS

The carbon black dust to be used for hurricane modification is almost pure organic carbon. It is manufactured by petroleum companies primarily as necessary ingredients to paints (for color pigments) and as a rubber reinforcing agent for auto tires. It is formed by the controlled incomplete combustion of fossil fuels (usually natural gas). Carbon black is inert and non-toxic. For the proposed concentrations needed for hurricane modification it is believed to be of no significant health hazard.

Being a primary ingredient in automobile tires, carbon black dust is deposited along road ways as tires wear out. It is estimated that approximately 1 lb/yr per tire of carbon material is released into the atmosphere from regular tire wear. This amounts to about 500 million lbs/yr of tire carbon release in the U.S. or about 1200 million lbs/yr for the globe. As each hurricane modification seeding experiment can be made for approximately 2-4 million lbs (i.e., 10-20 loaded C-5A aircraft each with 200,000 lbs of carbon dust), a possible global modification program involving 10-15 experiments per year would require putting into the atmosphere about 3-5 percent of the global deposition of carbon from automobile tires--certainly not an excessive amount of carbon. This is a miniscule fraction of the pollution coming from industrial contaminants. By contrast the total depletion of fossil fuels by the industrial nations of the world amounts to about 10^4 billion lbs/yr. This is between 10^5 to 10^6 times the fossil fuel to be used in

carbon black production for all the possible yearly global modification experiments. This program would not lead to significant future depletion of fossil fuels.

Particle Concentration. This study envisages dispersing carbon black in concentrations so as to cover approximately 10 percent of the horizontal area over a vertical thickness of 1/2 km. Ten percent area coverage of carbon black particles of 0.1μ size through an atmospheric boundary layer of 500 m thickness requires carbon black particle concentrations of $\sim 5000/cm^3$. This amounts to area densities of $\frac{1}{40}$ gm/m^2 or about 50 lb/km^2, certainly not an excessive mass of carbon per unit area. This particle concentration gives aerosol mass densities of but 50 micro gm/m^3 or $50 \times 10^{-6} gm$ per m^3.

The Environmental Protection Agency (EPA) in the Federal Register of Dec. 23, 1971 has set air contaminants standards by mean geometric average of weight of particles per cubic meter. Minimum levels representing the onset of undesirable pollution have been established as 70 microgram per m^3 or $70 \times 10^{-6} gm$ per m^3. Fig. 10-1 compares these proposed boundary layer carbon dust concentrations within the minimum EPA standards of pollution. Table 10-1 shows that during the period of 1957-1963 most U.S. cities and large towns far exceeded these levels. Maximum urban pollution levels were often 10-20 times higher than EPA safe levels. The proposed hurricane aerosol carbon dust seeding concentrations by mass are thus far below values typical of most urban areas. Most urban pollution

FOR CARBON BLACK PARTICLES OF 0.1 MICRON RADIUS AND DENSITY OF 2 gm/cm³

$$\text{MASS} \quad \sim \quad \tfrac{4}{3}\pi\rho r^3 \sim \quad 10^{-14} \text{gm/particle}$$

$$\text{AREA} \quad \sim \quad \pi r^2 \quad \sim \quad 3\times10^{-10} \text{cm}^2\text{/particle}$$

AVERAGE NO. OF PARTICLES PER cm³ IN LOWEST 500 METERS FOR 10% AREAL COVERAGE AND 120 CALORIES/10hr ABSORPTION	~ 5000
NO. OF CARBON PARTICLES PER m³ IF CARBON DISTRIBUTED OVER 500 m LAYER	$\sim 5\times10^9$
MASS OF CARBON PARTICLES PER m³	$\sim 5\times10^{-5}$ gm or 50 micrograms
HUD SPECIFIED MEAN DAILY AEROSOL MASS CONCENTRATION FOR MILDEST POLLUTION CON-CENTRATION MASS PER m³	~ 70 micrograms

Fig. 10-1. Magnitude of particle and mass concentration of proposed boundary layer carbon black seeding and comparison with HUD minimum pollution standards.

aerosols are larger (range $\sim 1\mu$ or 1,000 times volume of 0.1 μ particles) and in less concentration. Urban particles typically have radiation absorption characteristics much below that of the carbon black aerosols. Fig. 10-2 shows the typical size range of various classes of aerosol particles. The carbon dust to be used is smaller than most atmosphere aerosols.

TABLE 10.1

SUMMARY OF NASN SUSPENDED PARTICULATE SAMPLES FOR
URBAN STATIONS BY POPULATION CLASS, 1957–1963[a]

Pop. class	No. of samples	No. of stations[b]	Min. (μg/m³)	Max. (μg/m³)	Arith. mean (μg/m³)	Geo. mean (μg/m³)
1. 3 million and over	316	2	57	714	182	167
2. 1–3 million	519	3	34	594	161	146
3. 0.7–1.0 million	1191	7	14	658	129	113
4. 0.4–0.7 million	3053	19	18	977	128	112
5. 0.1–0.4 million	9531	92	10	1706	113	100
6. 50,000–100,000	5806	81	6	982	111	93
7. 25,000–50,000	1606	23	5	679	85	71
8. 10,000–25,000	484	6	11	539	80	63
9. <10,000	150	5	22	396	100	84

[a] From U.S. Dept. of Health, Education, and Welfare (115).

[b] 64 Stations participate every year; the remaining stations participated 1 or more years during the 7-year period. (Table from Stern, 1968) µg/m³ means micrograms per cubic meter.
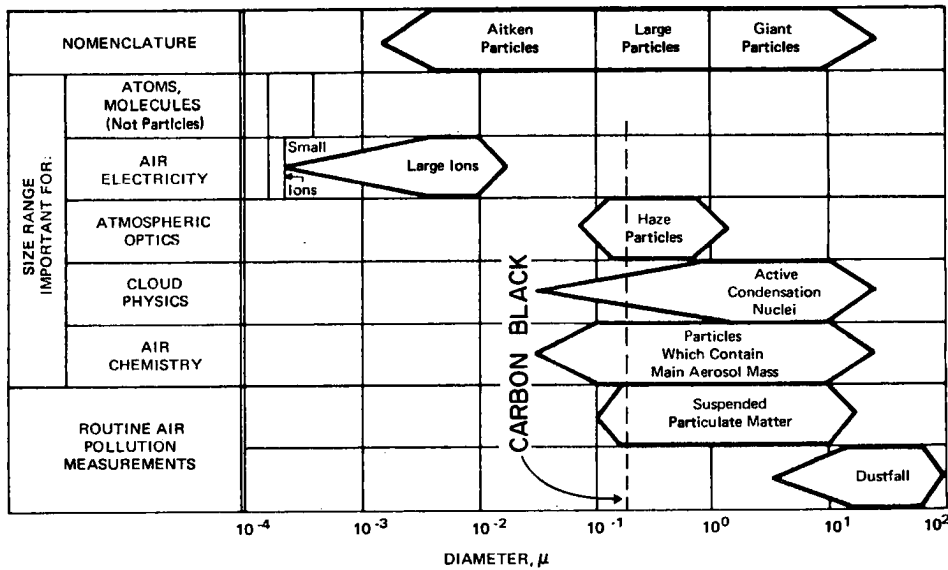
Fig. 10-2. Typical sizes of atmospheric particulate matter which are found in the earth's atmosphere (from NAPA Report AP-49, 1969), in comparison with 0.1µ carbon particles.

Particle Residency Time in the Atmosphere. As the carbon seeding

is to be accomplished in the boundary layer over the tropical oceans

where the turbulent mixing rates are high and where rapid particle

scavenging should occur, air pollution from 10-15 modification experi-

ments per year around the globe should prove to be a negligible factor

in adding to air pollution over the populated areas. Most particles

should be removed from the troposphere within a week. Atmospheric

residency times of the particles being advected into a hurricane should

be no more than a few days. Typical residency time of tropospheric

pollutants in the middle latitudes is only about 10 days (Martell, 1970,

AEC Report).

Visibility Reduction. As areal coverages of no more than 10-20%

are envisaged, mass densities of but 50-100 lb/km^2 should not unduly

restrict boundary layer visibilities. Boundary layer visibility may

be temporarily reduced to values no less than those observed in the

tropics in strong haze conditions. No significant visibility restriction

should occur at higher layers.

Health Hazard. The primary hazard to health from air pollution

comes from the intake and deposition of foreign aerosols within

the lower respiratory tract, particularly upon the alveoli sacs of the

lower lungs where oxygen and carbon dioxide are exchanged between

respired air and the blood. As discussed in the National Air

Pollution Control Administration Report No. AP-49 (U. S. Department

of Health, Education, and Welfare, 1969) this intake and deposition

upon the alveoli is strongly size dependent. Figs. 10-3 and 10-4 from

this report show that the larger aerosol particles of 5 - 100 μ are

filtered out in the nose and throat (nasopharyngeal). The very small

particles <.05μ are typically deposited on the walls of the lungs (other

than the alveoli through their natural molecular Brownean motion. These

very small particles which are not deposited in the alveoli are secreted

on the lungs and carried to the digestive tract to be filtered out of the

body without health hazard. The primary health hazard comes from

the deposition and retention of particles on the alveolar. The inter-

mediate sized aerosol particles in the size range of our carbon dust

particles ($\sim 0.1\mu$) -- the size to be used in the proposed modification

process--are least retained within the alveoli and represent a much

smaller health hazard than the other sized particles. In the carbon

dust particle concentrations envisaged for modification only a miniscule

number of particles will ever reach and be deposited on the alveolar.

Deposition of Carbon Particles in the Ocean. Most of the carbon

dust particles will be deposited by rainout or washout onto the ocean

surface. Being more dense than water ($\rho \sim 2\,gm/cm^2$) these nearly

pure carbon particles will eventually sink to the ocean floor.

Fall Velocity of Carbon Dust in Air and Water. The terminal fall

velocity of a small sphere (radius r) falling freely under gravity in a

viscous fluid with dynamic viscosity μ, has a velocity given by the

Stokes law. This velocity is $\sim 2/9\,gr^2 (\rho - \rho_o)/\mu$ where g is gravity,

and ρ, ρ_o are the density of the sphere and of the fluid. For lower
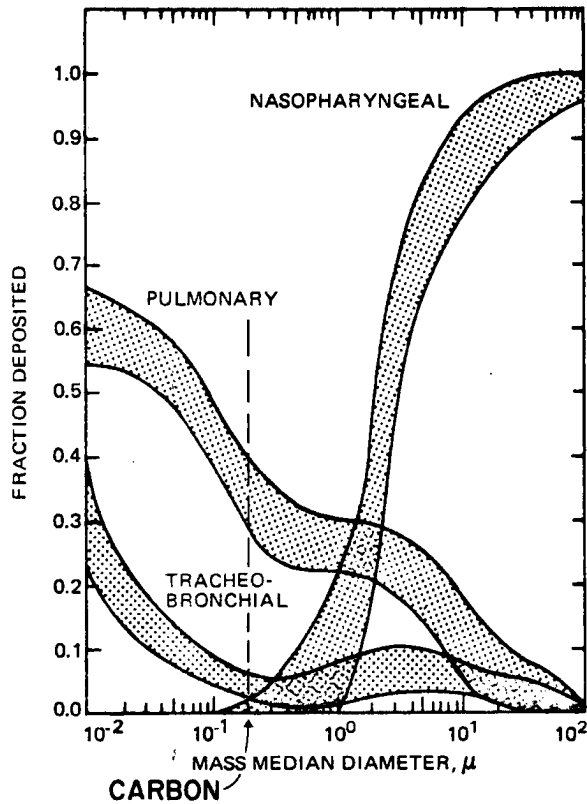
Fig. 10-3. Fraction of particles deposited in the three respiratory tract compartments as a function of particle diameter. (This figure shows the deposition efficiencies calculated by the Task Group on Lung Dynamics) (From NAPA Report AP-49, 1969). The dotted line shows the size of the 0.1μ carbon particles to be used.

Fig. 10-4. Calculated fraction of particles deposited in the respiratory tract as a function of particle radius. (This figure represents the calculated efficiencies of deposition of particles of various sizes in the tracheobronchial and alveolar regions of the respiratory system, and shows the size for minimum efficiency.) (From NAPA Report AP-49, 1969). The dotted line shows the 0.1μ carbon particles to be used.
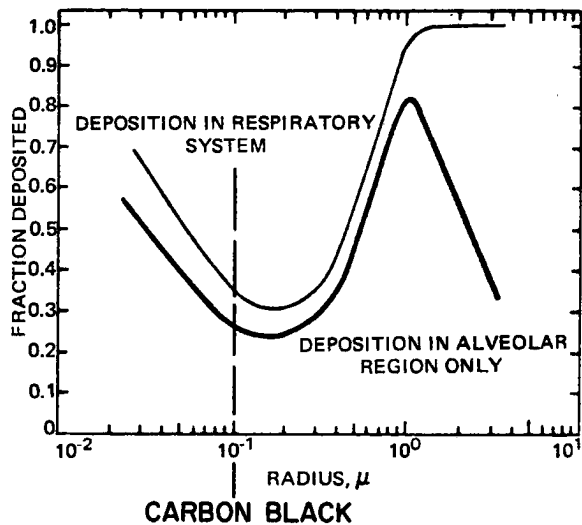
tropospheric tropical air, this terminal fall velocity for $0.1\,\mu$ radius carbon is $\sim 20\,cm/day$ — an insignificant amount. In water with higher density and dynamic viscosity the setting times are considerably slower. Experiments have shown that carbon dust reaching the ocean surface with wave action will become "well soaked" in a few days and will begin to settle at the Stokes law free fall velocity. 0.1μ radius carbon dust has a settling time in water of only $0.3\,cm/day$. Particles of this size will always remain near the ocean surface. This does not mean that the carbon dust cannot be removed from the ocean surface, however. Most of the $0.1\,\mu$ radius dust will not reach the ocean surface. Before the dust can sink through the atmospheric boundary layer to the ocean it will be removed by the scavenging process of rainout (particles becoming attached to raindrops during condensation) and washout (capture of particles by falling raindrops).

The carbon particles to reach the ocean surface will arrive only after substantial agglomeration and as such will sink into the ocean (after soaking) at rates on the order of about a meter per day. These settling rates will allow for the removal of the carbon from the ocean surface and eventual settling to the ocean floor in 5-10 years. These slow settling times should not effect the ecology of the oceans, however. Carbon is a highly inert substance that will not readily combine with other chemicals. It should have negligible influence on ocean fish or plant life.

Particle Washout. From information of the AEC Report (1970) on precipitation scavenging, it has been calculated that a rainfall amount of 1 cm with raindrop sizes of 0.1 cm radius should washout most of the 0.1μ carbon dust particles which are present in a vertical column of 0.5 km depth. A concentration of 5000 particles/cm^3 over a vertical depth of 500 m are the required amounts for modification. Each falling raindrop will capture by washout about 200-300 of the 0.1 μ particles. Agglomeration should occur for all the carbon particles captured by the individual raindrops. Agglomeration of 200-300 0.1 μ radius particles will increase the ocean Stokes particle settling time by a factor of ~15 to ~5 cm/day. This agglomeration by washout is, however, only a small part of the total particle agglomeration which will occur.

Agglomeration due to Rainout. Observational studies of particle residence times with lead and silver iodide tracers have shown that particle residency times determined only by washout are between 10 and 50 times too long. To explain this large descrepancy it is necessary to hypothesize a considerable agglomeration of aerosols as occurring in association with the condensation process. Particle capture with condensation is believed to result from a diffusiophoretic mechanism associated with rapid water vapor transfer to condensing drops and resulting nonuniformities in water vapor around the condensing drops.[6] Atmospheric aerosol residency times require a hypothesized rainout

---

[6]Personal discussion with M. L. Corrin.

agglomeration 10 to 50 times the rates normal to washout. Rainout agglomeration rates 10 to 50 times washout rates would lead to individual raindrop capture and agglomeration of about 2000 -10,000 0.1 μ radius carbon particles and, upon soaking with ocean wave action lead to a Stokes sinking velocity of about 0.5 to 2.5 m/day. These are the typical raindrops particle agglomerations and ocean settling times which are expected to occur in the actual modification experiments. As such, they will allow for the removal of the carbon particles from the ocean surface and their settlement to the ocean floor in a few years. The ocean currents will have a lot to do with the places and concentrations of ocean floor settling.

Deposition Concentrations. Although the carbon will be despensed at concentrations of about 50 lb/km^2, it is expected that it will be deposited on the ocean surface at concentrations of about one-tenth of the despensing amount, or at 5 lb/km^2 ($\sim$.002 gm/m^2). Concentrations of this amount would be difficult to detect. Carbon dust from 10 loaded C-5A aircraft would result in area deposition coverages equivalent to 5 lb/km^2 over only $\sim$1/100 of one percent of the global surface. Individual hurricane experiments should thus cause negligible contamination at the ocean surface. Carbon dust seeding of 20 hurricanes per year for 100 years would lead to a total global carbon dust deposition on the surface of about 2 lbs. per square mile.

Conclusion. The carbon dust seeding concentrations proposed for hurricane modification should have negligible effect on depletion of

fossil fuels. This modification proposal will cause no significant adverse pollution and/or health side effects either at the seeding location or over the populated land areas where some of the particles may be advected. The oceans should not be adversely effected in the future by the small mass to area depositions of carbon dust upon them. As the depositions of the carbon on the ocean surface will take place with considerable particle agglomeration, gravity (carbon density is twice that of water) should eventually remove these particles to lower levels. Chemically, carbon is a higher inert substance and will not disturb the ocean ecology.

11. CURRENT NOAA HURRICANE MODIFICATION PROGRAM AND COMPARISON WITH POTENTIAL OF CARBON DUST

The possibility of mitigating the destructive force of hurricanes by silver iodide seeding of the inner eye-wall of the storm was first proposed in 1961 by R. H. Simpson. Early experiments on hurricane Esther (1961) and Beulah (1963) were suggestive of some degree of success (Simpson and Malkus 1963, 1964). Later silver iodide treatment of the inner eye-wall of hurricane Debbie (1969) was associated with a reported reduction of the peak wind of 31 and 15 percent (Gentry, 1970). Because hurricanes have large natural variations of their intensity, it was impossible to tell how much (if any) of the wind changes were brought about by the silver iodide seeding (Hawkins, 1971). The Debbie results appeared encouraging, however.

The reasoning behind these silver iodide experiments and their results has been fully documented in the Project Stormfury Annual Reports of 1963 and 1971 (available from U. S. Navy Weather Service or the NOAA NHRL Miami office) and by Gentry (1971a, 1971b). Much of the background is based on the proven silver iodide cumulus enhancement techniques developed and tested by the NOAA Experiment Meteorological Laboratory under the direction of Joanne Simpson (Malkus and Simpson, 1964; Simpson and Simpson,1965; Simpson, 1970; Woodley, 1970; Simpson and Woodley, 1971; and other reports).

The physical justification for "silver iodide" seeding of the eye-wall cloud convection has, however, been questioned by some scientists.

Recently the National Hurricane Research Laboratory (Gentry and

Hawkins, 1970) has explored the consequences (through numerical

models and other physical reasoning) of altering the original cloud

eye-wall seeding hypothesis and moving the seeding treatment to rain-

bands just beyond the eye-wall cloud as shown in Fig. 11-1. This is

based on a hypothesis, similar to the theory of this paper, of prevent-

ing inflow from reaching the eye-wall by inducing extra cumulus con-

vection at larger radii. This produces a reduction of angular momen-

tum to the cloud eye-wall and leads to a reduction of the maximum

winds. The author supports the physical idea behind this more recent

silver iodide modification hypothesis. He questions only the magni-

tude of the influence that is possible.

HURRICANE MODEL
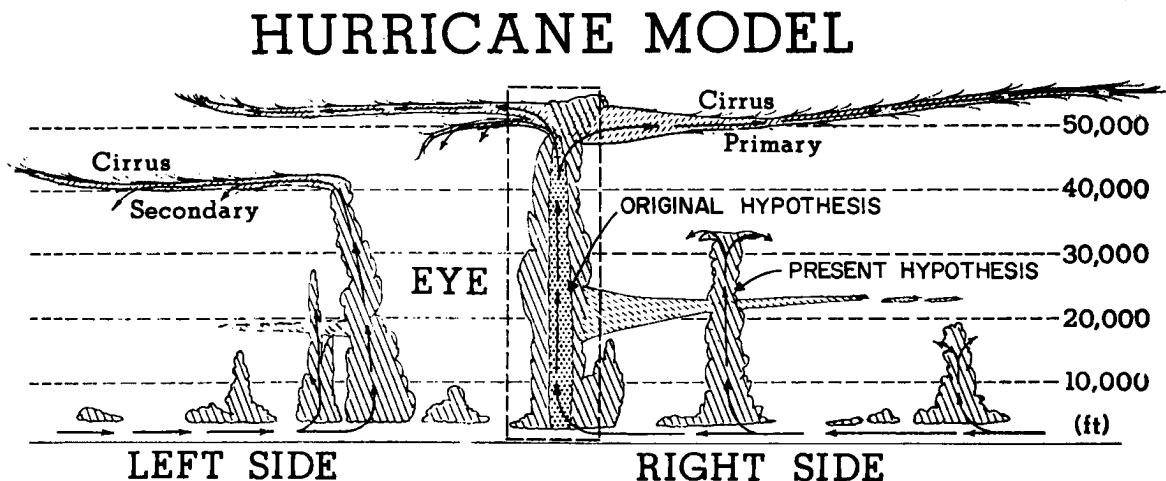
Fig. 11-1. Cross section of typical hurricane showing the places where silver iodide seeding was accomplished following the "original hypothesis" of R. H. Simpson (1961). The "present hypothesis" NOAA Stormfury silver iodide seeding location is shown to be at a radius beyond the eyewall cloud.

Comparison of Two Modification Schemes. The optimum artificial

heating rates from silver iodide seeding in the Stormfury project

have been tested in the Rosenthal model. They assume a heating of

$1/2^{\circ}$C/hr between levels of 300-500 mb at two grid points of radius 55

and 65 km. For this heating rate the Rosenthal model gives a maximum

eye-wall wind reduction of about 5 m/sec. This represents an artificial

heat source (if operationally possible) over a vertical depth four times

that of the boundary layer carbon dust heating and in an area of about

1/10 the area of the previously discussed carbon dust heating. This

$1/2^{\circ}$C/hr maximum assumed silver iodide heating from release of

heat of condensation gives (4 depth) x ($\frac{1}{10}$ area) x $\frac{24\,hrs}{10\,hrs} \sim 1.0$ or about

the same energy (if applied over 24 hours) to two interior grid points

as is gotten by applying the carbon black heating of $1/2^{\circ}$C/hr for 10 hrs

to two grid points just beyond the 400 km radius. In the silver iodide

case, the maximum wind reduction is about 5 m/sec. In the carbon dust

seeding case the reduction is 15 m/sec with the possibility of much

larger influence with higher heating rates for larger carbon concentra-

tions and areal coverages.

A comparison of these two heat sources is, however, not so mean-

ingful because much of-the extra convection which is brought about by

the silver iodide release of heat of fusion does not work to effect local

sensible temperature accumulation as does the radiation energy gain.

Much of the extra liberated heat of fusion goes to increased vertical

motion and potential energy gain which is exported to the surroundings

without local temperature increase. Much of the heat of fusion gain

and extra condensation which results is lost when many of the cloud

particles melt and evaporate at lower levels. Thus, most of the

silver iodide induced freezing and extra condensation which follows

does not bring about a local "long period" (i. e. -on a time scale larger

than that of the individual cumulus element) sensible temperature

accumulation. The silver iodide influence to beneficial hurricane

modification is hypothesized to occur in more of a dynamic fashion

from the rapid enhancement of the cumulus and the extra artificial

vertical motion (Simpson, 1970) which is believed to bring about an

increase of the mass transport out of the boundary layer.

Silver iodide heating requires the presence of preexisting convective

elements which, due to the typically large short term variations of the

inner convective region, is not always abundantly available. The carbon

seeding technique is not dependent on the inner storm variability. The

effectiveness of the silver iodide scheme is thus limited by both the

amount of super-cooled water available and by the cumulus enhancement

potential of the release of heat of fusion. Disregarding cost, the

potential for energy gain from carbon dust seeding in the hurricane

moat region is almost without limit.

The "carbon dust" modification hypothesis as outlined in this paper

is superior to the "silver iodide" hypothesis on the following grounds:

(1) It is based on a more direct physical model of interruption of the low level inflow through buoyancy enhancement. Man is more in control. He need not wait for cumulus to occur before acting as in the silver iodide seeding.

(2) Comparative results using the Rosenthal (op. cit.) model show the "carbon dust" hypothesis to be much more effective in reducing the inner core winds than the "silver iodide" hypothesis.

(3) The carbon dust scheme can be implemented in safer VFR flight conditions surrounding the storm without required knowledge of the highly variable inner cumulus cloud structure or navigation problems of getting the silver iodide into the super-cooled portion of the cloud.

(4) Since the influences of the carbon dust scheme are much larger than the silver iodide scheme, field testing to obtain statistical proof of modification will be much simpler with the carbon dust method.

The primary feature of the silver iodide scheme which is superior to the carbon dust scheme is the cost of implementation. The spreading of carbon dust will be more expensive. If the estimates of Section 9 on the damage reduction to modification cost ratio of carbon dust seeding are valid, however, then economic gain ratios of 10-100 to 1 should not invalidate the carbon dust scheme regardless of its cost in comparison with the silver iodide scheme.

Simultaneous Use of Both Carbon Dust and Silver Iodide Modification Schemes. It may prove beneficial to employ the silver iodide cumulus enhancement techniques in conjunction with the carbon dust seeding. This paper does not suggest that the current Project Stormfury program of seeding the rainbands beyond the radius of maximum winds in not beneficial, but only that its maximum wind modification

potential is limited in comparison with the carbon dust scheme. The recent Stormfury seeding hypothesis and that of the carbon dust seeding one are both based on the same physical idea of preventing inflowing mass from penetrating to the radius of the eye-wall convection. As the silver iodide techniques can be employed without great expenditure of funds (only a few seeding planes are needed) it may prove desirable to employ both techniques simultaneously.

Conclusion. The carbon dust hurricane modification hypothesis appears to be potentially superior to the silver iodide hypothesis in all regards except cost. As both techniques are directed to the goal of causing enhanced cumulus convection at a radii beyond the eye-wall radius, they both might be employed. For significant reductions of the hurricane inner core wind structure, however, the primary technique must be that of carbon dust.

12. SUMMARY DISCUSSION

This paper has been written for the purpose of opening up a dialogue on a new area of potential weather modification--namely meso-scale weather modification from solar energy interruption. It would appear that present day weather modification may need a broader scientific outlook. Nearly all the efforts over the last quarter century have been aimed at producing changes on the cloud scale through exploitation of the saturated water vapor pressure difference between ice and water. This is not to be criticized, but it is time we also consider the feasibility of weather modification on other time-space scales and with other physical hypotheses.

Hurricane modification is only one potential application of carbon dust seeding. It is likely that this same physical process can be beneficially utilized over oceans upwind from coastal areas in need of precipitation. The carbon dust heating might be utilized to generate weak meso-scale wind systems (and even in some cases produce weak tropical cyclones) which concentrate and enhance local convergence and induce extra rainfall over land as the ocean generated systems move inland. There are many coastal regions around the globe where significant precipitation enhancement of this type may be possible. It is time that we begin to expand our research efforts in these directions, and determine what realistic ratios of cost of experiment to economic gain would be. The very large advances in numerical modeling

in recent years should allow determination of realistic cause-effect relationships with regard to carbon dust heating influences.

Rainfall which occurs over the oceans is of little benefit to man. With growing global population densities the ultimate weather modification goal should be directed toward causing some of the rainfall which would normally occur over the oceans to, instead, fall over land. There are likely ways man can effect small but economically significant percentage alteration of land vs. ocean precipitation by employing more massive carbon dust seeding on a larger, say synoptic or possibly continental scale.

How to Get Started. This paper does not propose that we go out and attempt modification of a hurricane at this time. Actual hurricane modification with carbon dust should not be attempted until preliminary field testing and much more numerical modeling can be accomplished. We should first carry on a number of small scale field tests over the tropical oceans to carefully verify the influence of carbon heating in the real atmosphere. We must also conduct extensive numerical modeling experiments on the influence of heat sources on cumulus development and on the alteration of meso-scale flow patterns etc.

Initial Field Tests. We should first plan to spread carbon dust in sufficient quantity over the tropical oceans at a location where meteorological monitoring can be accomplished. Previous experiments as discussed by Frank (1973) were conducted with vastly insufficient amounts of carbon and over land. It

would appear that the minimum field test experiment to objectively verify the carbon heating influence should be accomplished with at least 50-100 thousand pounds of carbon dust--25 to 50% of one C-5A aircraft load. This would allow for 1000-2000 km^2 areal spread at 10% carbon coverage, or 300-600 km^2 at one-third carbon coverage. This 20 to 45 km side of a square carbon dispersal area should produce a heating influence large enough for accurate measurement and study with a) ground radar, b) aircraft: temperatures, moisture and carbon particle measurement, c) aircraft cloud pictures and d) the synchronous satellite. Numerical experiments will aid in determining what the minimum field test experiment should be. With easterly trade wind flow and the open Gulf of Mexico to the west, the Key West, Florida area could be a favorable location for initial field testing. If feasible, some modest field testing in the coming GATE experiment could be attempted. In the first experiments it may be possible to spread the carbon from surface sights with crop-dusting or other types of equipment without the need for aircraft dispersal. In the GATE experiment, dispersal might be accomplished from a few of the ships. Surface dispersal would be less complicated and less costly than that accomplished by aircraft. Pre-field testing work on methods and equipment of dispersion, size and diffusion character of the carbon dust, etc. must also be accomplished.

If minimum field test experiment results are encouraging, larger magnitude field testing from multiple aircraft could be accomplished at a later date. This field testing could gradually be expanded until it is deemed feasible to test on a mature storm or on the development of a meso-scale system.

Numerical Modeling Experiments. The extensive progress in numerical modeling in recent years allows for a variety of multiple testing of the influence of heat sources. Initial steps in this direction have already been made with the Rosenthal and Lopez models discussed in Sections 7 and 8. In addition it would also be desirable to test the carbon heat source in a variety of other numerical models such as those dealing separately with particle diffusion, planetary boundary dynamics, meso-scale flow patterns, the asymmetrical hurricane, etc. The knowledge potentially available from these existing and emerging numerical models should be fully exploited.

The initial field testing and all the model experiments could probably be accomplished in 3-4 years at a cost of about one-two million dollars. A decision to expand to more extensive field testing could be made after this first research phase. It would appear that an initial research outlay of one-two million dollars is well justified in terms of likelihood of success and potential benefit.

ACKNOWLEDGEMENTS

BIBLIOGRAPHY

Atomic Energy Commission Report, 1970: Precipitation Scavenging,
    AEC Symposium Series 22, 499 pp. (available from Nat. Tech.
    Infor. Ser., U. S. Dept. of Commerce, Springfield, Va., 22151).

Anthes, R. A., 1971a: Non-developing experiments with a three-level
    axisymmetric hurricane model. NOAA Technical Memorandum
    ERLTM-NHRL, 17pp. (available from NOAA NHRL Miami office).

_____, 1971b: The response of a three-level axisymmetric
    hurricane model to artificial redistribution of convective heat
    release. NOAA Technical Memorandum ERL-NHRL-92, 14 pp.
    (available from NOAA NHRL Miami office).

_____, S. L. Rosenthal, and J. W. Trout, 1971c: Preliminary
    results from an asymmetric model of the tropical cyclone. Mon.
    Wea. Rev., 99, 744-758.

Atkinson, G., 1971: Forecaster's guide to tropical meteorology. Un-
    published Air Weather Service (MAC) Technical Report No. 240,
    300 pp. (available from AWS, Scott AFB, Illinois).

Bell, G. J. and TSUI Kar-sing, 1972: Some typhoon soundings and
    their comparison with soundings in hurricanes. Unpublished Royal
    Observatory Report, Hong Kong, 28 pp.

Cabot Corporation, 1969: Preparation of aqueous carbon black disper-
    sions. Internal publication available from : Cabot Corporation,
    Special Blacks Division, 125 High Street, Boston, Mass.

Cox, S. K., 1969: Observational evidence of anomalous infrared cooling
    in a clear tropical atmosphere. J. of Atm. Sci., 26, 1347-1349.

_____, and S. L. Hastenrath, 1970: Radiation measurements over
    the equatorial central Pacific. Mon. Wea. Rev., 98, 823-832.

_____, and V. E. Suomi, 1969: Radiation in the free atmosphere.
    Dept. of Meteorology, Univ. of Wisconsin. Final unpublished report
    to ESSA Research Laboratories, 68 pp.

Cry, G. W., 1967: Effects of tropical cyclone rainfall on the distribu-
    tion of precipitation over the eastern and southern United States,
    ESSA Professional Paper 1, U. S. Dept. of Commerce, Environ-
    mental Science Services Administration, Washington, D. C., 67 pp.

BIBLIOGRAPHY (cont'd)

Dunn, G. E. and B. I. Miller, 1960: Atlantic Hurricanes. Louisiana
State U. Press, 377 pp.

Fritz, S., L. Hubert and A. Timchalk, 1966: Some inferences from
satellite pictures of tropical disturbances. Mon. Wea. Rev., 92,
231-236.

Frank, W. M., 1973: Characteristics of carbon black dust as a large-
scale tropospheric heat source. Colo. State Univ., Dept. of
Atmos. Sci. Research Report No. 195, 52 pp.

Garstang, M., 1967: Sensible and latent heat exchange in low latitude
synoptic scale systems. Tellus, 18, 1-17.

_____, and K. L. Warsh, 1970: Energy flux measurements at
the sea-air interface. J. of Marine Technology Soc., 4, 49-54.

Gentry, R. C., 1970: Hurricane Debbie modification experiments.
Science, 1968, 473-475.

_____, 1971: To tame a hurricane. Science Journal, 7, 49-55.

_____, and H. F. Hawkins, 1970: A hypothesis for modification
of hurricanes. Appendix B in Project Stormfury Annual Report
1970, (available from NOAA NHRL Miami office).

Giddings, M. E., 1966: An estimation of benefits to agriculture from
hurricane-induced rainfall. Dept. of Economics, Colo. State Univ.,
M. S. Thesis, 117 pp.

Goodyear, H. V., 1968: Frequency and areal distribution of tropical
storm rainfall in the United States coastal region on the Gulf of
Mexico. ESSA Technical Report, WB-7 (U. S. Dept. of Commerce,
Environmental Science Services Administration), Office of Hydrology,
Silver Springs, Maryland, 33 pp.

Graham, H. E., and G. N. Hudson, 1960: Surface winds near the cen-
ter of hurricanes (and other cyclones). Natl. Hurr. Res. Proj.
Rept. No. 39, Hydrometeorological Section, Hydrologic Services
Division, U. S. Weather Bureau, Washington, D. C., 200 pp.

Gray, W. M., 1967: The mutual variation of wind, shear and baro-
clinicity in the cumulus convective atmosphere of the hurricane.
Mon. Wea. Rev., 95, 55-73.

BIBLIOGRAPHY (cont'd)

Gray, W. M., 1968: Global view of the origin of tropical disturbances and storms. Mon. Wea. Rev., 97, 669-700.

_____, 1971: A climatology of tropical cylones and disturbances of the Western Pacific with a suggested theory for their genesis/maintenance, Unpublished NVVWEARSCHFAC Technical Paper No. 19-70, Navy Res. Facility, Norfolk, Virginia, 224 pp.

_____, 1972a: A diagnostic study of the planetary boundary layer over the oceans. Colo. State Univ., Dept. of Atmos. Sci. Report No. 179, 95 pp.

_____, 1972b: Cumulus convection and larger-scale circulations, Part III. Broadscale and meso-scale considerations. Colo. State Univ., Dept. of Atmos. Sci. Report No. 190.

Hawkins, H. F., and D. T. Rubsam, 1968: Hurricane Hilda, 1964. II. Sturcture and budgets of the hurricane on October 1, 1964. Mon. Wea. Rev., 96, 617-636.

Herbert, P. J. and C. L. Jordan, 1959: Mean soundings for the Gulf of Mexico area, National Hurricane Research Project Rept. No. 30, U. S. Dept. of Commerce, National Hurricane Research Lab., Miami, Florida, 10 pp.

Howard, R. A., J. E. Matheson, and D. W. North, 1972: The decision to seed hurricanes. Science, 176, No. 4040, 1191, 1202.

Hughes, L. A., 1952: On the low level wind structure of tropical cyclones, J. Meteor. 9, 422-428.

Izawa, T., 1964: On the mean wind structure of typhoons. Unpublished Japan Typhoon Res. Lab. Tech. Note No. 2, 45 pp.

Jelesnianshi, C. P. and A. D. Taylor, 1972: A preliminary view of storm surges, before and after storm modification. Unpublished intergovernment NOAA report to the Director of the National Hurricane Research Laboratory, 49 pp.

Korb, G., and F. Moller, 1962: Theoretical investigation on energy gain by absorption of solar radiation in clouds. Final Report on U. S. Army Signal Corp Contract No. DA-91-541-EUC-1612, 185 pp. (available from U. S. Army).

BIBLIOGRAPHY (cont'd)

Kuo, H. L., 1965: On formation and intensification of tropical cyclones through latent heat release by cumulus convection. J. of the Atmos. Sci., 22, No. 1, 40-63.

La Seur, N. E. and H. F. Hawkins, 1963: An analysis of hurricane Cleo (1958) based on data from research reconnaissance aircraft. Mon. Wea. Rev., 91, 694-709.

Lopez, R. E., 1972: A parametric model of cumulus convection. Colo. State Univ., Dept. of Atmos. Sci. Paper No. 188, 100 pp. (to be published in J. of Atmos. Sci.).

Malkus, J. S., and H. Riehl, 1960: On the dynamics and energy transformation in steady-state hurricanes. Tellus, 12, 1-20.

_____, and R. H. Simpson, 1964: Modification experiments on tropical clouds. Science, 145, 541-548.

Martell, E. A., 1970: Transport patterns and residence times for atmospheric trace constituents vs. altitude. Advances in Chemistry Series, 93, American Chemical Co., Washington, 421-428.

Marteney, P. J., 1965: Experimental investigation of the opacity of small particles. NASA Contractor Report No. NASA CR-211, Dept. of Commerce, Washington, D. C., April.

Matsuno, T., 1966: Numerical integrations of the primitive equations' by a simulated backward difference method. J. of the Meteorol. Soc. of Japan, Ser. 2, 44, 76-84.

Miller, B. I., 1964: On the filling of tropical cyclones over land. Mon. Wea. Rev., 92, 389-406.

National Air Pollution Control Administration, 1969: Air quality for particulate matter. National Air Pollution Control Administration Publication No. AP-49, U. S. Dept. of Health, Education and Welfare, Public Health Service, Consumer Protection and Environmental Health Service, Washington, D. C., 211 pp.

Ooyama, K., 1969: Numerical simulation of the life cycle of tropical cyclones. J. Atmos. Sci., 26, No. 1, 3-40.

Palmén, E. and H. Riehl, 1957: Budget of angular momentum and energy in tropical cyclones. J. of Meteor., 14, No. 2, 150-159.

BIBLIOGRAPHY (cont'd)

Project Stormfury Annual Reports, 1963 through 1971: (Available from National Hurricane Research Laboratory, NOAA, Miami, Florida).

Priestley, C. H. B., 1959: Turbulent transfer in the lower atmosphere. The Univ. of Chicago Press, 130 pp.

Riehl, H., 1954: Tropical Meteorology. McGraw-Hill, New York, 392 pp. (Chapter 11).

_____, 1963: Some relations between wind and thermal structure of steady state hurricanes. J. Atmos. Sci., 20, No. 4, 276-287.

_____, and J. Malkus, 1961: Some aspects of Hurricane Daisy, 1958. Tellus, 13, 181-213.

Roll, H. U., 1965: Physics of the Marine Atmosphere. Academic Press, New York and London, 426 pp.

Rosenthal, S. L. and W. L. Koss, 1968: Linear analysis of a tropical cyclone model with increased vertical resolution. Mon. Wea. Rev., 96, 858-865.

Rosenthal, S. L., 1970a: A survey of experimental results obtained from a numerical model designed to simulate tropical cyclone development. ESSA Technical Memorandum, ERLTM_NHRL 88, 78 pp. (available from NOAA NHRL Miami office), National Hurricane Res. Lab., Miami.

_____, 1970b: A circularly symmetric primitive equation model of tropical cyclone development containing an explicit water vapor cycle. Mon. Wea. Rev., 98, No. 9, 643-663.

_____, 1971a: A circularly symmetric primitive equation model of tropical cyclones and its response to artificial enhancement of the convective heating functions. Mon. Wea. Rev., 99, 414-426.

_____, 1971b: The response of a tropical cyclone model to variations in boundary layer parameters, initial conditions, lateral boundary conditions, and domain size. Mon. Wea. Rev., 99, 767-777.

BIBLIOGRAPHY (cont'd)

Rosenthal, S. L., 1971c: Hurricane modeling at the National Hurricane Research Laboratory (1970), Appendix C in Project Stormfury Annural Report 1970, (available from NOAA NHRL Miami office).

Saffir, H. S., 1972: An engineering study of structural damage caused by hurricane Camille in Mississippi. No. N22-197-72, Consulting Engineers, Coral Gables, Florida, 27 pp. (available from NOAA NHRL Miami office).

Schoner, R. W., and S. Molansky, 1956: Rainfall associated with hurricanes (and other tropical disturbances), National Hurricane Res. Proj. Report No. 3, (Hydrometeorological Section, Hydrologic Services Division, U. S. Weather Bureau), Washington, D. C., 305 pp. (available from NOAA NHRL Miami office).

Shea, D. J., 1972: The structure and dynamics of the hurricane's inner core region. Colo. State Univ., Dept. of Atmos. Sci. Report No. 182, 134 pp.

Sheets, R. C., 1968: On the structure of hurricane Dora (1964). National Hurricane Res. Lab. Rept. No. 83, 64 pp. (available from NOAA NHRL Miami office).

Simpson, J., 1970: Cumulus cloud modification: Progress and Prospects. A Century of Weather Progress, American Meteorological Society publication, 143-155.

Simpson, J. S., and R. H. Simpson, 1965: Experimental cumulus dynamics. Reviews of Geophysics, 3, 387-431.

Simpson, J., and W. M. Woodley, 1971: Seeding cumulus in Florida: New 1970 results. Science, 172, 117-126.

Simpson, R. H., and J. S. Malkus, 1963: An experiment in hurricane modification: Preliminary results. Science, 142, 498.

_____, 1964: Experiments in hurricane modification. Scientific Amer., 211, 27-37.

Stern, A. C., 1968: Air Pollution, Vol. 1. Academic Press, New York, 694 pp.

Sundqvist, H., 1970: Numerical simulation of the development of tropical cyclones with a ten-layer model. Part I, Tellus, 22, 359-390.

BIBLIOGRAPHY (cont'd)

Sugg, A. L., 1968: Beneficial aspects of the tropical cyclone. J. of Appli. Meteor., 7.

Turner, D. B., 1969: Workbook of atmospheric estimates. Public Health Service Publication No. 999-AP-26, 84 pp.

Williams, K. T., 1970: A statistical analysis of satellite-observed trade wind cloud clusters in the western North Pacific. Atm. Sci. Paper No. 161, Dept. of Atmos. Sci., Colo. State Univ., Fort Collins, 80 pp.

Woodley, W. L., 1970: Rainfall enhancement by dynamic cloud modification. Science, 170, 127-132.

Yamasaki, M., 1968: Detailed analysis of a tropical cyclone simulated with a 13-layer model. Papers in Meteorology and Geophysics, 19, No. 4, 559-585.

Yanai, M., 1961: A detailed analysis of typhoon formation. J. Meteor. Soc. Japan, 39, 187-214.

_____, 1968: Evaluation of a tropical disturbance in the Caribbean Sea region. J. Meteor. Soc. Japan, 46, 86-109.

_____, and T. Nitta, 1967: Computation of vertical motion and vorticity budget in a Caribbean easterly wave. J. Meteor. Soc. Japan, 45, 444-466.

Vonder Haar, T. H., and K. J. Hanson, 1969: Absorption of solar radiation in tropical regions. J. of Atmos. Sci., 26, 652-655.

Zipser, E. J., 1969: The role of organized unsaturated convective downdraft in the structure and rapid decay of an equatorial disturbance. J. of Appl. Meteor., 8, 799-814.

APPENDIX A

The (Rosenthal, 1970b, 1970a, 1971b) symmetric hurricane model is representative of the current state of the art as may be verified by comparison with models developed by Ooyama (1969), Sundqvist (1970) and Yamasaki (1968). In their overall features all these models compare very well. The National Hurricane Research Laboratory has recently developed a hurricane model (Anthes et al., 1971) which eliminates the assumption of circular symmetry and, therefore, is more advanced than those cited in this text. This modification experiment will later be tried on this asymmetric model.

Review of the Model. The reader concerned with mathematical details should refer to Rosenthal (1970a). The model storm is an isolated, stationary, circularly symmetric vortex. The vertical structure of the atmosphere is represented by seven levels and geometric height is the vertical coordinate. The levels correspond to pressures of 1015, 900, 700, 500, 300, 200 and 100 mb in the mean tropical atmosphere. All variables are defined at all levels. The primitive equations govern the horizontal motion. The hydrostatic assumption is employed.

The continuity equation is simplified as follows. The local rate of change of density is neglected and a climatological density (a function of height alone) is used to evaluate the vertical and horizontal mass flux terms. The external gravity wave is eliminated by demanding that the vertical integral of the horizontal mass divergence vanish.

In the experiments discussed here, the radial limit of the computational domain is 440 km. The system is open at the lateral boundary. The lateral boundary conditions require that the relative vorticity and horizontal divergence vanish. In addition, the radial derivatives of potential temperature and specific humidity are also required to vanish.

Through a generalization of the procedure suggested by Kuo (1965), the model simulates convective precipitation (and the macroscale heating due to this latent heat release) as well as the enrichment of the macroscale humidity due to the presence of the cumuli. Convection may originate in any layer provided that the layer has a water vapor supply from horizontal convergence and that conditional instability exists for parcels lifted from the layer. Non-convective precipitation is also simulated. Details are given by Rosenthal (1970a).

Time derivatives are estimated by forward differences except in the case of specific humidity where a Matsuno (1966) type integration is employed. Advective derivatives are calculated by the upstream method except for the case of humidity where a conservation form of the equations is used. All nonadvective space derivatives are calculated as centered differences.

The drag coefficient is represented by Deacon's empirical relationship (Roll, 1965, p. 160) which is a linear function of surface-wind speed. The sensible and latent heat fluxes at the sea surface are calculated by the bulk aerodynamic equations and the surface drag is

represented by the usual quadratic stress law. The exchange coefficients for sensible and latent heat are equal to the drag coefficient. The turbulent flux convergences that appear in the thermodynamic and water vapor continuity equations are evaluated through the assumption that the fluxes have a linear variation over height and are zero at and above the height of the 900 mb level. This is based on the assumption that at 900 mb and above, fluxes produced by small scale turbulence are insignificant in comparison to those produced by cumulus-scale motions.

The sea temperature is an external parameter and, for experiments discussed here, is taken $2^{\circ}C$ greater than the initial sea-level air temperature (initially, the latter is horizontally uniform for all experiments). Since the sea-level air temperature varies with time according to the thermodynamic equation, the air-sea temperature difference varies both with radius and time as the model hurricane evolves.

Radial resolution is 10 km and the time step is 2 minutes. A lateral mixing coefficient of $2.5 \times 10^{3} \; m^{2} \; sec^{-1}$ is used for all prognostic variables.

The Control Experiment. The model is initialized with hypothetical data representative of a weak vortex (Rosenthal, 1970a). With judicious choices of static stability, humidity, sea temperature, etc., a hurricane-like vortex ultimately is developed. For discussions of the circumstances under which models of this type do not produce hurricanes, see Rosenthal (1971c) and Anthes (1971). The structure of the mature storm is, in general, highly realistic.

For the control experiment (Experiment S-35) employed in this report, initial conditions are established as follows. Climatological potential temperatures (a function of height alone and very nearly those of the Hebert and Jordan (1959) mean hurricane season sounding) are specified. With a lower boundary condition of 1015 mb, hydrostatic base-state pressures and temperatures (Table A 1) are computed for the levels above the surface.

Table A 1. Standard Values of Thermodynamic Variables

Level	Height	$\overline{\theta}$	$\overline{T}$	$\overline{p}$
	(m)	(°K)	(°K)	(mb)
1	0	300	301.3	1015.0
2	1054	303	294.1	900.4
3	3187	313	282.6	699.4
4	5898	325	266.5	499.2
5	9697	340	240.8	299.2
6	12423	347	218.9	199.5
7	16621	391	203.1	101.1

The initial temperature field is then specified by

$$T_{i,j} = \overline{T}_i + T_* \left(\text{Cos} \left(\frac{\pi}{r_{max}} \right) r_j + 1 \right) \text{Sin} \left(\frac{\pi}{z_7} \right) z_i$$

where i and j are, respectively, height and radial indices, $\overline{T}_i$ is the standard temperature (Table A 1), $T_* = 0.16°K$, $r_{max} = 440\,km$, and z_7 is the height (Table A 1) of level 7. The initial pressure at level 7

is then taken to be the standard value (Table A 1) and the hydrostatic equation is integrated downward to obtain the remainder of the initial pressure field. Finally, the gradient wind equation is solved for the initial tangential wind while the initial radial and vertical motions are taken to be zero. The initial surface wind reaches a maximum of 7 m sec^{-1} at a radius of 250 km. The central pressure of the vortex is 1013 mb. A base state relative humidity is specified as a function of height (Table A 2). By use of the data given by Table A 1, a base state specific humidity is calculated. The initial specific humidity is then assumed horizontally homogeneous and equal to this base state value.

Table A 2. Initial Values of Relative Humidity at the
Information Levels

Level	Height	Relative Humidity
	(meters)	(percent)
1	0	90
2	1054	90
3	3187	54
4	5898	44
5	9697	30
6	12423	30
7	16621	30

Although Experiment S-35 has been discussed elsewhere (Rosenthal, 1971c), a detailed summary is presented here since we wish to emphasize different points.

Figure A-1 summarizes the control's life cycle in terms of central pressure and maximum sea-level wind. Pressure is not defined at zero radius because of a horizontal staggering of variables. As a consequence, central pressure values are taken from a grid point 5 km from the storm center at sea-level. The initial conditions are clearly arbitrary and, therefore, the early portions of the integration are not especially significant. In particular, the rather long "organizational" period (168 hours) required for the vortex to begin intensification is easily altered by changing such arbitrary parameters as the scale and/or intensity of the initial vortex, the size of the computational domain and the lateral boundary conditions (Rosenthal, 1971c). The values of some rather poorly defined physical parameters also strongly effect the organizational period (Rosenthal and Koss, 1968; Rosenthal, 1970a; Rosenthal, 1971c).

The rapid intensification of the storm to the mature stage (from 192 to 240 hours, Fig. A-1) is fairly typical of real hurricanes. Indeed cases exist where deepening of this magnitude has occurred in as little as 12 to 24 hours. The long, quasi-steady, mature stage is fairly typical of hurricanes which remain over the ocean without encountering cold surface waters or unfavorable surrounding flow patterns.
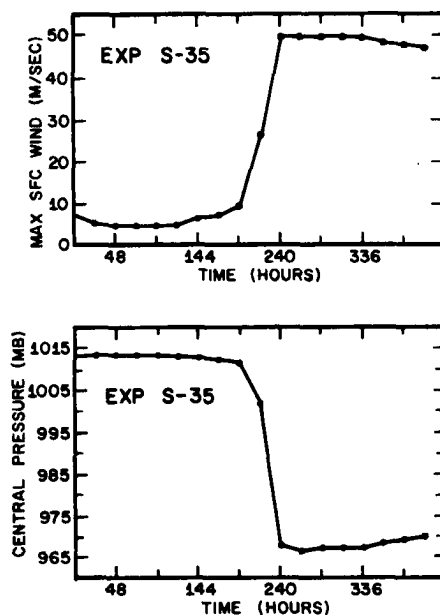
Fig. A-1.   Results from experiment S-35.   Top, maximum
surface wind as a function of time.   Bottom, central
pressure as a function of time.   Taken from
Rosenthal (1971c).

Fig. 8-1 (in the text) illustrates the wind field at 312 hrs and is

representative of the mature stage between 240 and 336 hours.   The

strongest winds are concentrated in a narrow zone near the storm

center.   The strongest vertical motions and condensation rates as

represented by the rainfall rate, (analogous to the hurricane eye wall)

are also concentrated in an extremely narrow zone which extends

from slightly outside to slightly inside the wind maximum.   The radial

motions show that virtually all of the storm's inflow occurs in the

lower kilometer of the atmosphere while significant outflow occurs

only in the high troposphere.   The transverse circulation is then

characterized by inflowing air very close to the surface, ascent in

the vicinity of the wind maximum and outflow at high levels.

Close to the sea surface, the tangential wind is controlled by the opposing effects of angular momentum conservation as air spirals inward and loss of angular momentum to the ocean through surface drag. This then explains the close association of the eyewall and the wind maximum since it is in the eyewall region that large centrifugal and Coriolis effects prevent further inward penetration of the air and hence force ascent to take place. Inflow is concentrated close to the sea surface because the rotational stability of the mature vortex does not allow inward penetration unless absolute angular momentum (following a parcel) is rapidly dissipated (Rosenthal, 1971c) and surface drag provides the only sink sufficient to allow significant penetration. The outflowing branch of the circulation in the high troposphere is largely controlled by conservation of absolute angular momentum since frictional forces are small at these levels.

The fact that the wind maximum and the isotachs inward of the maximum are essentially vertical is a consequence of the control of the midtropospheric wind field by vertical transports of absolute angular momentum (Rosenthal, 1970b).

APPENDIX B

Characteristics of the Air Force C5A Aircraft

PERFORMANCE		
High cruise speed		470 knots
Long range cruise speed		440 knots
Aerial delivery drop speed		130 - 150 knots
Rate of climb at sea level, standard day at basic mission* weight		2,100 ft/min
Take-off distance over 50 feet at basic mission* weight		7,500 ft
Landing distance over 50 feet with 100,000 lb payload at midpoint of 2500 nm radius mission, sea level, 89.5°F, wet grass runway		4,000 ft
Design payload—2.5 g		220,000 lb
—2.25 g		265,000 lb
Range with 220,000 lb payload		3,050 nm
Range with 112,600 lb payload		5,500 nm
Ferry range		7,200 nm

*Basic Mission 100,000 lb payload, 5,500 nm

WEIGHTS		
Flight design gross weight—2.5 g		728,000 lb
Flight design gross weight—2.25 g		764,500 lb
Basic mission weight		712,000 lb
Maximum landing weight (9 fps sink rate)		635,050 lb
Operating weight		323,904 lb

CARGO COMPARTMENT					
Length excluding ramps					121.1 ft
Length including ramps					144.6 ft
Height					13.5 ft
Width					19.0 ft
Total volume, including ramps					34,734 cu ft
Palletized volume including ramps (36 463L pallets)					19,020 cu ft
Forward loading opening	height	. 13.5 ft		width	19.0 ft
Aft loading opening	height	. 9.5 ft*		width	19.0 ft
Loading opening height above ground (forward or aft)					54 inches
Loading opening height above ground (level-kneeled)					73 inches

*With the ramp lowered to the ground, aft cargo opening will accommodate vehicles or other loads up to 12.5 feet high.

PERSONNEL CAPACITY		
Crew		8
Alternate crew		6
Courier seating		8
Troops—upper troop compartment		75

FUEL SYSTEM		
Capacity (JP-4)		49,000 U.S. gallons (318,500 lb)
Single point refueling rate		2,400 U.S. gallons/min (15,600 lb/min)
Jettison rate		1,380 U.S. gallons/min (8,970 lb/min)

LANDING GEAR		
Number of wheels		28 (4 nose and 6 each on 4 main gear bogies)
Tires, nose and main		43 x 17-20, Type VII, 26 ply rating
Main landing gear tread—outer tires		35.9 ft
—main struts		25.9 ft
Wheel base		72.8 ft